FREIBURGER SCHRIFTEN
ZUR HYDROLOGIE

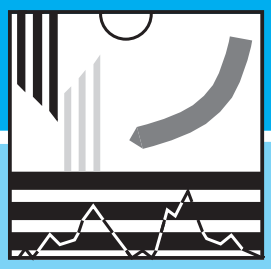

Band 9

Jens Lange

A non-calibrated rainfall-runoff model for large arid catchments, Nahal Zin, Israel

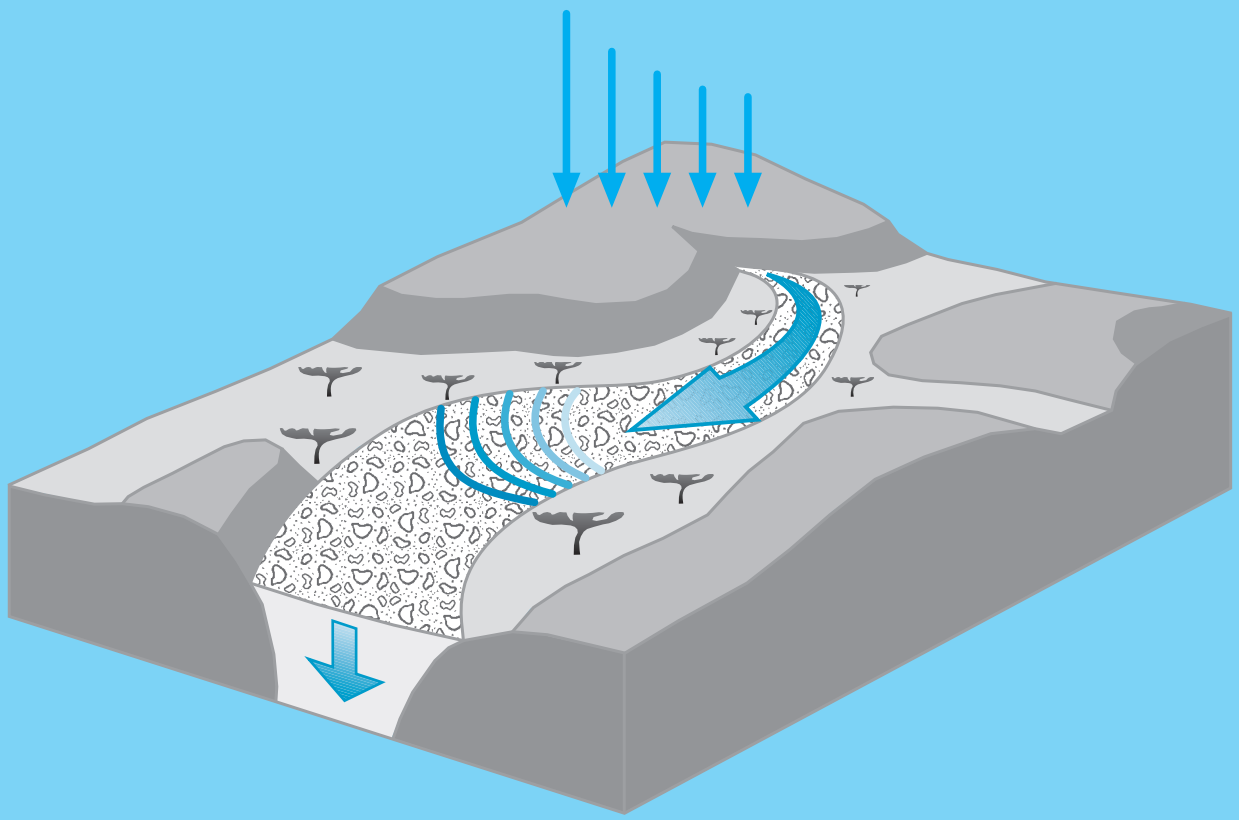

Institut für Hydrologie der Universität Freiburg i.Br.

Jens Lange

A non-calibrated rainfall-runoff model for large arid catchments, Nahal Zin, Israel

Unterstützt durch / Supported by:

Förderverein Hydrologie an der Albert-Ludwigs-Universität
Freiburg im Breisgau

FREIBURGER SCHRIFTEN ZUR HYDROLOGIE

Band 9

Jens Lange

A non-calibrated rainfall-runoff model for large arid catchments, Nahal Zin, Israel

1999

Institut für Hydrologie der Universität Freiburg i. Br.

Freiburger Schriften zur Hydrologie

Herausgegeben von / Edited by:

Prof. Dr. Christian Leibundgut
PD Dr. Siegfried Demuth

Institut für Hydrologie, Universität Freiburg i. Br.

Schriftleitung / Editorial office:

Ingeborg Vonderstraß

Verlag und Vertrieb / Published and saled by:

Institut für Hydrologie
Universität Freiburg i. Br.
im Selbstverlag
Anschrift / Address: Fahnenbergplatz, D-79098 Freiburg i. Br.
Germany

ISSN 0945-1609

Preface

This dissertation belongs to studies of catchment hydrology carried out at the Institute of Hydrology, University of Freiburg. Nevertheless there are two main differences: First, the humid zone is left as an arid catchment is investigated and, second , a non-calibrated model is presented. Thereby an important contribution to the current discussion about problems in calibration and validation of hydrological catchment models is provided. For runoff-, groundwater recharge- and water balance studies in arid areas a new tool is provided based on innovative methods.

The editors would like to express thanks to all Israeli partners, especially to the colleague Asher P. Schick, for supporting this study and for the fruitful co-operation.

The Editors
Christian Leibundgut and Siegfried Demuth

Contents

Abstract

Much field based hydrological research has been conducted in arid environments mainly in microscale studies. Two main processes dominate arid zone flood generation:

(a) the generation and spatial concentration of surface runoff as a direct response to localized high intensity rainfall and

(b) transmission losses into the dry channel alluvium.

The present study seeks to incorporate this knowledge into a rigorous analysis of single high magnitude events in a large arid catchment. This required a new appropriate tool, i.e. a rainfall-runoff model not depending on calibration with hydrometric streamflow data.

Hence a non-calibrated rainfall-runoff model was developed for the 1400 km^2 arid catchment of Nahal Zin, northern Negev, Israel. The model used spatially distributed rainfall input applied over a catchment which was disaggregated into different terrain types according to hydrologically relevant surface characteristics. Hortonian overland flow generation on each type was parametrized independently using values of initial loss and temporal decay of infiltration determined from existing field experiments. Delimited by topography, this catchment-wide pattern of rainfall excess was distributed over more than 800 tributary catchments (model elements). Runoff delivery from the model elements to the adjoining channel segments was timed by applying a mean response function determined in an environmentally similar experimental catchment. Inside the channel network the MVPMC3-method of the Muskingum-Cunge technique was used for streamflow routing accounting for channel dimensions and roughness. For each channel segment a constant infiltration rate was applied to account for transmission losses and discontinued when the wetting front reached the bottom of the available alluvial storage.

In the Zin catchment neither of the two large floods used for model application was completely documented. For both of them the model helped to analyze flood generation:

- In the uppermost catchment a localized, convective rainstorm caused the high magnitude flood of October 1979. A rainfall radar had not yet been installed and only the routing component of the model could be tested with field data. Nevertheless, areas of major cell activity and runoff generation could be reasonably reconstructed by a reversed use of the Zin model as a ‘runoff-rainfall model’. Both simulated and gauged hydrographs showed that even large floods may totally disappear flowing on dry arid channels for long distances.
- For the October 1991 event data from six rainfall recorders and a rainfall radar were available, both showing a huge squall line. However, gauging stations were destroyed and peak discharges had to be reconstructed post-factum. The fit of the peak discharges was encouraging as simulations fell within the uncertainty range of reconstructed field values. Simulated runoff generation took place in almost the entire catchment, still the spatial pattern revealed the trajectories of the inner core rainfall cells. The postponed response of an upper tributary directly sharpened the main flood peak. Then the peak did not decrease significantly downstream. Preceding inflows from tributaries caused an initial wetting of the alluvium. The

following main flood crossed over a nearly saturated channel alluvium with a high flow velocity. Hence the effect of transmission losses on flood peaks may be limited when additional parts of a catchment are active.

Total maximum model uncertainty was estimated including the uncertainty ranges of each model parameter. The different event characteristics directly affected parameter sensitivity and model uncertainty. Maximum model parameter error of the diminished October 1979 peak was governed by transmission loss parameters and exceeded 300 %. During 1991 only 90 % was determined for this value and infiltration characteristics of the terrain were more relevant. Still comparisons to existing calibrated or regionalized models showed that the present approach may be regarded as superior when runoff responses (e.g. rare high magnitude discharges) and flow processes (e.g. concentration times and flow velocities) are simulated in conditions or areas where no field data exist. Hence the model may be reasonably applied to ungauged catchments simulating the dangers and benefits of desert floods. This may yield a more dependable flood control (i.e. a ‘field based estimate’ of extreme discharges and flood concentration times) and estimates of runoff volumes available for groundwater recharge at the mouth of large dryland rivers.

Zusammenfassung

Umfangreiche hydrologische Forschungsarbeiten fanden in der Vergangenheit vor allem in kleinen ariden Einzugsgebieten statt. Es zeigte sich, daß hauptsächlich zwei Prozesse die Entstehung von Abflußereignissen in Trockengebieten dominieren:

(a) Bildung und räumliche Konzentration von Oberflächenabfluß als direkte Antwort auf räumlich eng begrenzte Niederschläge von hoher Intensität und

(b) Infiltrationsverluste in das trockene Gerinnebett.

Die vorliegende Arbeit möchte sich dieses Wissen zunutze machen und es in eine gründliche Analyse von einzelnen Extremereignissen in einem großen ariden Einzugsgebiet einfließen lassen. Dafür war jedoch als geeignetes Werkzeug ein Niederschlags-Abfluß-Modell notwendig, das nicht auf die Kalibrierung mit gemessenen Abflußdaten angewiesen ist.

So wurde ein nicht-kalibriertes Niederschlags-Abfluß-Modell im 1400 km^2 großen ariden Einzugsgebiet des Nahal Zin, einem Wadi im nördlichen Negev Israels, entwickelt. Als Eingangsgröße verwendet das Modell ein räumliches Niederschlagsmuster. Dieses wurde im Gebiet auf verschiedene Oberflächentypen verteilt, die zuvor anhand von wichtigen hydrologischen Eigenschaften ausgeschieden worden waren. Die Bildung von Horton-Oberflächenabfluß wurde unabhängig für jeden Oberflächentyp parametrisiert. Hierzu wurden Anfangsverluste und zeitliche Abnahmen von Infiltrationsraten aus Feldversuchen herangezogen. Das räumliche Muster von gebildetem Oberflächenabfluß wurde dann auf über 800 Teileinzugsgebiete (Modellelemente) verteilt, die durch die Topographie vorgegeben waren. Eine mittlere Antwortfunktion, die in einem ähnlichen Einzugsgebiet ermittelt worden war, löste den Zufluß der einzelnen Modellelementen in angrenzende Gerinnesegmente zeitlich auf. Im Gerinnenetz beschrieb die MVPMC3-Methode des Muskingum-Cunge-Verfahrens unter Berücksichtigung von Gerinnedimension und Rauhigkeit den Wellenablauf. Eine konstante Infiltrationsrate vollzog in jedem Gerinnesegment die Abflußverluste in das Gerinnebett nach. Diese wurden gestoppt, wenn die Feuchtefront die Grenze des verfügbaren Flußbettspeichers erreicht hatte.

Im Nahal Zin war keines der zwei großen Abflußereignisse, die für eine Modellanwendung zur Verfügung standen, komplett meßtechnisch erfaßt. So half das Modell bei beiden Ereignissen, die Abflußentstehung zu analysieren.

- Im Oktober 1979 erzeugte eine räumlich eng begrenzte, konvektive Niederschlagszelle ein Großereignis im oberen Teil des Einzugsgebiets. Zu dieser Zeit existierte noch kein Niederschlagsradar, so daß nur die Wellenablaufkomponente des Modells mit gemessenen Daten verglichen werden konnte. Trotzdem konnten Hauptzonen des gefallenen Niederschlags und der Abflußbildung sinnvoll rekonstruiert werden. Dies war durch eine Umkehrung des Modells in ein ‘Abfluß-Niederschlags-Modell’ möglich. Sowohl simulierte als auch gemessene Abflußganglinien dokumentierten, daß Abflußereignisse völlig verschwinden können, wenn sie lange Strecken in trockenen ariden Gerinnen zurücklegen.

- Im Oktober 1991 zeigten sowohl sechs Niederschlagsschreiber als auch ein Niederschlagsradar ein umfangreiches System aus linienhaft aufgereihten Niederschlagszellen. Jedoch wurden sämtliche Abflußmeßstationen zerstört und Abflußspitzen mußten nachträglich rekonstruiert werden. Die Modellergebnisse paßten gut zu den rekonstruierten Abflußspitzen, sie lagen in deren Unsicherheitsbereichen. In nahezu dem gesamten Einzugsgebiet fand Abflußbildung statt, deren räumliches Muster noch die Zugbahnen der einzelnen Konvektivzellen erahnen ließ. Die verzögerte Reaktion eines oberen Teileinzugsgebietes führte zu einem direkten Aufsteilen der Abflußspitze, die im weiteren Verlauf kaum noch abnahm. Dies war der Fall, weil vorauseilende Abflußspitzen von unteren Teileinzugsgebieten das sonst trockene Gerinnebett aufgesättigt hatten. Die folgende Hauptabflußwelle schoß danach über ein fast gesättigtes Alluvium. Dies mag als Beispiel dafür dienen, daß Gerinnebettverluste nur bedingt auf Abflußspitzen wirken können, wenn wichtige Teileinzugsgebiete aktiv sind.

Die Unsicherheitsbereiche der einzelnen Modellparameter erlaubten es, die maximale und die gesamte Modellunsicherheit abzuschätzen. Hierbei wirkten sich unterschiedliche Ereignischarakteristika auf die Modellunsicherheit und auf die Sensitivität einzelner Parameter aus. Im Oktober 1979 überstieg die maximale, von der Parametrisierung herrührende Modellunsicherheit 300 % und war von Parametern geprägt, die die Gerinnebettverluste beschrieben. Im Oktober 1991 betrug dieser Wert nur 90 % und Infiltrationscharakteristika der Oberflächen wurden bedeutender. Dennoch zeigten Vergleiche zu bestehenden kalibrierten und regionalisierten Modellen, daß das neu entwickelte Modell jenen Ansätzen dann überlegen ist, wenn Abflußentstehung (z.B. seltene Extremabflüsse) oder Fließprozesse (z.B. Konzentrationszeiten oder Fließgeschwindigkeiten) zu Bedingungen oder in Gebieten simuliert werden sollen, für die keine Geländemessungen vorliegen. Folglich kann das Modell in ungemessenen Gebieten sinnvoll zur Vorhersage von positiven und negativen Auswirkungen von Trockengebietsabflüssen eingesetzt werden. Dies kann zu einem verläßlicheren Hochwasserschutz (durch eine ‘geländebasierte’ Abschätzung von extremen Abflüssen und deren Konzentration) sowie zu Abschätzungen der Wasservolumina führen, die zur Grundwasserneubildung im Mündungsbereich großer Trockengebietsflüsse zur Verfügung stehen.

1 Introduction

A complete understanding of the individual runoff responses of various catchments is only guaranteed by a thorough analysis of the underlying processes of flood generation. These processes differ from one climatic regime to another. In humid areas soil infiltration usually is in excess of occurring rain intensities. During single storm events most rain infiltrates and mixes with water from preceding events stored in the underground. Following various subsurface pathways water of *'different history'* reaches a channel and induces flood generation. Moreover, in almost all areas vegetation is the point of first contact of rainfall. In the catchment scale this complex interplay of different processes can hardly be followed, i.e. the *three-dimensional* pattern of the single (mostly subsurface) flow processes can hardly be identified.

Except for terrain with active erosion or sedimentation (e.g. recent channel alluvium, mobile sand dunes), infiltration rates of the sparsely vegetated arid areas do not reach the rain intensities of high magnitude convective rainstorms. During these events Hortonian overland flow accumulates on the ground surface, concentrates quickly and induces episodic floods in ephemeral streams. While a huge amount of flood water may be lost travelling on dry channel beds, runoff contribution from indirect subsurface storages is negligible. Hence water of the *'same history'* makes up desert floods. Flood generation processes are inherent with accentuated spatial variability but limited to the surface, hence to only *two dimensions*.

The complexity of flood generation in humid areas has caused a widespread application of conceptual rainfall-runoff models. In these approaches complex hydrological processes are approximated by simple, physically meaningful conceptualisations (e.g. linear reservoirs). Usually their parameters are not measurable but have to be assessed by model calibration, i.e. by fitting simulated with gauged runoff data. As a consequence, high quality hydrometric data are required for a successful model application, a precondition often fulfilled in the perennial streams of developed countries in humid areas. In most arid zone countries, however, financial means are too short to install and maintain a hydrometric gauging network, the reason why almost all arid catchments are ungauged. And even if gauging stations exist, measurement problems during high magnitude desert floods considerably reduce data quality. Still only calibrated rainfall-runoff models have been applied to arid catchments so far.

The present study aims to contribute to the understanding of high magnitude events in a large arid catchment. This requires a new appropriate tool, i.e. a rainfall-runoff model not depending on calibration by hydrometric streamflow data but taking into account the dominant processes of arid zone flood generation. Compared to humid areas these processes are simpler, as event water (of the same history) is redistributed within only two spatial dimensions. This fact encouraged the establishment of a non-calibrated approach in a 1400 km^2 arid catchment, despite the knowledge that the determination of the spatial pattern of the various model parameters would demand considerable time and effort. To cope with the large modelling scale recent techniques were chosen (e.g. rainfall radar and a GIS-framework providing facilities of airphoto analysis and spatial modelling).

Applying a new type of model this tool must be tested carefully. Tests of model performance included validation with gauged or reconstructed streamflow data and sensitivity/uncertainty evaluations. Scarcity of data limited hydrological analyses to two high magnitude events. As the model input by convective raincells was studied in detail, this information could be transferred to an ungauged tributary and to changed catchment properties. As a result contributions to two problem areas of water resources management were provided: a field- based estimate of high magnitude discharges and assessments of the effects of an alteration of catchment properties induced by climatic change.

The present study represents an outcome of the close cooperation between the Department of Geography, The Hebrew University of Jerusalem, Israel, and the Institute of Hydrology, Freiburg, Germany. Both the local field experience of the Israeli research team and the 30-year database of the hyper-arid Nahal Yael research catchment were indispensable prerequisites. The 'Förderverein Hydrologie an der Albert-Ludwigs-Universität Freiburg i. Br.' provided financial help for a five-months period of field mapping and data collection, January - June 1996**.** Digital radar data were provided by Mekorot, Electro-Mechanical Service Ltd., hydrometric runoff data by the Israel Hydrological Service.

Within the joint research project 'Floodwater alluvium relations', funded by the Government of Baden-Württemberg, a dam breach induced flash flood simulation was carried out (SCHICK et al. 1996). The U.S.-Israel BiNational Science Foundation, the Israel Electric Corporation and the Jewish National Fund provided assistance in the construction of the dambreak. While aspects of sediment dynamics and temporal behaviour of channel bed infiltration were studied elsewhere (SCHICK et al. 1996, SCHICK et al. 1997, LANGE et. al. 1998), the measured field data provided an excellent framework for a field-based model test.

2 General aspects

2.1 Arid zone hydrology

2.1.1 Water balance and temporal scales

The water-balance equation, the fundamental equation of hydrology, is the essential part of any hydrological model. It largely depends on the climatic zone and the time scale considered. The hydrological regime of most arid environments is governed by single, episodic flood events in dry channels as a direct response to localized high intensity rainfall. The *long-term* water balance of arid areas is dominated by evaporation losses from bare soil (PILGRIM et al. 1988). Because of the sparse vegetation cover interception losses are generally negligible and only along stream channels phreatophytes are responsible for considerable transpiration. In the arid Tabalah catchment, Saudi Arabia, for example, total evapotranspiration losses accounted for 95 % of the rainfall, only 3 % contributed to surface runoff. From the latter 3 % about 75 % recharged alluvial aquifers (ABDULRAZZAK et al. 1989).

In the *short time scale* of ephemeral runoff events (several hours up to one or, rarely, two days) the amount and spatial redistribution of rainfall through surface runoff is most decisive for the water balance. Evaporation losses from open water surfaces may be disregarded due to a rapid spatial concentration of flow. Moreover, low air temperatures and high cloudiness prevail during storm and runoff events (YAIR & LAVEE 1985). For a single runoff event a time-sequence of two types of surface flow losses is characteristic:

(a) first, widespread infiltration or detention losses occur spontaneously at or near the location where the rainfall arrives at the surface (*direct losses*),

(b) second, linear transmission losses into the riverbed alluvium of the stream channels occur after surface flow has been generated and has spatially concentrated (*indirect losses*).

The type of loss also has an ecological impact. The shallow storages recharged by direct losses are quickly emptied by evaporation within several days after the event, while the alluvial storages filled by indirect losses are deeper, more permanent and may serve as water storage for vegetation or local population. Especially in large arid catchments all components of the event-based water balance are inherently entwined with an accentuated spatial heterogeneity to be accounted for.

2.1.2 Climate and rainfall

During most of the year arid regions are located beneath semi-permanent anti-cyclones into which moist air, rain-bearing frontal systems or tropical cyclones penetrate only rarely (GRAF 1988). Lacking precipitation is the main feature of drylands usually

associated with immense variations in space and time. Data from the southern Negev, Israel and the central Sahara provide an example of temporal variability: a 24-hour rainfall can be expected to exceed the mean annual value by a factor of three to four in a 20- to 30-year period (SCHICK 1988). SHARON (1972) detected a large spatial variability of short term rainfall in southern Israel. Analysing the daily rain amounts of three stations within 15 km of each other, only 20 % of the values showed the same order of magnitude. These characteristic features of arid zone rainfall are caused by localized high intensity showers. Analyzing data records from 1951 to 1992, maximum rain intensities in the Negev desert exceed 220 mm hr^{-1} measured in October 1979 by a rainfall recorder located in the town of Mitzpe Ramon. Inside the semiarid Walnut Gulch catchment, Arizona, USA even more than 330 mm hr^{-1} were recorded (GOODRICH et al. 1997). Convective raincells, responsible for high magnitude runoff events, form due to the destabilizing effect (of the atmosphere) of enhanced surface temperatures in arid regions (SHARON & KUTIEL 1986). Arid areas, where greatest runoff volumes result from synoptic scale depressions with low rain intensities, e.g. in the arid western New South Wales, Australia (CORDERY et al. 1983), are in minority in a global scale.

With the help of radar techniques the characteristics of convective raincells have been widely studied (e.g. BURGESS & LEMON 1990, DWD 1995). During the initial development stage of a storm life cycle updrafts push moist unstable air aloft. Rainfall commences only later during the mature and dissipating stages. In general three different types of storms exist:

(a) *Single cell* storms of limited extent (approx. 5 km) typically do not produce severe weather. Their whole life cycle usually does not exceed 20-30 minutes.

(b) *Multicell* storms consist of clusters or lines of single cells moving together with each cell in a different stage of the storm life cycle.

(c) *Supercell* storms develop stable and intense up- and downdrafts that may coexist for long periods of time. They are the largest storms (approx. 15 km) and responsible for the most extreme weather. A life time of up to twelve hours has been documented (PAUL 1973).

Often transitional stages between multi- and supercell storms exist. Studies in the southern Negev and in Sinai experienced both moving stormcells (SCHICK 1968, SHARON 1972) and quasi stationary ones (SCHICK & LEKACH 1987).

Different classification schemes for climatic regimes in drylands exist depending on temperature and precipitation. Most widely used is the UNESCO (1979) classification in which the degree of aridity is based on the ratio of mean annual precipitation to mean annual potential evaporation estimated by the Penman approach. If this ratio drops below 0.2 the regime is arid, up to 0.5 semiarid conditions prevail. For the Sinai and Negev deserts, Egypt and Israel, GERSON et al. (1985) proposed a local scheme based on the spatial distribution of vegetation and diagnostic soil associations, as well as on the relative significance of geomorphic processes (e.g. mechanical weathering). According to mean annual precipitation the climatic regimes of drylands were subdivided as follows:

(a) semiarid - 400-250 mm yr^{-1}

(b) moderately arid - 250-150 mm yr^{-1}

(c) arid - 150-80 mm yr^{-1}

(d) extremely arid - < 80 mm yr^{-1}.

SCHICK (1988) defined hyperarid areas as areas with less than 50 mm of mean annual rainfall.

2.1.3 Runoff generation and overland flow

In contrast to humid areas, overland flow following the ideas of HORTON (1933) is generally assumed to be the dominant mechanism of runoff generation throughout the arid zone. It may be defined as flow of water over the land surface towards a stream channel and is the initial phase of surface runoff. If rainfall intensity at any time during a storm exceeds the infiltration rate of a soil surface, water accumulates on top. After surface depressions have been filled, water spills over to run downslope. On plane surfaces (e.g. paved urban areas or a laboratory flume) a thin film or even sheet of flowing water may develop often termed as sheet flow. On natural slopes, however, topographic irregularities direct most runoff water into lateral concentrations. Following anastomosing paths these concentrations often give the appearance of flow in a wide braided channel. Hence no simple description or modelling of the hydraulics of overland flow is possible (EMMETT 1978). In arid regions plant cover and organic matter on the ground surface are sparse. The soil surface largely is the first point of contact by rainfall. Thus physical and chemical properties of surficial material play a primary role in runoff generation. Characterizing the surface properties two kinds of landscapes may be distinguished:

(a) terrain where rocky or debris mantled slopes dominate and

(b) terrain with thick unconsolidated sediments of fluvial or aeolian origin.

In rocky deserts underlying rocks are usually exposed or covered by either a thin veneer of debris or shallow lithosols. At the base of most slopes colluvium accumulates. Infiltration rates of bare rock surfaces are low (only a few mm hr^{-1}) and vary only little due to differences in rock type or jointing (GREENBAUM 1986, SALMON & SCHICK 1980). However, infiltration characteristics may significantly differ with slope position. On rocky upslope areas, on the one hand, huge amounts of runoff may be generated immediately after the onset of rain. Infiltration rates of the colluvial base, on the other hand, are one order of magnitude higher and allow losses of runoff originating from upslope areas. Different aspects of this flow discontinuity were studied on a limestone slope in the arid northern Negev desert (YAIR 1992).

Infiltration characteristics of unconsolidated sediments mainly depend on grain size distribution and the tendency to surface sealing. Only a minority of the global deserts is covered by aeolian sands, for example 15 % of the Sahara (MABBUTT 1977). In many of these sand fields final infiltration rates exceed 100 mm hr^{-1} (AGNEW & ANDERSON 1992). Nevertheless, even inside an arid sand dune area a biological topsoil crust may reduce infiltration significantly and lead to runoff (YAIR 1990). The formation of surface crusts is

even more accentuated in sediments with a high content of silt and clay. During high intensity storms raindrops disperse the soil matrix and form a stable surface layer of reduced permeability (RÖMKENS et al. 1990). Most runoff in silty loessial arid terrain is caused by these crusts. The effects of rock fragments on surficial properties is more complex. They have been reported to both increase and decrease infiltration (BRAKENSIEK & RAWLS 1994). This ambiguous impact is also evident inside the Zin catchment: while on loessial slopes a stone clearing significantly increases runoff (EVENARI et al. 1982), stable stony pavements on old alluvial terraces seal the surface (GERSON & AMIT 1986).

2.1.4 Wadi flow and transmission losses

Arid ephemeral streams remain dry for most of the year and flow only occasionally as a direct response to runoff generating rainstorms. SCHICK (1988) reviewed the characteristics of flashy high magnitude floods in rocky arid catchments located in the southern Negev and in Sinai. They were geomorphologically highly efficient modifying the landscape by erosion and deposition of huge amounts of debris. Flow rose from insignificant levels to high and short flood peaks within several minutes forming 'walls of water'. Direct observation of one of these floods indicated supercritical flow with surface velocities as determined by floats of about 5 m s^{-1}. In these environments much of the characteristics of small flashy floods were preserved even in large catchments reaching peak values of up to 1650 m^3 s^{-1}.

In arid and semiarid areas the time spans between single flood events are usually long. Hence ephemeral floods mostly travel on a dry channel bed allowing for significant infiltration losses into the channel alluvium on their way downstream. For a long time these transmission losses resulting in a downstream decrease of runoff have been observed (e.g. RENARD & KEPPEL 1966). During a flood event different processes (e.g. air entrapment, scour and fill) are active modifying the intensity and amount of transmission losses. Silt carried by flood waters can effectively seal the alluvial surface even during flood events at unexpectedly high flow velocities (CREAR et al. 1988). The interplay of scour and fill is complex and not fully understood. It prohibits accurate quantification of loss volumes making reach-scale studies essential for a further insight (WHEATER et al. 1997).

2.1.5 Data collection

Hydrological gauging stations are rare in arid environments, since most countries belong to the third world and financial means necessary for installation and maintenance are lacking. For instance, SEHMI & KUNDZEWICZ (1997) claim that African networks of hydrometric stations are in decline. Because of the accentuated spatial and temporal variability of arid zone rainfall, the calculation of spatial rainfall distribution by interpolation of coarse gauging networks may cause substantial errors. For runoff simulations in semiarid catchments a minimum density of one gauge per 4 km^2 has therefore been recommended (MICHAUD & SOROOSHIAN 1994b).

In large arid basins the only practical tool to derive an accurate picture of catchment wide rainfall is the use of rainfall radar. By this technique a large area can be covered in real time from a single point with a relatively high spatial and temporal resolution. Although additional information may be obtained by multi-parameter techniques (e.g. dual polarization radar), only single frequency measurements of the back scattered radiation have been used widely and implemented operationally (COLLIER 1996). They require a relationship between radar reflectivity and rainfall intensity (Z-R relationship) which is mostly obtained by raingauge adjustment. The WPMM-method (ROSENFELD et al. 1994) may significantly increase the accuracy of this procedure (MORIN et al. 1995). However, high quality data sets of different events being measured by several rain gauges and radar scans are required. Due to the curvature of the earth, the elevation of the deepest detectable sampling volume increases with the distance from the radar location. Therefore at long ranges errors originating from variations in the vertical profile of reflectivity are usually more dominant than those caused by changes in the Z-R-relationship due to a varying drop size distribution (JOSS & WALDVOGEL 1990). The effective range of a rainfall radar depends on the type of precipitation. While for convective rain (the most prominent rain type in arid areas) ranges of 150 km still enable meaningful measurements, snow or widespread rain may only be scanned in the immediate vicinity of the radar station (Fig. 2.1).

Standard runoff gauges measure the water stage by floats or pressure transducers. They require rating, i.e. direct discharge measurements, to relate stage to discharge. In the bed of arid ephemeral stream channels particles up to gravel sizes become unstable at flows with depths of only 0.5 m (GRAF 1988). Hence the direct measurement of velocity by current meters becomes difficult or even impossible during high flow. A common alternative is to compute discharge indirectly using the slope-area method. This method adapts a uniform-flow equation (the Manning equation) using channel characteristics, water-surface profiles and a roughness coefficient. Thereby it is neglected that cross-sectional geometry may permanently change during a flood event. As a result, hydrometric streamflow data in most arid and semiarid channels are inherent with unavoidable uncertainty. Moreover, gauging stations are frequently destroyed by the huge erosive power of high magnitude events and data records are incomplete (e.g. GREENBAUM et al. 1998).

Using morphological and sedimentary evidence peak stages of historic and recent floods may be reconstructed post-factum by paleoflood methodologies (BAKER 1987, KOCHEL & BAKER 1988). Where flow boundaries produce markedly reduced flow velocities during times of high flow, suspended sediments are deposited. These slackwater deposits are minimum paleostage indicators, since some flood water must have been above them at the time of emplacement. Absolute high water indicators, including scour marks, lines of silt, driftwood or organic debris, are more accurate. Owing to reduced biological activity in arid and semiarid settings, both slackwater deposits and high water marks may be preserved for long times. Bedrock-confined reaches are preferable for paleoflood analysis, since they accommodate high discharges by largely increasing flow depth and show a high cross-sectional stability. Historic peak stages are transformed to paleodischarge estimates by slope-area calculations (DALRYMPLE & BENSON 1967) or hydraulic modelling. As a hydraulic model the HEC-2 procedure (HYDRAULIC ENGINEERING CENTER 1982) is often used. It generates water surface profiles using step-back-water evaluations for various

discharges. Since ages of slackwater deposits may be assessed using radiocarbon dating, paleoflood hydrology may also augment existing flood records obtained by conventional gauging resulting in a more accurate flood frequency analysis (e.g. GREENBAUM et al. in press).

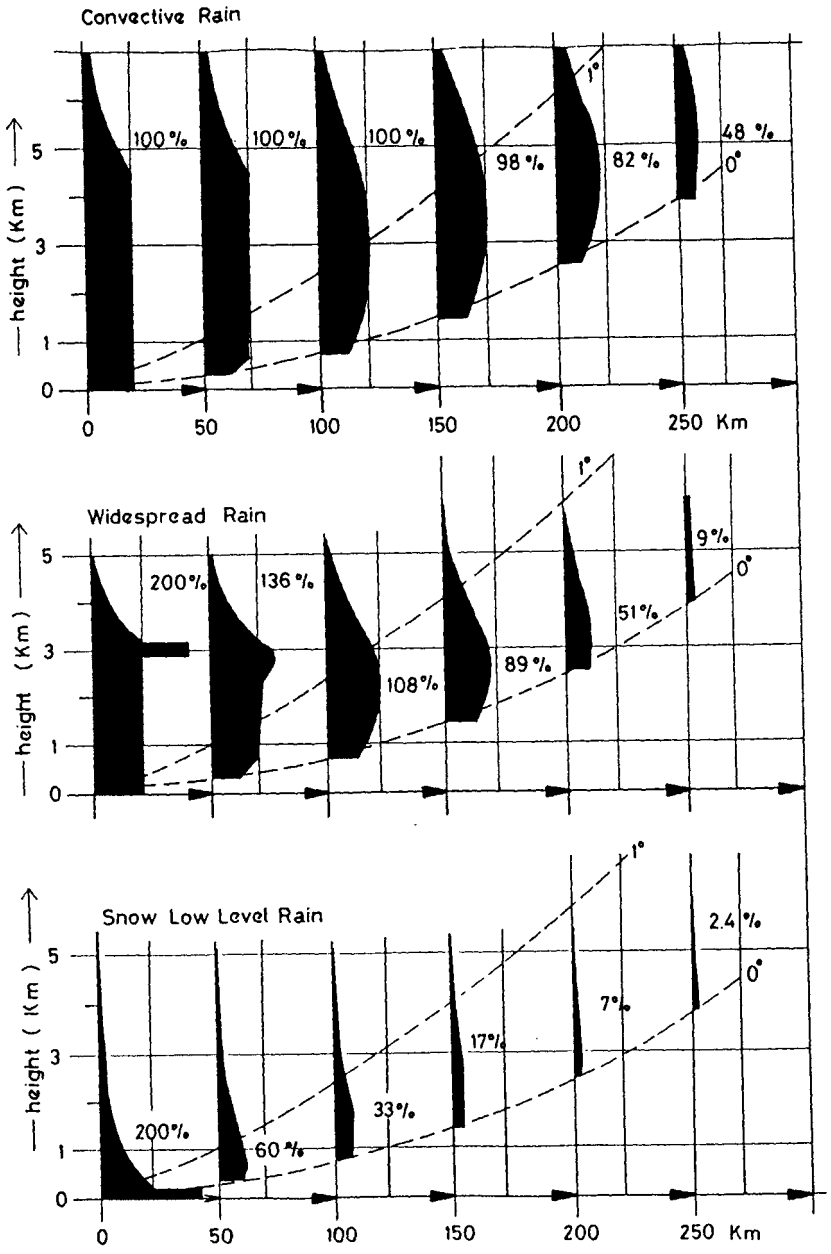

Fig. 2.1 **Vertical profiles seen by a 1-deg beam radar at various ranges. The number in each figure gives the percentage (referred to the true value measured at the ground) of the rain rate deduced from the maximum reflectivity of the profile** (JOSS & WALDVOGEL 1990)

2.2 Rainfall-runoff modelling

2.2.1 Classification and basic definitions

Since in the present discussion of hydrological modelling no unique and generally accepted terminology is used in the hydrological community (REFSGAARD 1996), some basic definitions are useful as a preamble to the present study. In its widest sense, a hydrological model is a mathematical tool to interpret hydrological processes and always is a simplified representation of the real world. According to DOOGE (1992) hydrological modelling is concerned with 'the accurate prediction of the partitioning of water among the various pathways of the hydrologic cycle'. As such, all hydrological models should solve the water balance equation, the basic equation in hydrological science. The following discussion concentrates on hydrological models investigating the rainfall-runoff process with precipitation as input and runoff as output. Due to the wide range of modelling purposes, data constraints and spatial and temporal scales a great variety of these models exist. Different classification schemes have been proposed (e.g. CHOW et al. 1988, TODINI 1988, LEAVESLEY 1994, SINGH 1995, REFSGAARD 1996). The following scheme (Fig. 2.2) provides a general overview using the classification criteria randomness, spatial discretization and model structure. To find the desired hydrological model one should ask the following questions:

(a) Is there a need to consider randomness?

(b) Is there a need to consider spatial variations of model input or parameters?

(c) To what extent the governing physical laws have to be considered?

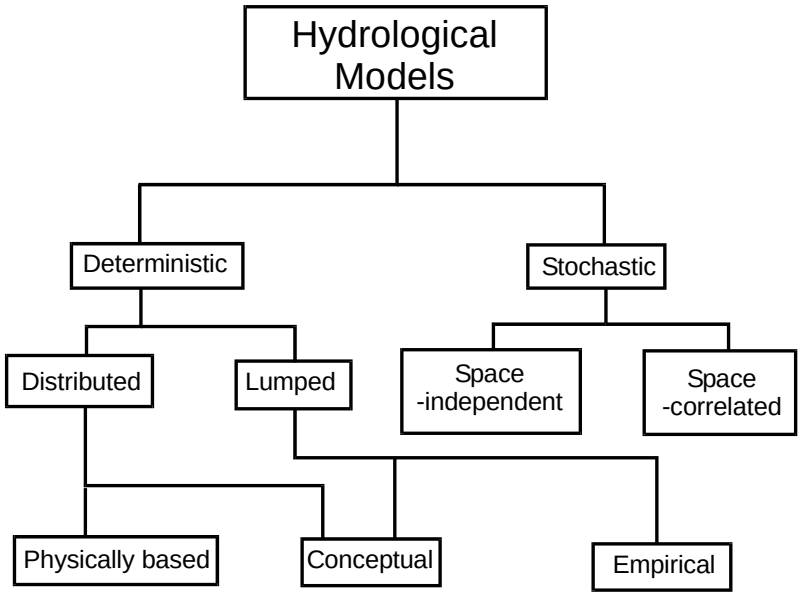

Fig. 2.2 Classification scheme of hydrological models (CHOW et al. 1988, modified)

Randomness is not considered in a *deterministic* model; a given input (rainfall) always produces the same output (runoff). The outputs of a *stochastic* model are at least partially random. A deterministic *distributed* model considers the hydrological processes taking place at various points in space. It may either be *physically based*, i.e. reproducing the rainfall-runoff process only by physical principals on the conservation of mass and momentum, or *conceptual* reflecting these principals in a simplified approximate manner. In deterministic *lumped* models hydrological systems are spatially averaged or regarded as a single point in scale without dimensions. Since hydrological processes generally are space-dependent, spatial lumping always includes crude conceptualization. *Empirical* models do not explicitly consider the governing physical laws of the processes involved only relating input to output through some (empirical) transform function. Stochastic models are termed *space-independent* or *space-correlated* according to whether or not random variables at different points in space influence each other. For each criterion in the classification scheme not only the extremes but also intermediate types exist.

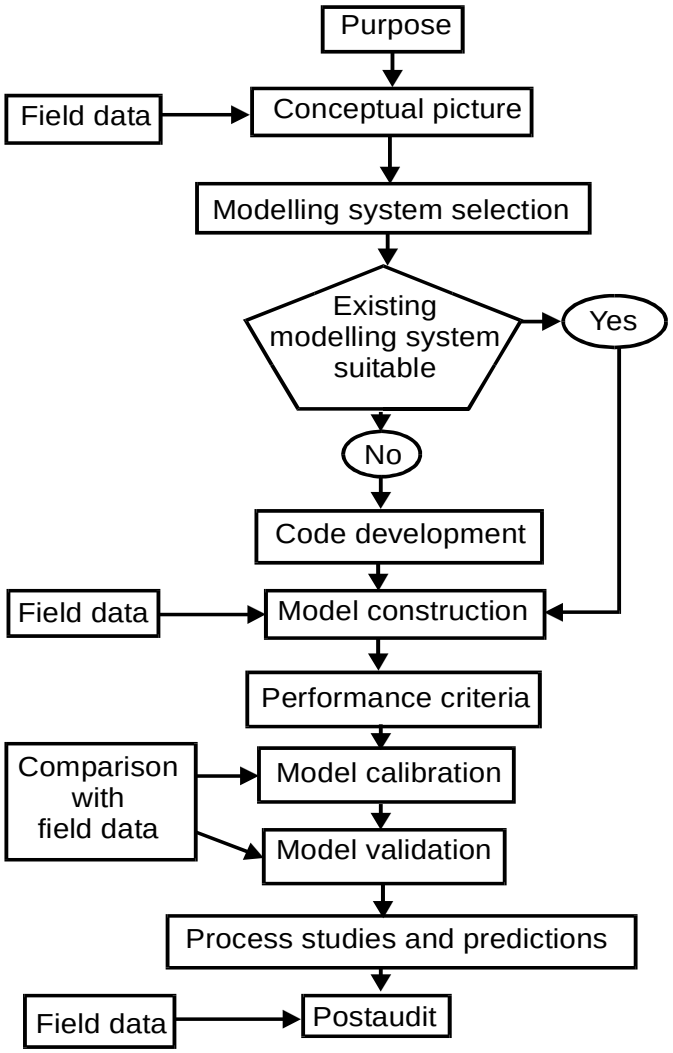

Fig. 2.3 Schematic modelling protocol (REFSGAARD 1996, modified)

REFSGAARD (1996) proposed a general procedure for applying models (Fig. 2.3). First the *purpose* of the model application should be defined containing type and accuracy of the desired model output. Based on this purpose the user should establish a *conceptual picture* comprising the key hydrological processes in the catchment and the corresponding limits of simplification and accuracy assumed to be acceptable a the hydrological model. This is followed by the selection of a *suitable modelling system* (existing computer codes, software packages for hydrological modelling). In case no suitable modelling system exists, a *code development* has to take place including a thorough check of the numerical solutions obtained. With this modelling code a *model construction* has to be made in a catchment with collected field data. This involves spatial discretisation and a selection of preliminar parameter values. The next step is to define *performance criteria* that should be achieved in subsequent calibration and validation steps. During *model calibration* preliminar parameter values are manipulated to reproduce catchment response within the range of accuracy specified in the performance criteria. In other words, a calibrated rainfall-runoff model **always** contains parameters determined comparing model simulations with gauged streamflow data. Only if a gauging station exists in a catchment, a model application is possible. *Model validation* implies that the model is applied to another period or site than used for calibration without changing the calibrated model parameters. Then the model may be used for *process studies and predictions*. Finally, several years after the modelling study, a *postaudit* is possible to evaluate the model's predictions in other catchments.

2.2.2 Historical overview

Several historical reviews of rainfall-runoff models are available (e.g. CHOW et al. 1988, TODINI 1988, LEAVESLEY 1994). A first attempt to predict runoff from rainfall, the 'rational method', may be traced back to the mid-19th century. Using a simple formula this approach calculates peak runoff rates from data on rainfall intensity and catchment characteristics. It is still widely used for the design of storm sewers in small urban catchments. To determine hydrograph shape the concept of 'isochrones' (lines of equal travel time) was developed during the 1920s followed by the 'Unit Hydrograph' (SHERMAN 1932). These two methods can be seen as the first basic rainfall-runoff models, as they introduced a rainfall-runoff transfer function. In the 1950s mathematical techniques (Laplace- and Fourier transformations) enabled to determine the Unit Hydrograph. Later on solutions of simplified differential equations yielded the shape of the rainfall-runoff transfer function describing the outflow of a single reservoir or a cascade of reservoirs (e.g. NASH 1958). In the following decade these single conceptualizations were subdivided into a number of interconnected elements each representing the response of a particular subsystem. Initiated by the Standford Watershed Model (CRAWFORD & LINSLEY 1966) a great variety of these conceptual hydrological models has appeared up to the present date.

In parallel it was tried to reproduce the rainfall-runoff process only by physical principles on the conservation of mass and momentum. Physically based, distributed models were developed (e.g. SHE, ABBOTT et al. 1986a,b) describing three-dimensional water fluxes only with the help of the basic differential equations (Richard's, Darcy and Saint-Venant).

In small-scale research studies this model type has been applied successfully, whereas in large catchments data requirements impose considerable lumping and conceptualization (STORM & REFSGAARD 1996).

2.2.3 Scale and modelling

Hydrological processes span about eight orders of magnitude in space and time (KLEMES, 1983). Therefore the question of scale is fundamental for all modelling efforts. For a given process large spatial scales tend to be associated with large temporal scales and vice versa. The time interval (temporal scale) used for internal computations depends on that of the available input and that desired for the model output. Models may be *event-based* using time steps of hours or minutes. For most applications longer time intervals (daily, monthly or yearly) are sufficient. The spatial scale reflects the size of a hydrological system to be modelled. *Microscale* systems are homogeneous enough to enable the application of fundamental laws describing internal hydrological processes (BECKER 1992). These systems include laboratory flumes, runoff plots (*local scale*) or even intensely observed hillslopes (*hillslope scale*). *Mesocale* systems are usually represented by catchments of different sizes (*catchment scale*). They play a central role in hydrological modelling, as issues in applied hydrology and water resources management are usually related to catchments. *Macroscale* systems include regions (*regional scale*) or the entire globe (*global scale*). According to BECKER (1992) microscale systems may have sizes up to 10^{-1} km^2, mesoscale systems range from 10^{-1} to 10^3 km^2 and macroscale systems exceed 10^3 km^2.

In general three different scales may be distinguished (BLÖSCHL & SIVAPALAN 1995): the *process scale* where hydrological processes occur, the *observation scale* where hydrological data are collected and the *modelling scale* used in models. Ideally all of them should be the same which is rarely feasible in reality. For instance, problems occur when large scale processes are observed by point scale measurements or long term trends must be estimated from short data records. Scaling techniques have been developed to bridge these gaps in both directions. *Upscaling* refers to transferring information from a small scale to a larger scale, while *downscaling* means the opposite (GUPTA et al. 1986). In lumped models the spatial modelling scale is represented by the entire catchment, while in distributed approaches this scale is defined by the size of the single model elements, the smallest spatial units (grid size or sub-catchments) accounted for (*element scale*). Model parameters need to be spatially uniform within a single model element. As *effective parameters* they represent the internal variability of the sub-element scale.

In several runs of TOPMODEL (BEVEN & KIRKBY 1979), a gridbased rainfall-runoff model, WOOD et al. (1988) increased the size of the element scale and compared the variability of hydrological response (quantity of generated runoff) between the single model elements. Fluctuations broke down at an element scale of 1 km^2, which they called ‘Representative Elementary Area’ (REA) in catchment runoff. It was postulated that beyond the REA scale a transition was possible from a distributed description to a statistical treatment of spatial variability in runoff generation. Hence an absolute spatial scale for sound effective parameters was obtained, representing the ideal element scale for

a distributed rainfall-runoff model. BEVEN (1995) interpreted the REA as a point at which the local patterns of runoff generation are sufficiently well integrated, before non-stationarity in catchment characteristics (e.g. geology, physiography, land use etc.) or hydrological processes starts to increase the variances at larger scales. He concluded that, if a REA scale exists, it might vary between environments and processes. Indeed, in other catchments gauged runoff data did not support a 1 km^2 REA (WOODS et al. 1995) and it depended on catchment properties and climatic conditions (BLÖSCHL et al. 1995). Moreover, the REA was relative to the resolution of hydrological modelling indicating that the number of single model elements was more important for a minimum in spatial variability than their size (FAN & BRAS 1995). Hence a REA of 1 km^2 should only be regarded as a rough guideline in the search for an appropriate spatial disaggregation in a distributed model.

2.3 Developments in research

2.3.1 Field studies

SCHICK (1968) analysed a large rainstorm flood occurring on March 1966 in the southern Negev and adjoining parts of Jordan. Total rainfall was enclosed in a long strip not more than 80 km wide, while the area of violent rainfall - certain areas underwent a rainfall representing over 200 % of the mean annual amount - covered an inner strip of only a few kilometres width. Runoff coefficients varied between 20 and 50 %. Walls of water rushed down the dry channels with estimated flow velocities of more than 5 $m^3 s^{-1}$.

COSTA (1987) reviewed the largest historic rainfall-runoff floods from small catchments (0.39 - 370 km^2) in the entire conterminous United States. Twelve floods were identified to be the largest ever measured. For all of them post-flood surveys and subsequent calculations by the slope-area method provided indirect measurements of peak discharges. All events occurred in the semiarid and arid parts of the western and south-western United States where mean annual precipitation ranges from 114 to 676 mm yr^{-1}. Estimated peak flow velocities ranged between 3.47 and 9.97 m s^{-1} with high Froude numbers (between 0.81 and 2.49). This indicated critical or even supercritical conditions during peak flow. Shear stresses and unit stream powers were several hundred times greater than in floods of large rivers (e.g. Mississippi, Amazon).

SCHICK & LEKACH (1987) studied a high magnitude flood in a small catchment in the Sinai desert, Egypt where annual rainfall can be estimated at 30 - 40 mm. Wadi Mikeimin drains 12.9 km^2 of steep basement rocks flowing into Wadi Watir, a 3860 km^2 catchment entering the Red Sea at Noueiba. Floodmarks, geomorphic effects and other indirect evidence were used to study post-factum storm rainfall, runoff and erosion-deposition characteristics. In the uppermost catchment peak discharges up to 100 $m^3 s^{-1}$ were reconstructed, while the complete Mikeimin catchment only yielded 68.5 $m^3 s^{-1}$. The high values of generated runoff in the headwaters were explained by a highly localized, quasi-stationary and very intense cloudburst. In total 6200 m^3 of sediment were deposited in an alluvial fan at the mouth of Wadi Mikeinim. The main channel of Wadi Watir was not

active during the flood of January 1971 and was blocked at the junction. In November 1972 a medium flood in Wadi Watir breached the Mikeimin fan. Its hydrograph was characterized by distinct and sharp peaks (Fig. 2.4). The large catchment size of Wadi Watir and the characteristics of the 1972 rainstorm (50 - 70 mm of total rainfall distributed fairly unevenly over 48 hours) lead to the conclusion that intra-event damming and breaching of tributary fans (comparable to the Mikeinim fan) might have been the cause for the extreme flood bores.

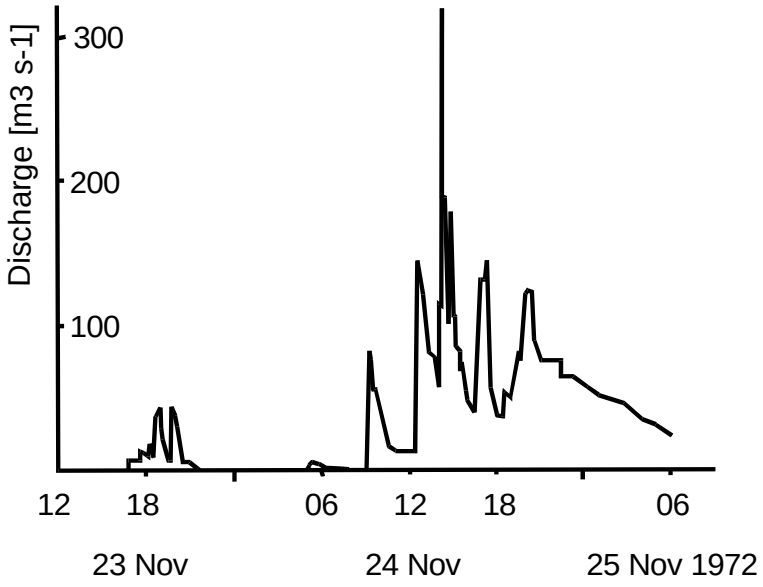

Fig. 2.4 The November 1972 Wadi Watir flood (SCHICK & LEKACH 1987)

The 597 km^2 Wadi Ghat catchment drains the Asir Mountain range, south-west Saudi Arabia, towards the Red Sea. Annual precipitation is 322 mm and approximately 90 % of the catchment consists of rocky outcrops and shallow soils. WALTERS (1989) reported about a unique flood event which occurred in April 1985. Three raingauges located inside the catchment and seven in its surrounding facilitated the reconstruction of the spatial rainfall distribution in a hourly time step. During four hours a rain cell crossed the catchment from west to east. Maximum recorded rainfall (177.4 mm) fell within 3 hours reaching a maximum intensity of 115.4 mm hr^{-1} in the south-eastern part of the catchment. This intense rainfall caused a large flash flood at the Wadi Ghat gauging station peaking at 3200 m^3 s^{-1}. Comparing flood volume with spatial weighted rainfall, determined by the Thiessen polygon method, a runoff coefficient of 27.2 % resulted. Frequency analysis indicated that hourly rainfall had a return period exceeding 200 years, while recorded peak discharge could be expected on an average of once every 143 years.

GREENBAUM et al. (1998) analysed one high magnitude rainstorm flood occurring in Nahal Zin, the present study area, in October 1991. Since findings of this study serve as important input for the present study, this event is further described later on (Chapter 7).

The rainfall pattern was determined using temporal intensity patterns at a point ('fingerprints'), intensity factor maps (KELWAY & HERBERT 1969) and a spatial evaluation of the time at which maximum rainfall intensity occurred at a given point. Then the results were validated by rainfall radar data. This thorough analysis yielded a complete different picture of rainfall intensities than might have been portrayed if based on available raingauge data only. The flood hydrograph was reconstructed using techniques of paleoflood hydrology. A three-peak, 7×10^6 m^3 flood was reconstructed reaching a main peak of 550 m^3 s^{-1} with an estimated recurrence interval of 40-50 years.

2.3.2 Rainfall-runoff models for drylands

SHANAN & SCHICK (1980) developed a lumped model for runoff plots and a 3.45 km^2 catchment in the arid northern Negev, Israel. More than 60 events used for calibration enabled a successful simulation of daily runoff values at the plot scale, whereas at the catchment scale the differential effects of various factors could not be separated. LAVEE (1986) simulated the runoff response of arid runoff plots by a complex distributed model without calibration. Since no channel processes were taken into account, model applications were restricted to small intensely measured arid hillslopes. KOTWICKI (1987) applied the conceptual lumped rainfall-runoff model RORB3 (LAURENSON & MEIN 1983) to the 450,000 km^2 arid Lake Eyre catchment in Australia. Because of short streamflow records available for calibration only rough estimates about past inflows into the lake were possible.

HUGHES AND SAMI (1994) introduced a compromise between a complex, physically based, distributed model and a simple empirical approach. Most of the input parameters could be derived from maps or by field work but for some of them calibration was still necessary. ALLAM (1990), NOUH (1990) and AL-TURBAK (1996) used modelling approaches based on the Geomorphologic Instantaneous Unit Hydrograph (GIUH) (RODRIGUEZ-ITURBE & VALDES 1979) in several semiarid and arid catchments of Saudi-Arabia. Although the size of the largest catchment was 600 km^2, the maximum number of rainfall gauges used for calibration with measured hydrographs was four. SHARMA et al. (1996) incorporated remotely sensed data into a GIS-based rainfall-runoff model for a small 5.47 km^2 arid catchment. Still calibration was necessary for two model parameters. HUGHES (1997) reviewed the application of different hydrological models within the southern African region. Generally both monthly and daily time step models could be applied where good quality data sets for calibration were available. Within the more arid parts of the region problems arose because of inadequate rainfall data and the poor empirical simulation of channel transmission losses. SHARMA & MURTHY (1998) developed a package of simulation models to predict flow hydrographs in the Indian arid zone. Regression relations and simple conceptualizations (leaky reservoirs or triangular approximations) were used to minimize the amount of observed data required for calibration. 79 gauged hydrographs enabled model applications to nine different study catchments.

The data base of the semiarid experimental catchment Walnut Gulch, Arizona, USA, facilitated the successful application of different rainfall-runoff models. In this 150 km^2 catchment the dense network of rain gauges and the long data record of streamflow are

unique for the semiarid zone (RENARD et al. 1993, GOODRICH et al. 1997). With the help of this background LANE (1982) developed a simplified conceptual rainfall-runoff model approximating the runoff response by runoff volume, peak rate and duration of flow. Runoff volume was estimated by the Curve Number Method (SOIL CONSERVATION SERVICE 1985). Peak discharge, flow duration and transmission losses were determined applying several regression relations resulting from the analysis of gauged events. This approach required only a minimum of observed data for calibration. Moreover it could be used to estimate runoff rates and amounts from ungauged semiarid catchments transferring the used regression relations. GRAYSON et al. (1992) applied a relatively simple distributed model to a 4.4 ha tributary of Walnut Gulch. Without calibration simulations were disappointing. A model fit improved the results, but then the simulations at the catchment outlet did not differ markedly even when two completely different processes of runoff generation (Hortonian overland flow and partial area runoff) were assumed; only the spatial pattern of flow characteristics was different. KARNIELI et al. (1994) presented a semi-distributed model for two 6.28 and 14.7 km^2 tributaries of Walnut Gulch. Only after the input parameters were calibrated and optimized a good model fit was reached. MICHAUD & SOROOSHIAN (1994a) compared different model types in the complete catchment. Even after calibration a lumped model applying Curve Numbers and a Unit Hydrograph performed very poorly. KINEROS (SMITH et al. 1995), a complex distributed model specially developed for semiarid catchments, could be reasonably applied without calibration. After calibration model accuracy improved only little, but then the simulations of KINEROS were similar to those of a distributed Curve Number model. WHEATER et al. (1997) calibrated a distributed two parameter rainfall-runoff model inside Walnut Gulch using a daily timestep. Even peak discharges could be simulated by this simple approach, since a well defined relationship between flow volumes and flood peaks was determined in the runoff records.

3 Research need and objective

Following dictionaries, (e.g. BLACK DOG & LEVENTHAL PUBLISHERS INC. 1995), *science* may be defined as a 'department of systematized knowledge that is an object of study'. *Technology* may be defined as 'applied science, a method of achieving a practical purpose for the sake of society'. KLEMES (1988) transferred this controversial distinction to hydrology and complained that most hydrological scientists are busy solving technological problems. These actions include the development of different kinds of hydrological models. The rapid development of computer technology, has promoted the creation of mathematical models based neither on adequate theory nor on adequate data. According to KLEMES (1988) bad examples for these models are:

(a) many probabilistic hydrological models and

(b) complex conceptual (deterministic) models with calibrated parameters.

Hence a hydrological model should be regarded as a mathematical (technological) tool for hydrological science. This tool should be based on sound data and should include the dominant hydrological processes of the catchment it is applied to.

The present study wants to incorporate knowledge from existing small scale field experiments into a rigorous, spatially distributed analysis of single high magnitude events in a large arid catchment. The input (the spatial rainfall distribution) is to be followed through the system (the catchment with its direct and indirect water losses) down to the output (the flood hydrograph). Such a deterministic input-output analysis requires a suitable rainfall-runoff model and is still missing. Existing field based studies describe high magnitude floods by summarizing available data (e.g. SCHICK 1968, WALTERS 1989) or by post-factum analysis (e.g. SCHICK & LEKACH 1987, COSTA 1987, GREENBAUM et al. 1998).

As summarised in Chapter 2, much field based hydrological research has been conducted in arid environments mainly in microscale studies. Two main processes dominate arid zone flood generation:

(a) generation and spatial concentration of surface runoff as a direct response to localized high intensity rainfall and

(b) transmission losses into the dry channel alluvium.

These processes are inherently tied to an accentuated variability in space and time. Still arid zone catchment response is comparatively simple, since indirect subsurface runoff components, decisive in wetter climates, are negligible. However, data records of the episodic arid flow events are poor and rarely provide enough information for model calibration. This is especially true for high magnitude events, where during peak discharge stage-discharge transformations are inaccurate because no rating curves exist and supercritical flow may occur. Also the erosive power of these floods causes cross-section instability and often destroys existing gauging stations.

Hence an appropriate rainfall-runoff model for high magnitude events in a large arid catchment should be a deterministic non-calibrated approach. As such it should be spatially distributed, should incorporate existing field knowledge and only field derived parameters. Following the relevant literature, these findings, although available, have not adequately been incorporated into arid catchment modelling. Existing arid catchment modelling studies entirely depend on calibration with gauged streamflow data, a technique originally developed for humid catchments with indirect runoff components but often long data records. This seems to be a common dilemma in arid areas, since also techniques used in hydrological design and water resources management are frequently borrowed from the humid zone (WHEATER 1994).

Inside the semiarid Walnut Gulch experimental catchment the unique runoff records facilitated the successful use of calibrated models. Calibrated rainfall-runoff models may also perform well in humid areas with perennial rivers, or in low yielding catchments where channels are characterized by periodic flows during wet seasons (YE et al. 1997). Under these circumstances the information content of the runoff data may be enough to calibrate several model parameters. However, a good runoff prediction by a calibrated model does not necessarily mean that the parameters have been determined precisely and that they may be related to physically measurable catchment characteristics being the prerequisite to model ungauged catchments (MEIN & BROWN 1978). Moreover, satisfactory model calibration may also be performed accounting for the wrong hydrological processes, e.g. partial area runoff instead of Hortonian overland flow (GRAYSON et al. 1992). In reversal, this means that statements on internal catchment processes based on calibrated models may be misleading. Even totally incorrect modelling concepts can yield reasonable results, as long as only the simulated runoff is used to evaluate the modelling (UHLENBROOK et al in press). In a recent general discussion on distributed modelling, REFSGAARD et al. (1996) recommended that in distributed models almost all parameters should not be subject to calibration. BEVEN (1996) advocated simpler distributed models, based on data collected at appropriate scales.

In a semiarid setting the long history of research inside Walnut Gulch fulfilled the extensive data requirements needed for a non-calibrated run of KINEROS. The limited data available in large arid catchments make a non-calibrated application of this complex distributed model difficult and the existing ‘semiarid’ parameterization can hardly be transferred as differences in vegetation density and soil depth are too pronounced. For the same reasons existing semiarid regression relations are not transferable.

The objective of the present study is three-fold:

(a) First, a distributed, non-calibrated and field based rainfall-runoff model will be *developed* for high magnitude events in large arid catchments. Model parameters will be determined by techniques suitable for the large modelling scale. These techniques will use field measurements and results of existing experiments carried out in the study catchment itself or nearby. Hence parameterization will not depend on an existing local runoff gauging station and the model may be applied to ungauged catchments. Model uncertainty will be analysed and model results will be tested with measured runoff data.

(b) Second, this model will be used as a tool to *analyse* internal hydrological processes active during two high magnitude events. Main emphasis will be put on the spatial pattern of runoff generation, the temporal sequence of tributary responses and the downstream development of flow characteristics.

(c) Third, the model will be used to *predict* catchment responses under conditions with no field evidence. Extreme discharges will be estimated for an ungauged tributary and possible hydrological effects of climatic change induced catchment changes will be simulated.

4 Study area

4.1 Location and climate

From geographical as well as climatological points of view the Negev Desert, Israel belongs to the Saharo-Arabian deserts which are part of the global northern desert belt (Fig. 4.1). For a long period of time it has been under the influence of subtropical anticyclones producing slowly subsiding air masses which absorb moisture from the atmosphere and the ground surface.

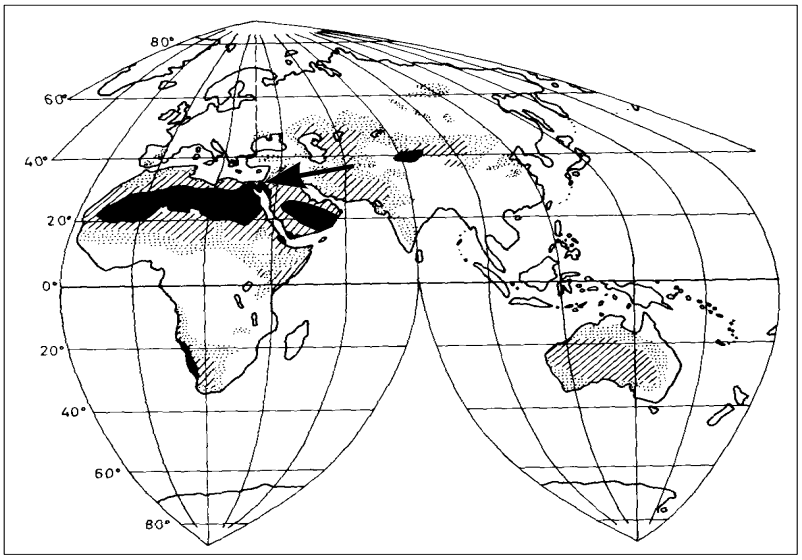

Fig. 4.1 The deserts of the world
black: extremely arid, hatching: arid, strippled: semiarid,
arrow: the Negev (EVENARI et al. 1982, modified)

Nahal (Wadi) Zin is one of the major arteries draining the rocky northern part of this desert into the Dead Sea. Elevations inside the 1400 km^2 catchment range from less than 300 m below to more than 800 m above sea level (Fig 4.2).

The Nahal Zin catchment experiences hot and dry summers with occasional winter rains whose annual average ranges between 50 and 100 mm increasing gradually to the north-west (Fig. 4.3). In general, the rainfall is produced by two types of storms. On the one hand, widespread storms are of the frontal type extending from large cold lows passing north of the country. These storms produce only moderate intensities (peak values seldom exceeding 40 mm hr^{-1}) but may last for many hours. On the other hand, localized storms occur as convective cells in conjunction with the *Red Sea Trough* extending into Israel from the Sudanese low pressure centre (BAR-LAVY et al. 1977). Due to surface heating the time of enhanced raincell activity is late afternoon and early evening (KUTIEL & SHARON 1980). These storms have short duration with maximum intensities of more than

120 mm hr^{-1} (SHARON & KUTIEL 1986) and are responsible for the largest floods in the Negev Desert (SCHICK 1988).

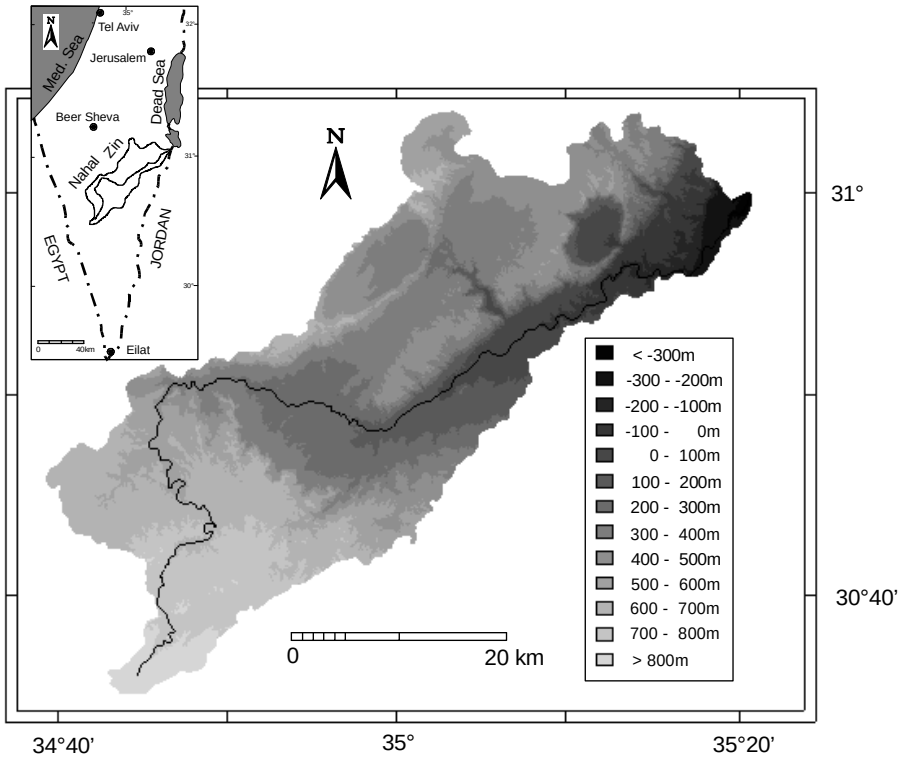

Fig. 4.2 Location map and elevations

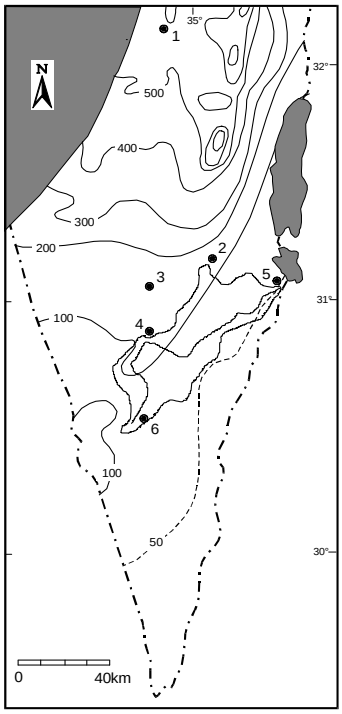

Five meteorological stations are situated in the surrounding of Nahal Zin (Fig. 4.3). From the time when the first station was installed (Mashabe Sade in 1951) until now there has been no period with all the stations operating simultaneously. Studying all high intensity events (maximum rain intensity exceeding 15 mm hr^{-1}), very rarely the same event is recorded by more than one station (Fig. 4.4) This points to the high spatial variability of arid zone rainfall. The maximum intensity recorded on 22/10/1979 at Mitzpe Ramon (224 mm hr^{-1} over a period of 5 min) represents a true high magnitude event which will be analysed in detail in Chapter 9.

Fig. 4.3 Mean annual rainfall and meteorological stations in the vicinity of Nahal Zin
(1) Rainfall Radar, (2) Dimona,
(3) Mashabe Sade, (4) Sde Boker,
(5) Sdom, (6) Mitzpe Ramon
(SHARON & KUTIEL 1986, modified)

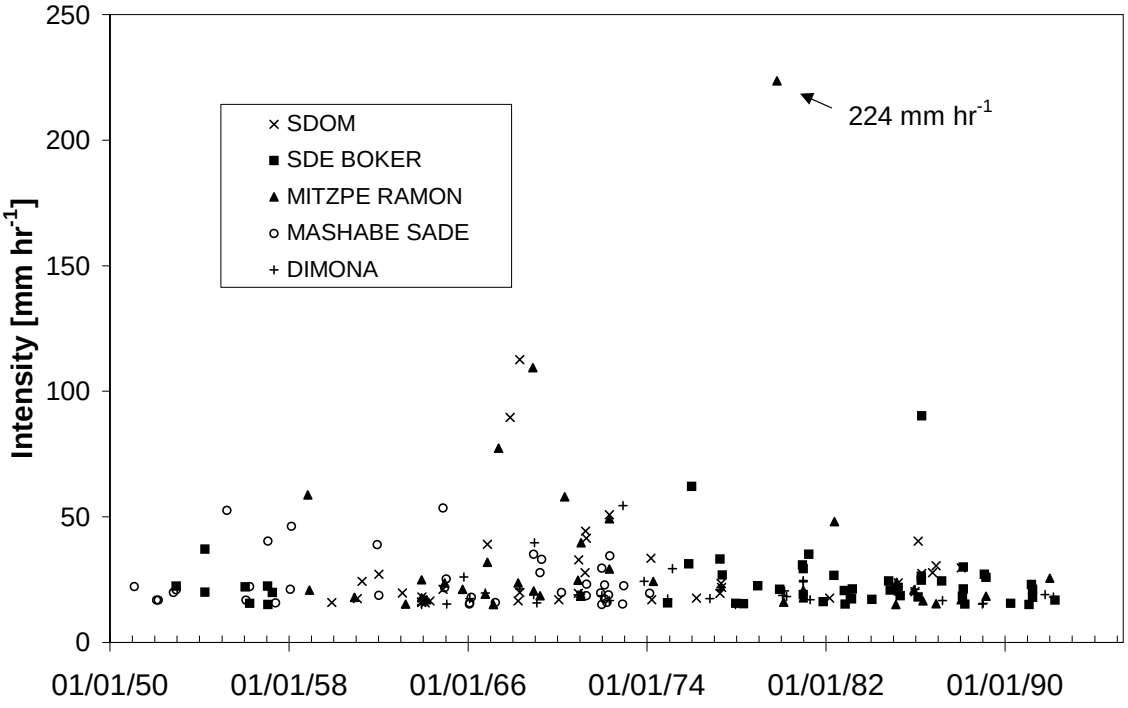

Fig. 4.4 High intensity rain events recorded by the five meteorological stations in the vicinity of Nahal Zin

4.2 Morphological units

The morphology of the Nahal Zin catchment is dominated by distinct units (Fig. 4.5). The upper south-western part of the Nahal Zin catchment drains the Avdat Plateau. Together with other high plateaus it represents the highest erosion surface preserved in the Negev (ZILBERMAN, 1989). Hammada soils on hard carbonatic rocks dominate the terrain and the valleys are filled with loessial silty sediments. The Zin Valley, a deeply entrenched wide erosional canyon on friable soft sediments, separates the Avdat Plateau from the remaining north-eastern catchment which is dominated by the Northern Negev Fold Belt. Here the anticlines form hilly ridges attaining up to 700 m in elevation and are mainly composed of bare limestone. Three of these northeast-southwest trending anticlines are partially included into the Nahal Zin catchment: The Hatira, Hazera and Ramon Anticlines. They are asymmetric with gentle north-western (5° - 7°) and steep south-eastern (35° - 90°) flanks (RODED 1983). The synclines of the Northern Negev Fold Belt are filled with soft sediments forming elongated, flat bottomed valleys. The Oron Syncline widens in its northern part where it is covered by aeolian sands of the Rotem Plain. Generally the morphological units of the Fold Belt follow the geological structures. Clear exceptions are deep erosion cirques (‘Makhteshim’) in the crests of the anticlines

representing relief inversion as low topographical features on high geological structures. The drainage of Makhtesh Gadol and Makhtesh Katan contributes to Nahal Zin, while the largest Makhtesh, Makhtesh Ramon, only forms the southern catchment boundary. In its last kilometres before it reaches its alluvial fan at the southern end of the Dead Sea, Nahal Zin is entrenched into soft marls of the Arava Rift Valley.

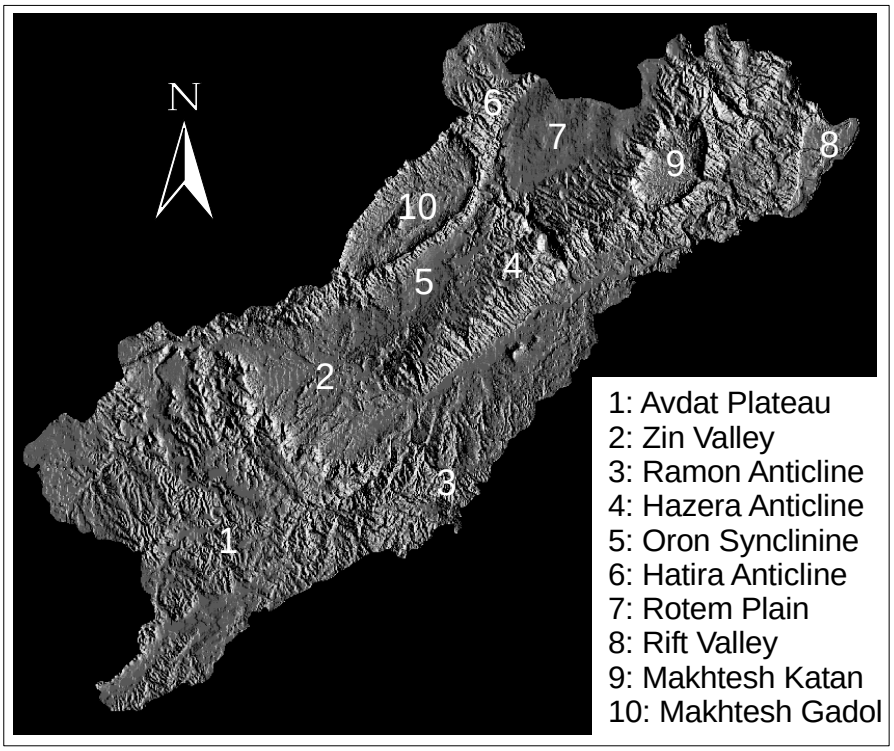

Fig. 4.5 Morphological units of the Nahal Zin catchment

4.3 Geology and landscape development

The first rigorous description of the geological history of Israel was given by PICARD (1951). BENTOR & VROMAN (1949-1960) mapped the geology of southern Israel including the northern Negev (scale 1:100,000). Their results were included into the first country-wide geological map published by the Geological Survey of Israel in 1965 (scale 1:250,000). Later on more detailed geological mapping was undertaken, because mineral resources were discovered in the Zin catchment (mainly phosphorite and quartz sand that are still exploited today). These mapping campaigns yielded two high quality 1:50,000 geological maps (RODED 1983, YECHIELY et al. 1994). ZILBERMAN (1989) studied the landscape development of the central and north-western Negev in detail.

In general the catchment geology is dominated by two carbonatic sequences (Fig. 4.6):

(a) Resistant marine limestone (Jurassic in the core of the Makteshim, Upper Cretaceous along the anticlinal ridges, Eocene of the Avdat Plateau);

(b) Chalky-marly sediments, partly with flint cover (Upper Cretaceous in the Zin Valley and along the synclines, Pleistocene in the Arava Rift Valley).

(c) Only in the Makhteshim the friable Lower Cretaceous Sandstone is exposed, while the Rotem Plain is covered with Pleistocene aeolian sand.

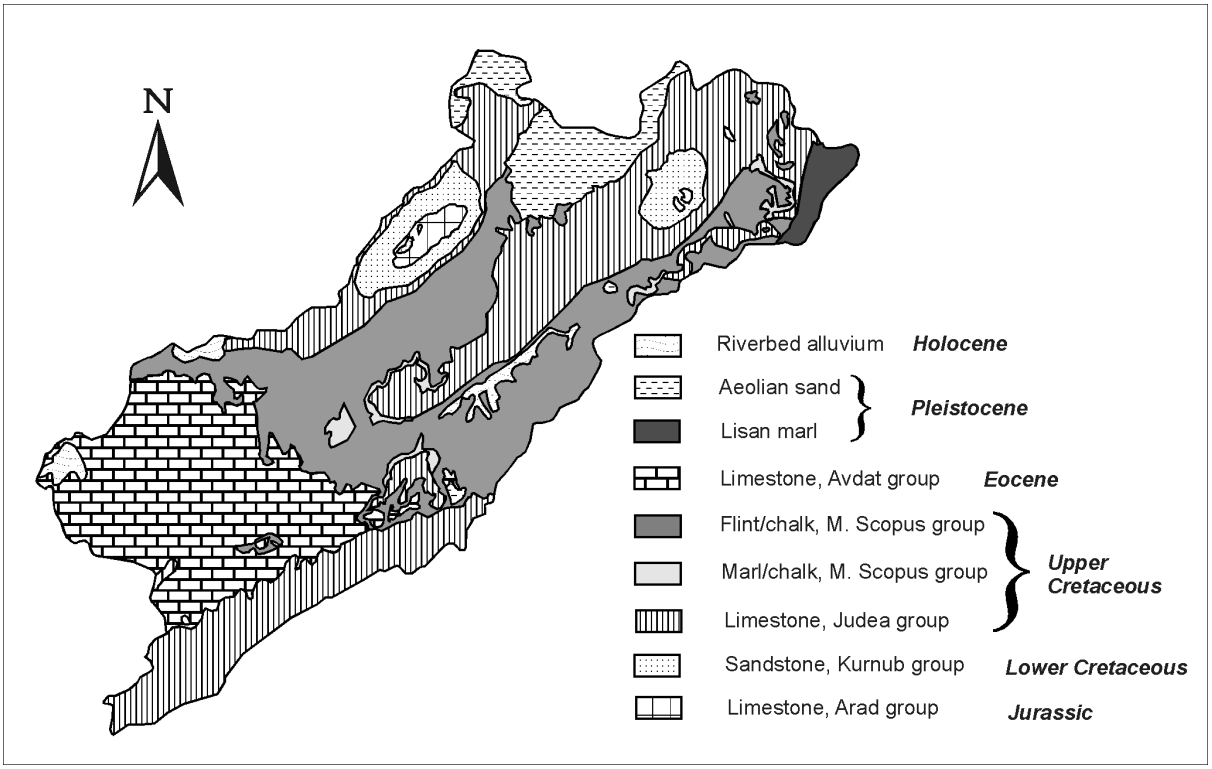

Fig. 4.6 Geological overview of Nahal Zin

The oldest rocks exposed in the area are of Middle Jurassic age. In this time a shallow sea with high biogenic activity deposited a series of marls and limestones. During the early Cretaceous „Nubian“ conditions prevailed and continental sandstones were accumulated in considerable thickness. Inside Nahal Zin Cretaceous sandstones and Jurassic marine rocks can be found inside the two Makhteshim where erosion is most advanced. A marine transgression during lower Cretaceous put an end to continental conditions for a considerable period of time. A mighty series of carbonates (limestones, dolomites and marls) were deposited in a warm epicontinental sea. Today these resistant Cenomanian and Turonian carbonates make up the anticlinal ridges of the Northern Negev Fold Belt. During the Senonian high structural areas partly rose above sea level and were subjected to erosion, while in synclinal basins chalky-marly sediments accumulated. Today large outcroppings of these soft sediments can be found in the Zin Valley. Only at Campanian times a marine transgression covered the folded structures. From this time the main chert

member originates covering large areas of today's synclines as it is very resistant to erosion. The relations between land and sea remained more or less the same until the end of the Eocene.

During the Oligocene most of the area was uplifted above sea level and the present morphological structure began to be formed. The drainage system flowed towards the west on an extensive low-relief landscape (peneplain). The amount of denudation was rather limited, evident from relics of the Oligocene peneplain (Avdat Plateau) with middle to upper Eocene sediments. Tectonic activity during the early Miocene was associated with folding activity along the existing anticlines. Forming transversal valleys the new relief was incised by the westward flowing streams whose catchment area extended far to the east to the margins of the Arabo-Nubian Massif. The Arava Valley was not yet established as an inland basin. In the late Miocene or early Pliocene a major tectonic event, probably the most significant in the history of the region, established the morphological valley along the Arava and uplifted the Northern Negev Fold Belt. A rejuvenated high energy fluvial system established a new water divide along the fold belt and deposited coarse clastic sediments. Still most of the present Nahal Zin catchment was drained towards the north-west by the ancient Nahal Besor.

A westward retreat of the broad young Zin Valley at the end of middle Pleistocene captured the entire eastern and southern catchment area of Nahal Besor. This explains the distinct turn of the drainage direction from north to south-east at the entrance of the Zin Valley. At present the transition from ancient drainage to the Mediterranean Sea to young high energy drainage to the Dead Sea is marked by steep waterfalls both in the tributaries and in the main channel (e.g. the Avdat Waterfall; Fig. 4.7). All over the Pleistocene, different climatic cycles can be distinguished, each reflecting three climatic regimes which prevailed in the following order (ZILBERMAN 1989):

(a) a moist climate associated with considerable loess accumulation, stream channel infilling and floodplain development (these floodplains represent the abandoned high terraces of today),

(b) a semiarid climate characterized by stable conditions along the stream valleys and by extensive human settlement,

(c) an arid climate with erosion along the stream valleys and sand penetration.

Thick mantles of loess and loessial soils have developed in the northern and north-western Negev during the middle and late Quarternary. Changes in the clay content and several calcic horizons point to the climatic cycling. Average rates of loess deposition of 0.1 mm yr^{-1} were estimated (GERSON et al. 1985). The Arava Rift Valley was covered by Lake Lisan - the precursor of the Dead Sea (BENTOR & VROMAN 1960). This lake existed from 70,000 - 60,000 to 15,000 -12,000 years BP. When the lake reached its highest level (-180 m) its size was about 220 km long and 7 - 15 km wide (GOODFRIEND et al. 1986). Marly lake sediments were deposited all over this area. During the Holocene, a period dominated by arid climate, high energy floods formed the present narrow stream channels.

Fig. 4.7 The Avdat Waterfall during a flood (Photo by Hydrological Service)

The formation of the most distinct morphological features, the Makhteshim, is discussed controversially. Three of them are known from the Negev around Nahal Zin (Makhtesh Katan, Gadol and Ramon) and one from the eastern Sinai desert, Egypt (Makhtesh Hallal). AMIRAN (1950) and PICARD (1951) proposed the following model: Stream channels incised into the steep south-eastern limestone flanks of the anticline and finally exposed the friable sandstone. The rapid erosion of the sandstone followed by the collapse of the limestone-roof formed a deep valley along the fold axis. Issar (1983) thought that a higher piezometric head of Tertiary groundwater may have karstified the Cretaceous limestones and accelerated erosional processes. Following the principles of PICARD, ZILBERMAN & EIDELMAN (1994) discovered a unique combination of lithological sequence, structural framework and paleomorphology that lead to the development of a Makhtesh. Transversal valleys, incised into the anticlines by north-west flowing streams during the early Miocene, were filled by fluvial sediments later on. East-flowing high energy streams, draining to the subsiding Arava, re-opened these valleys and eroded the friable sandstone. They captured other east-flowing streams and drained the complete Makhteshim through one opening predefined by a Miocene valley.

4.4 Vegetation and soils

Phytogeographically the Nahal Zin catchment belongs to Saharo-Arabian region with its typical low shrub species and very sparse vegetation cover (YAALON 1981). On rocky slopes of the Avdat Plateau or on the northern anticlinal ridges, where pockets of soil receive an accumulation of rainwater from the surrounding rocks, the vegetation is diffuse just as on the loessial plains and stabilized dunes. With increasing aridity and less rocky outcrops (e.g. in the lower Zin Valley and Arava Rift Valley) vegetation gradually becomes restricted to depressions and runnels where moisture conditions are more favourable. Trees generally are very scarce, a few Acacia and Tamarix are found in wadis and stream channels.

DAN et al. (1981) and GERSON et al. (1985) described the soils types in the dry regions of Israel This served as a basis for the field campaigns inside the Zin catchment. On the gently sloping Avdat Plateau bare limestone outcrops alternate with small pockets of gypsic or calcic Hammada soils. These 'rocky' soils contain gravel from the local bedrock mixed with a fine earth fraction derived from reworked loess or airborne dust. In only small, isolated parts of the upper Zin catchment flat loessial terrain, typical for wide areas of the north-western Negev, can be found. There relatively thick (> 40 cm), quite uniform loessial soils with a stable surface crust develop. Steep mountain slopes, found along the anticlinal ridges, are usually bare of any soil cover. On alluvial terraces along the main channels gravely Reg soils develop. Their typical soil profile consists of a surficial stone cover (desert pavement), a gravel-free or gravel-poor B-horizon and a gravely C-horizon. Soil thickness ranges between 30- 40 cm (Holocene age) to more than 100 cm (Pleistocene age). In the Zin Valley, in the synclines of the Northern Negev Fold Belt and in the Arava Rift Valley mechanical weathering has formed shallow calcareous desert lithosols in situ on the unconsolidated carbonate rocks (marl and clay). Where flinty strata are common, flint gravel accumulates on top and forms a stable pavement inducing the same Reg soil development as on abandoned alluvial terraces.

Two main surficial processes govern the infiltration characteristics of these soil types:

(a) Soils with a high silt content develop a stable surficial crust due to raindrop impact (e.g. MORIN & BENYAMINI 1977, RÖMKENS 1990, LUK et al. 1993). Clay-rich soils, are more resistant to surface crusting because of higher soil stability and desiccation cracks (e.g. ZHANG & MILLER 1993, YAIR et al. 1980a). Since the grain size distribution of aeolian loess is largely dominated by the silt fraction, surface crusting and sealing is widespread on the Loessial and Hammada soils in the upper Zin catchment. Here stone clearing may enhance runoff generation significantly (EVENARI et al. 1982). The Lithosols on the marly sediments in the middle and lower catchment contain less silt. Here crusts are less stable and more permeable.

(b) Small stones and gravel accumulate on top of plain gravelly soils due to the erosion of the finer material (DAN et al. 1982, GERSON & AMIT 1986). Because of physical weathering the sizes of stones and gravels decrease with time. Surfaces older than 50 - 70 000 years are veneered by a complete cover of angular gravel less than 10 cm in size forming a smooth and stable desert pavement. Fragments from resistant rocks (limestone, dolomite and flint) are most prominent. A vesicular horizon

underneath formed by entrapped air reduces infiltration furthermore (EVENARI et al. 1974). In the Nahal Zin stable stony pavements are mainly found on Pleistocene alluvial terraces and on Campanian flint surfaces.

Erosion on the elevated parts of the catchment is severe due to the arid climate, steep slopes and absence of vegetational cover. Most weathering products are constantly carried away and are deposited as alluvial deposits in the valleys along the stream channels. The spatial extent of the riverbed alluvium, digitized from topographical maps (scale 1:50,000 by THE SURVEY OF ISRAEL, JERUSALEM, ISRAEL), reflects the main morphological units (Fig. 4.8).

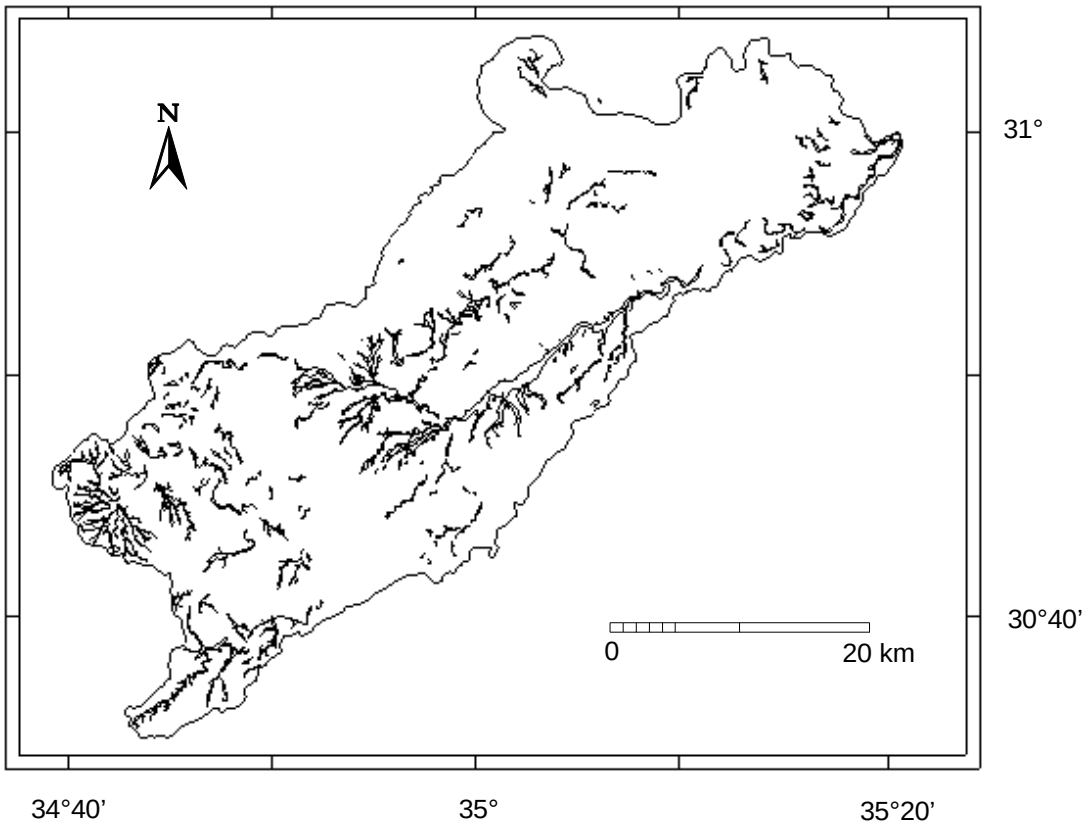

Fig. 4.8 Distribution of reaches with deep riverbed alluvium

On the Avdat Plateau riverbed alluvium is widely spread mainly consisting of fine, silty material. Aeolian loess was washed from the hillslopes and deposited into the stream valleys. Further downstream the alluvial sediment coarsens with increasing stream power. It is mainly concentrated in the Zin Valley and in the synclines of the Fold Belt. The anticlinal ridges and the Makteshim are locations of pronounced erosion devoid of considerable channel alluvium.

4.5 Surface drainage and underground storages

The catchment of Nahal Zin is part of the endorheic Dead Sea catchment. It is characterized by a distinct relief, a high drainage density and several main tributaries (Fig. 4.9). The Avdat Plateau is drained by the upper Nahal Zin and Nahal Avdat, both meeting upstream of the Avdat Waterfall. Then Nahal Zin turns eastward entering the Zin Valley. Despite the friable soft sediments the main channel is still confined. Nahal Aqev joins the upper Zin Valley draining an elongated rocky catchment deeply entrenched into the Avdat Plateau. At the end of the Zin Valley Nahal Hava enters the main channel. This tributary resembles the upper Zin in lithology and surface characteristics but represents a hydrological 'shortcut' with steeper and shorter channels and accelerated runoff concentration. Downstream this confluence Nahal Zin flows over a section which is covered by thick coarse alluvium. It changes into a wide braided channel with a maximum width of several hundred meters. In this reach a substantial part of the flow is lost. The largest tributary of Nahal Zin, Nahal Hatira, enters just downstream this section. Over the next 20 km Nahal Zin forms a narrow canyon entrenched into hard carbonate rocks. Here the flows of Nahal Hazera join the main channel before it falls down the lower waterfall at the main fault of the Arava Rift Valley. On its final 15 km Nahal Zin eventually reaches its alluvial fan off southern end of the Dead Sea.

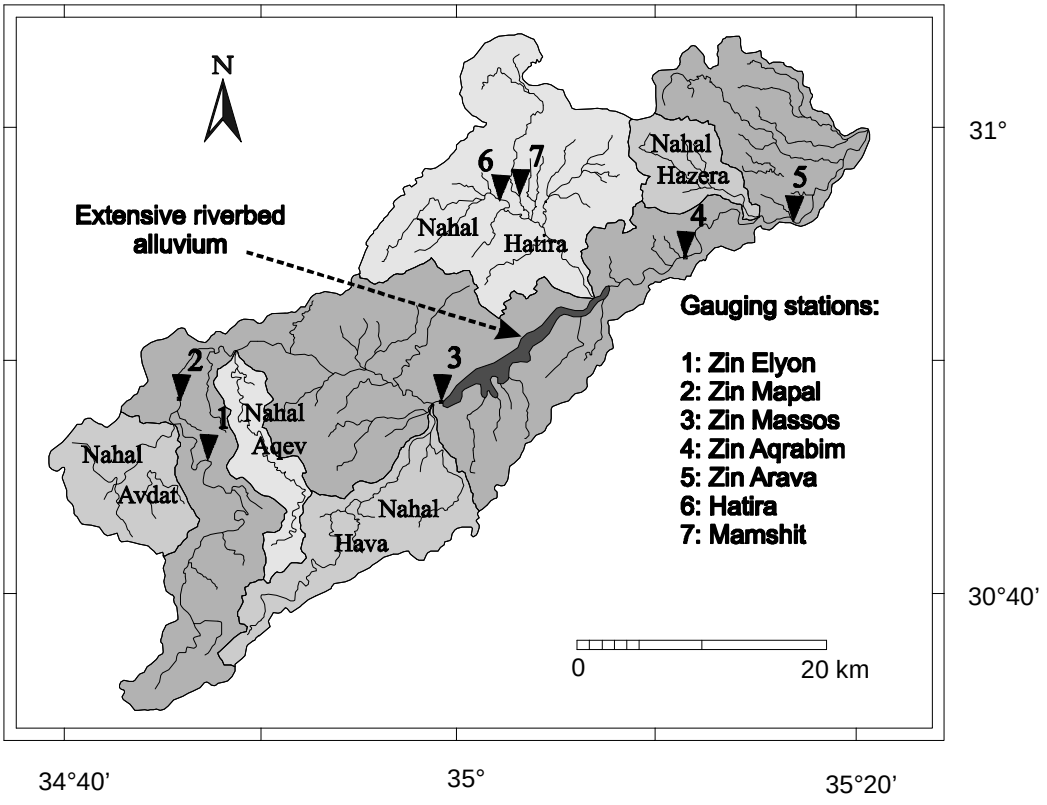

Fig. 4.9 Hydrometric network and main tributaries of Nahal Zin

Throughout the drainage network the Israel Hydrological Service installed seven runoff gauging stations, five in the main channel and two in the tributaries (Fig. 4.9). GREENBAUM et al. (1998) and MEIROVICH et al. (1998) summarized parts of this data (Tab. 4.1). The record of Zin Elyon in the uppermost catchment is incomplete as it was destroyed by a flood and rebuilt at another site. For the present study single event data were not available and the station had to be completely excluded from further analysis. Zin Mapal is located on a narrow rocky section just upstream the Avdat Waterfall. Zin Massos was established at the end of the Zin Valley recording the flow of the upper half of the catchment including the fast responding Nahal Hava. At the Aqrabim station two effects are balancing: considerable transmission losses into the extended riverbed alluvium upstream and the tributary inflows from Nahal Hatira. These inflows are measured twice before reaching the main channel (stations Hatira and Mamshit). The lowermost tributaries remained ungauged for most of the time, since the gauging station Arava was in operation for only three years.

Tab. 4.1 Gauging stations inside Nahal Zin, Station properties and largest flood events on record
(MEIROVICH ET AL. 1998, GREENBAUM ET AL. 1998, modified)

Station	Drainage area km^2	Years of observation	Total number of flow events	Flow events per year	Maximum Discharge m^3s^{-1}	Maximum Volume 10^6 m^3
Hatira	66	15	47	3.1	300*	1.5
Mamshit	64	42	109	2.6	99	0.7
Zin Elyon	135	36	63	1.8	552	1.6*
Zin Mapal	233	43	54	1.3	551	6.0
Zin Massos	660	37	84	2.3	572	5.7*
Zin Aqrabim	1130	29	65	2.2	550*	7.0**
Zin Arava	1230	3	7	2.3	275	3.0

* reconstructed
** estimated

The three most important gauging stations in the main channel, Mapal, Massos and Aqrabim, were evaluated on an unofficial rating scale of the Israel Hydrological Service (BEN-ZVI oral comm. 1998). The quality of the hydrometric records of Mapal are average to good. This gauging station is located on a stable bedrock cross section; it is partly rated and good records of Manning n and high water marks exist. The Massos gauging station offers only average quality records. The bottom of the cross section is mobile, though deep scouring is inhibited by its gravelly character; slope-area evaluations are applied to calculate the discharge. The Aqrabim station provides good quality records based also on a concrete control before being discontinued in 1983. Even if gauging stations are rated by velocity-area discharge calculations applying current meters, systematic and random uncertainties cannot be avoided. The difference between alternative measurements may approach 20 % (MOSLEY & MCKERCHAR 1993). In small Swiss rivers BÄNZIGER (1994) determined 10 % of mean deviation of current meter ratings from salt dilution measurements. Thus, for the hydrometric data of the Zin stations an error range of 15 % for Aqrabim, 20 % for Mapal and 25 % for Massos is estimated. The range for Massos equals the estimate of KIRBY (1985) for slope-area discharge evaluations.

Geological surveys reveal only very few karstic caves or shafts in the limestones of the Nahal Zin catchment, e.g. in the canyon of Nahal Hava (ZILBERMAN 1993). These systems are fossil and completely filled with fluvial sediments. Well developed and widespread underground karstic features (including dolines) have not been found all over the Negev. Therefore it may be concluded that the region has not been under a sufficiently humid climate for a long enough duration to enable karst development (GERSON 1982). In the synclinal valleys, where the groundwater converges, thick impermeable beds isolate the water table from the surface (ROSENTHAL et al. 1987). Hence the two large aquifer systems in the region, the Cenomanian limestone (Judea Group) aquifer and the lower Cretaceous (Nubian) sandstone aquifer have to be regarded as largely disconnected from surface hydrology, a common phenomenon in arid zones (PILGRIM et al. 1988). Only local surficial aquifers in the alluvial fills of the channels are directly replenished by ephemeral floods. The perennial springs of Ein Aqrabim and Ein Zin are fed by the largest local aquifer inside the Zin Syncline and create the Aqrabim Oasis.

5 Model structure and parameters

5.1 General aspects

In catchment-scale applications the extensive data requirements of distributed rainfall-runoff models involve considerable lumping and the use of effective parameters for spatial sub-units. As a result, the spatial resolution of applied physically based models is seldom detailed enough to claim the physical basis of the original model code (STORM & REEFSGAARD 1996). For effective model parameters the present model uses spatially homogeneous sub-units determined by geomorphological analysis with the help of airphotography, topographic maps and several field campaigns.

These spatial sub-units are typical for the different parameter groups:

(a) characteristic terrain types represent the spatial sub-units for runoff generation,

(b) sub-tributaries represent those for runoff concentration,

(c) channel segments/types represent those for channel routing and transmission loss parameters.

This non-rigid spatial subdivision enables maximum accuracy with minimum spatial distribution. Since all sub-units share a common coordinate system, a quick transfer from one spatial distribution to the other is possible. Only a Geographic Information System (GIS) provides an independence from a rigid spatial distribution of model parameters, representing a main advantage of spatially related data processing. In the present model an ARC-INFO framework was used.

Rainfall is event-based, since rain amount and intensity differ considerably from event to event. Hence it is not part of the present non-calibrated model itself but represents the input. The model uses a catchment-wide grid of rainfall intensities [mm hr^{-1}] in a time step of 1 min. This information may be gained from the interpolation of a dense network of recording raingauges, from rainfall radar (as during October 1991) or from a physically based two-dimensional rainfall model (as during October 1979). In Chapters 8 and 9 the rainfall input of two high magnitude events will be discussed in detail.

This chapter summarises model operation in a concise form, while details on parameter determination inside Nahal Zin follow in Chapter 6. Model parameters are given in italic followed by their respective units. In general the model code may be termed ‘field-based’, as not a single model parameter is fitted by calibration with measured streamflow data. Instead, all parameters are determined in the field by techniques suitable for the large modelling scale. These techniques include field measurements and results of existing experiments carried out inside Nahal Zin or nearby. Figure 5.1 provides a schematic flowchart of the model including the different types of spatial subdivision.

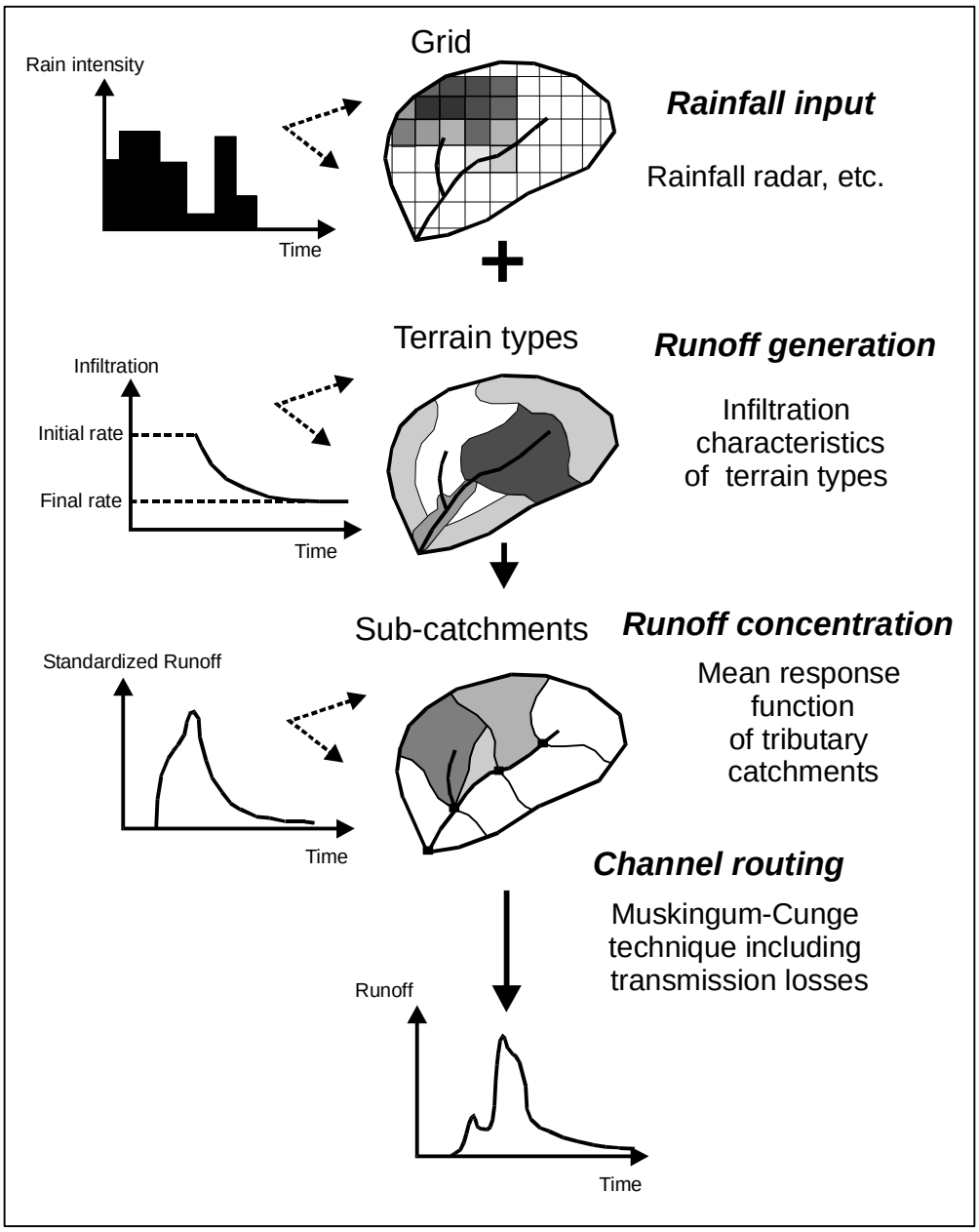

Fig. 5.1 Schematic flowchart of the non-calibrated rainfall-runoff model

5.2 Runoff generation

According to hydrologically relevant surface characteristics the catchment is spatially disaggregated into different terrain types representing the sub-units for parameter determination. Mapping is governed by airphoto analysis together with thorough ground truthing. Hortonian overland flow generation is generally accepted to be the dominant

process of runoff generation in arid and semiarid catchments (e.g. YAIR & LAVEE 1985). This concept calculates generated runoff as rainfall that falls in excess of infiltration when the rain intensity exceeds the infiltration capacity of the soil (HORTON 1933). Knowing the rainfall rate and neglecting interception losses due to the sparse arid vegetation, only the temporal decay of the soil infiltration rate dictates runoff generation. In the model Hortonian runoff generation is parameterized independently for each terrain type.

After the accumulated rain has reached the *initial loss* [mm], Hortonian runoff is calculated as rain that falls in excess of the infiltration which drops down from an *initial rate* [mm hr^{-1}] to a *final rate* [mm hr^{-1}] (Fig. 5.1). The temporal decay does not follow a mathematical function but is directly derived from rainfall simulator experiments, as are the values for initial loss and initial/final infiltration rate. Hence these values include all dominant processes for arid zone runoff generation (e.g. crust wetting, detention losses, etc.). The initial loss is increased by a *scale transition factor* [mm] to account for processes that are active in a larger scale, namely losses of runoff into the colluvial base of a slope (YAIR 1992) or channel transmission losses. Comparisons of measured runoff responses between slopes and small catchments yield quantitative estimates of this factor. Light rains up to a few millimetres which precede large rainstorms have, generally, a negligible effect and are disregarded in the model. They mostly fall over a long time span and infiltrate into the thin debris cover without spatial concentration. Subsequently most of the water is lost by evaporation within a few hours.

5.3 Runoff concentration

The channel network is divided into segments which are adjoined by small sub-catchments (model elements) delineated according to topography. Within the GIS the catchment wide information on amount [mm] and onset [min] of Hortonian runoff (as calculated by the runoff generation routine) is distributed to the different sub-catchments. Then lateral runoff delivery from the model elements to the channel segments is timed describing runoff concentration. Based on relevant field data this process can only be assessed analysing measured rainfall and runoff of single events in an arid catchment of a size similar to the model elements. For the present study the unique data record of Nahal Yael, a 0.6 km^2 research catchment near Eilat, southern Negev, was available (SCHICK 1988, SCHICK & LEKACH 1993).

Several conceptualisations of runoff concentration exist, usually based on the Unit Hydrograph concept (SHERMAN 1932). The Unit Hydrograph represents the direct runoff hydrograph resulting from a unit impulse (usually 1 mm) of rainfall excess generated uniformly over the drainage area within an effective duration. Generally this concept should be well applicable to arid zone catchments, since they quickly react on short high intensity rainstorms by surficial direct runoff components. However, detailed studies on the spatial distribution of arid zone rainfall revealed an accentuated non-uniformity of event rainfall in Nahal Yael (SHARON 1970) and even along a 0.1 km^2 arid hillslope (YAIR et al. 1980b). This was confirmed by the striking variation of recorded rainfall onsets inside Nahal Yael which will be discussed in Chapter 5. Hence determining a Unit

Hydrograph based on spatially and temporally uniform rainfall excess may be assumed to gain no additional accuracy compared to a simple mean response function. Moreover, applying the Unit Hydrograph would introduce theoretical conceptualization into an otherwise purely field based model code. The mean response function consists of a *hydrologic timelag* [min] and a *standardized shape*. Both may be determined directly by a simple averaging of flood arrival times and event hydrographs of gauged storm events.

5.4 Channel flow and transmission losses

The spatial disaggregation for this part of the model, the subdivision of the drainage network into channel segments delimited by channel nodes, is predefined by the sub-catchments used to parameterize runoff concentration. Flow is routed from node to node accounting for lateral inflow and transmission losses. Flow routing procedures are mathematical tools to describe the flow of linearly concentrated water through stream channels of a catchment. Among others CHOW et al. (1988) and FREAD (1985, 1993) provided comprehensive reviews of different methods. In *lumped/hydrological* routing procedures flow is computed at only one point at the lower end of a channel reach. The storage within this reach is described by arbitrary empirical functions whose parameters are not measurable and usually have to be determined by calibration with gauged outflow hydrographs. *Distributed* routing procedures describe the flow process at several points along a watercourse accounting for channel properties such as cross sectional geometry, slope, flow length and channel roughness. They are based on the differential equations of one-dimensional unsteady flow, the Saint-Venant equations. Firstly developed by Barre de Saint-Venant in 1871, these equations consist of a continuity and a momentum part. Latter contains terms for the physical processes governing the flow momentum, namely acceleration, pressure, gravity and friction forces.

Simplified distributed flow routing models have been developed using the full continuity equation while neglecting terms in the momentum equation. LIGHTHILL & WHITHAM (1955) introduced the simplest type of a distributed routing model, the *kinematic wave* model. It neglects pressure and acceleration terms assuming that friction and gravity forces balance each other. The *diffusion wave* model neglects acceleration but incorporates the pressure term. The *dynamic wave* model considers the entire Saint-Venant equations.

CUNGE (1969) developed an approximate solution for the diffusion wave model modifying the Muskingum routing procedure. In a space-time discretized network, where a flood is calculated from channel node to channel node at different time steps, this solution is represented by linear algebraic equations (CHOW et al. 1988):

$$Q_{i+1,\,j} = C_1\, Q_{i,\,j} + C_2\, Q_{i,\,j-1} + C_3\, Q_{i+1,\,j-1} \qquad (5.1)$$

$$C_1 = (\Delta t - 2KX) / (2K(1 - X) + \Delta t) \qquad (5.2)$$

$$C_2 = (\Delta t + 2KX) / (2K(1 - X) + \Delta t) \quad (5.3)$$

$$C_3 = (2K(1 - X) - \Delta t) / (2K(1 - X) + \Delta t) \quad (5.4)$$

where Δt is the time step, $Q_{i+1,\ j}$ is the unknown discharge at the next node at the present time step, $Q_{i,\ j}$ is the discharge at the present node at the present time, $Q_{i+1,\ j-1}$ is the discharge at the next channel node at the last time step, $Q_{i,\ j-1}$ is the discharge at the present channel node at the last time step, K is a storage constant having dimensions of time and X is a weighting factor expressing the relative importance inflow and outflow have on the storage;

$$K = \Delta x / v_k \quad (5.5)$$

$$X = 0.5\ [1 - (Q_{REF} / B\ v_k\ S_0\ \Delta x)] \quad (5.6)$$

where Q_{REF} is the reference discharge, Δx the distance step, B the width of the water surface, S_0 the energy slope and v_k the kinematic wave celerity.

For a wide channel, where the hydraulic radius approaches the flow depth, the following approximation is valid:

$$v_k \approx 5/3\ v \quad (5.7)$$

where v (the flow velocity) may be obtained applying a uniform flow formula such as the Manning equation:

$$v = (R_0^{2/3}\ S_0^{1/2}) / n \quad (5.8)$$

where R_0 is the hydraulic radius, S_0 the energy slope and n the Manning roughness coefficient.

Different modes of the Muskingum-Cunge method exist due to the value of Q_{REF} chosen (PONCE & CHAGANTI 1994). *Linear modes* use a constant reference flow making the routing parameters K and X constant in time. They require an a-priori estimation of this flow and do not incorporate wave steepening. *Non-linear modes* re-calculate the routing parameters at each time step using available Q-values of previous time- and distance steps for Q_{REF}. They account for the fact that different discharges travel at different celerities. Thereby a steepening of a flood front may be described important for ephemeral floods in arid channels. For the present model the non-linear MVPMC3-method (PONCE & CHAGANTI 1994) is applied using the maximum available information for Q_{REF}:

$$Q_{REF} = (Q_{i,\ j} + Q_{i,\ j-1} + Q_{i+1,\ j-1}) / 3 \quad (5.9)$$

Channel geometry is represented by a compound section consisting of inner channels and bars (Fig. 5.2). At the beginning only the percentage of the cross section covered by inner channels is covered by the flood. Only at bankfull stage the complete cross section (including inner channels and all bars) is inundated. In between the width is linearly interpolated. The temporal behaviour of channel transmission losses during flood events is largely unknown. Tracer studies provided evidence that the infiltration rate at the very beginning of a flood may be smaller than later on (LANGE et al. 1998), which is in contradiction to common infiltration models. In infiltrometer tests a constant infiltration rate was reached very soon (KÜLLS et al. 1995). For the present model a constant infiltration rate was chosen to parameterize channel transmission losses. In the compound channel section two different infiltration rates are assigned to bars and inner channels. In each time step the wetted area is multiplied by the infiltration rate to obtain the volume of channel loss subtracted from the actual discharge. This subtraction is stopped when the available storage for channel losses is filled, represented by the depth of the active alluvium.

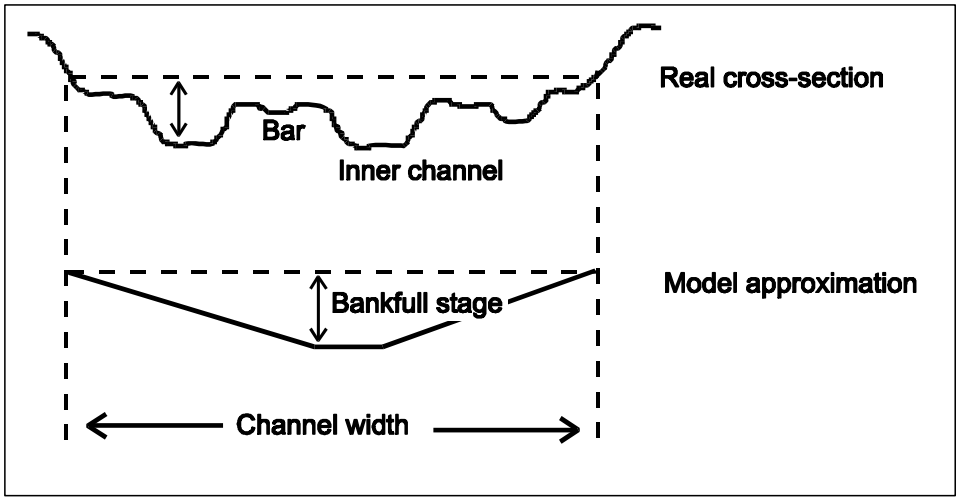

Fig. 5.2 Simplified representation of cross-sectional geometry

Model parameters to be determined for each channel segment are: *channel length* [m], *percentage covered by inner channels*, *channel width* [m], *bankfull stage* [m], *Manning n*, constant *infiltration rates* [mm hr^{-1}] for inner channels and bars and the *depth of the active alluvium* [m]. To limit the amount of needed input data several parameters (percentage covered by inner channels, bankfull stage, Manning n, infiltration rates and depth of the active alluvium) may be assigned uniformly for channel types classified in the field.

6 Parameter determination

6.1 Runoff generation

6.1.1 Spatial disaggregation

Within the Nahal Zin catchment, typical for arid environments, almost no vegetation covers the surface. Therefore remote sensing is a valuable tool to study hydrologically relevant surface characteristics. On aerial photographs the spatial extent of the characteristic terrain types can be mapped (VAN ZUIDAM 1986). These terrain types represent the spatial sub-units for parameter determination. For instance loose sediments can be distinguished from rocky slopes or plateaus and ages of alluvial deposits may be characterized by the intensity of surficial stone accumulation and desert varnish (BULL 1991). About 60 black and white airphotos of different scales were scanned, rectified and incorporated into the GIS. The complete main channel and about 90 % of the catchment could be covered (Fig. 6.1). Gaps in the coverage were mainly due to a security censorship (e.g. military objects and a nuclear research plant). Geological maps (scale 1:50,000) served as additional data sources. All this information was supplemented by a specific field campaign. As a result 21 different terrain types were mapped inside the Nahal Zin catchment (Fig. 6.2).

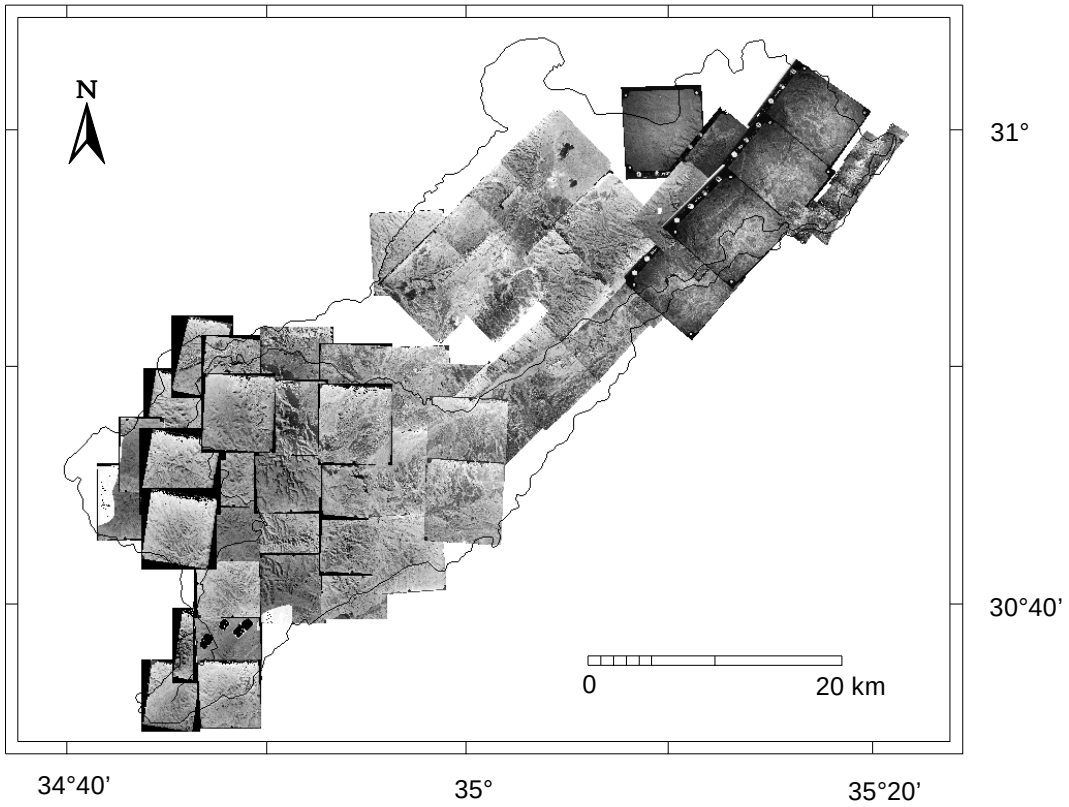

Fig. 6.1 Aerial photo coverage of the Zin catchment

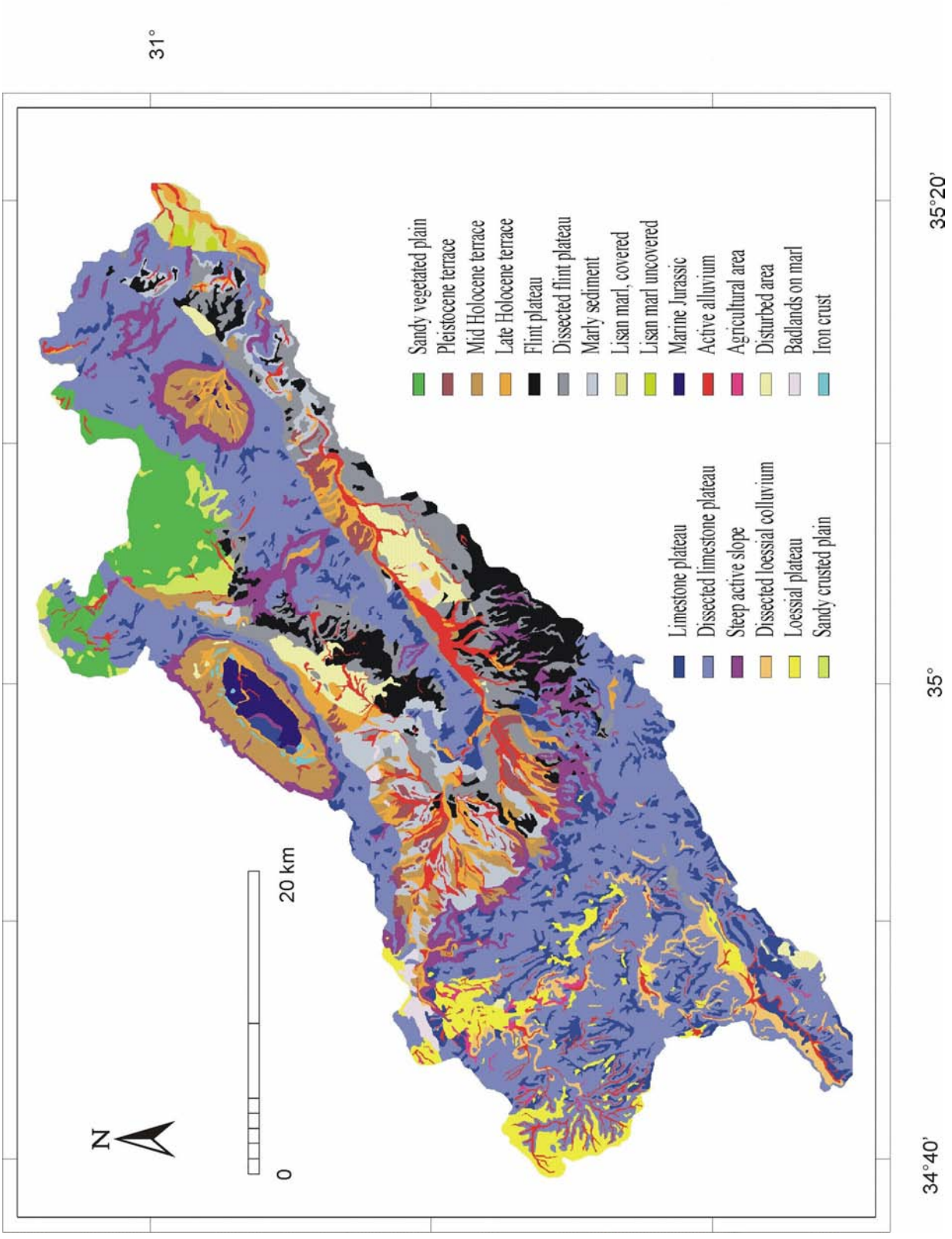

Fig. 6.2 Terrain types inside Nahal Zin

6.1.2 Parametrization

To provide the necessary model parameters (initial loss and final infiltration rate) each terrain type was studied directly in the field. Examples of the most important terrain types are given in the annex (Fig. A1-A13). Investigations concentrated on the surficial cover governing infiltration characteristics and runoff generation. For some terrain types experimental results of runoff plots or heavily instrumented hillslopes were available (terrain types 1,2,8,9,10,20), while the infiltration rates and initial losses of others were assessed studying the development of surface crusts, vesicular horizons and stony pavements on top.

For scale transition two additional catchment scale processes were taken into account:

Slope losses: on terrain types consisting of a rocky upslope area with a colluvial base (terrain types 2 and 12), runoff generated on the upper rocky part may be lost at the interface between the rocky and colluvial parts resulting in a discontinuity of runoff (YAIR 1992), this process is not active on plain surfaces or uniform slopes.

Channel losses: as the catchment size increases, more and more water flowing on dry channels disappears (SCHICK 1988, BULL 1997). This process is active within each terrain type when experimental results from runoff plots are transferred to the scale of small catchments.

Comparisons of runoff responses between slopes and small catchments (YAIR & KLEIN 1973, SHANAN & SCHICK 1980, YAIR 1992) made it possible to estimate how these processes could be quantified. For both the initial losses were increased by a scale transition factor of 2.5 mm. In case of a very sandy channel alluvium (terrain types 6,7) the value for channel losses was increased to 4 mm. Table (6.1) provides an overview of the model parameters which is followed by a detailed description of the results of the field campaign.

(a) *Terrain type 1* consists of rocky plateaus of resistant limestones. It can be found all over the Avdat Plateau and along the crests of the anticlinal ridges covering 7.4 % of the catchment. Bare rocky outcrops dominate the terrain, only patches of shallow lithosols (A-C-profile) may be found. On small runoff plots (0.25 m^2) SALMON & SCHICK (1980) and GREENBAUM (1986) studied the hydrological characteristics of rocky surfaces. They were characterised by very small values of initial loss and final infiltration rate. Magmatic lithologies (e.g. Gneiss, Granite) showed minimum values (about 1 mm initial loss, 0-1 mm hr^{-1} final infiltration rate). The infiltration rates for bare limestone increased slightly (about 2 mm initial loss, 5 mm hr^{-1} final infiltration rate). Near Sde Boker, YAIR (1987, 1992) extensively studied the runoff response of an entire arid limestone hillslope (rocky headwater area in the upper part of the slope and colluvial mantle downslope). Infiltration characteristics of the rocky headwater area amounted to 1-3 mm of initial loss and 0 mm hr^{-1} of final infiltration rate. To represent scale transition in the Zin model only channel losses were taken into account for these plain limestone plateaus. The following parameters resulted: 4.5 mm of initial loss and 5 mm hr^{-1} of final infiltration rate.

Tab. 6.1 Infiltration characteristics of the different terrain types

Terrain type	No.	Area in the entire catchment [%]	Initial loss [mm]	Final infiltration rate [mm hr^{-1}]
Limestone plateau**	1	7.4	4.5	5
Dissected limestone plateau**	2	37.0	7	15
Steep active slope	3	5.8	10	30
Dissected loessial colluvium	4	2.0	10	20
Loessial plateau	5	3.3	7.5	15
Sandy crusted plain	6	1.1	9	15
Sandy vegetated plain	7	4.7	11	50
Pleistocene terrace**	8	1.8	6	8
Mid Holocene terrace**	9	4.9	7	12
Late Holocene terrace**	10	4.4	11	40
Flint plateau	11	5.8	6	10
Dissected flint plateau	12	7.6	8	20
Marly sediment	13	4.4	9.5	15
Lisan Marl, uncovered	14	0.6	7.5	12
Lisan Marl, covered	15	0.2	6	8
Marine Jurassic	16	0.9	7.5	10
Active alluvium*	17	4.4	-	-
Agricultural area*	18	0.3	-	-
Disturbed area*	19	2.6	-	-
Badlands on marl**	20	0.6	9.5	20
Iron crust	21	0.2	7	20

* terrain where all rain infiltrates
** terrain type with performed field experiment

- *Terrain type 2* may be characterized as dissected limestone plateau. It consists of small upper slope area (comparable to terrain type 1) and a colluvial mantle at the slope bottom. This type covers 37.1 % of the catchment and is found in the entire Avdat plateau and along the anticlinal ridges. SHANAN & SCHICK (1980) studied the runoff response of a typical 3.45 km^2 catchment located in the Avdat Plateau. As initial loss they determined 7 - 8 mm, infiltration rates were not quantified, however, only daily amounts. The extensively measured arid limestone hillslope mentioned above (YAIR 1987, 1992) represents a perfect example for terrain type 2 providing relevant hydrological data. Losses of generated runoff on the rocky parts upslope into the colluvial mantle increase both initial losses and infiltration rates. Therefore scale transition from rocky runoff plots to entire hillslopes consists of both channel- and slope losses. The initial losses of terrain type 1 were therefore increased by 2.5 mm to reach 7 mm. For a final infiltration rate a value of 15 mm hr^{-1} was assessed, similar to the rates measured on a stony colluvial soil (YAIR 1987).

- *Terrain type 3* consists of steep slopes with active erosion processes. It is found at the cliffs of the Zin Valley, in the surroundings of the Makhteshim and along deeply entrenched valleys in the anticlines. This terrain type covers 5.8 % of the catchment. In contrast to terrain type 2, almost the entire slope delineates a unit covered by a young, non-stabilized and highly infiltrating colluvium originating from limestone and marly lithology. No discontinuity of runoff leads to slope losses. Soil formation did not have enough time to develop a stable surficial crust or pavement. Large boulders

on the surface increase roughness and detention losses. GREENBAUM (1986) determined about 7.5 mm initial loss and about 30 mm hr^{-1} of final infiltration rate on runoff plots located on a similar young colluvial surface (a riser of a Pleistocene alluvial terrace). To account for scale transition (channel losses) the initial loss was increased for this terrain type (10 mm), while the final infiltration rate was left unchanged.

- *Terrain type 4* may be characterized as highly dissected uniform loessial colluvium. Located in the upper Avdat Plateau it represents a remnant of a Pleistocene valley fill covering 2.0 % of the catchment area. Still no stable crust or vesicular horizon inhibits infiltration. The texture is silty to sandy allowing a rather deep penetration of the infiltrating water. An active calcic horizon at a depth of about 20 cm confirms this fact. Slopes are less steep than on terrain type 3, still the high percentage of sand in the soil matrix leads to enhanced infiltration. Including scale transition (channel losses) model parameters amounted to 10 mm of initial loss and 20 mm hr^{-1} of final infiltration rate.

- *Terrain type 5* is made of plain loessial plateau surfaces in the upper catchment covering 3.3 % of the catchment area. On hard material with fine texture (mainly silt and clay) a stable crust has developed. The origin of this material is aeolian or partly redistributed fluviatile with almost no stones at the surface. YAIR (1987) determined an initial loss of 5 mm and a final infiltration rate of approximately 15 mm hr^{-1} for runoff plots on a stoneless loessial soil. To obtain an estimate for the entire terrain type initial losses were increased by 2.5 mm to account for channel losses. The resulting model parameters were: 7.5 mm of initial loss and 15 mm hr^{-1} of final infiltration rate.

- *Terrain type 6* is represented by a sandy vegetationless plain. A stable silty crust has formed at the almost stoneless surface. This terrain type makes up a south-western fringe of the sandy Rotem Plain covering 1.1 % of the total catchment. YAIR (1990) showed that even sand dune areas may respond quickly to rainfall if stable crusts cover the permeable sandy soil. Hence for the infiltration rates of this terrain type not the underlying sand, but the stable silty crust on top is decisive. Compared to the crust of terrain type 5 a great difference is apparent: Once the stable silty crust is eroded (mainly due to channel incision), sandy, highly infiltrating material appears. Therefore channel losses were increased (4 mm). Model parameters for the entire terrain type were assessed the following way: 9 mm of initial loss and 15 mm hr^{-1} of final infiltration rate.

- *Terrain type 7* may be found on the sandy Rotem Plain, covering 4.7 % of the total catchment. In contrast to terrain type 6 there is no cohesive silty crust on top, as a rather dense vegetation cover has formed. Only patches with biological crust as found in Nizzana (YAIR 1990) exist. Vertical water movement is most distinct around bushes and shrubs, where roots reach depths of 20 - 30 cm. High initial losses are caused by the vegetation cover due to interception losses and high surface roughness. Similar to terrain type 6 above, the sandy channel alluvium increases channel losses. For the whole terrain type an initial loss of 11 mm and a final infiltration rate of 50 mm hr^{-1} were estimated.

- *Terrain type 8* represents Pleistocene alluvial terraces. They are the highest of a sequence of terraces found along the Zin Valley and in the synclines covering 1.8 % of the total catchment. A deep Reg soil limits infiltration, as a stable stony desert pavement, a stable silty crust and an underlying vesicular horizon have developed. GREENBAUM (1986) studied the infiltration characteristics of these surfaces. While initial losses (about 3.5 mm) were considerably higher than on rocky terrain, final infiltration rates (8 mm hr^{-1}) were similar. Accounting for channel losses (2.5 mm) an initial loss of 6 mm and a final infiltration rate of 8 mm hr^{-1} were assigned to this terrain type.

- *Terrain type 9* is of similar origin than terrain type 8 above, the age, however, is considerably younger. Predominant areas of these Mid Holocene alluvial terraces are located in the synclines and in the Zin Valley covering 4.9 % of the total catchment. Pedogenis did not have time enough to develop a surface seal as distinct as on the Pleistocene terraces of terrain type 8. The stony pavement is not as well sorted, vesicular horizons and surficial crusts are not as stable. Also for this terrain experimental results of GREENBAUM (1986) could be used to describe the infiltration characteristics. Accounting for channel losses the values for the entire terrain type were 7 mm of initial loss and 12 mm hr^{-1} of final infiltration rate.

- *Terrain type 10* represents the youngest alluvial terraces. They are of late Holocene age covering 4.4 % of the total catchment. Also these low terraces are found along the major water courses in the Zin Valley and the synclines. High infiltration rates prevail, since no stable crust or surficial pavement has formed. Over the entire depth of the soil profile soil material is largely unsorted. Experimental results by GREENBAUM (1986) revealed very high infiltration rates. For the whole terrain type (including channel losses) the following model parameters resulted: 11 mm of initial loss and 40 mm hr^{-1} of final infiltration rate.

- *Terrain type 11* consists of plateaus covered by Campanian flint. This lithology is very resistant to erosion, accumulates on top of the soil developing a stable pavement. Mainly located in the synclines this terrain type covers 5.8 % of the catchment,. A well developed vesicular horizon is found underneath pointing to effective surface sealing. Some large flint particles penetrate through the vesicular horizon into the silty-sandy matrix underneath enhancing the infiltration rates. For the model initial losses were mainly governed by the well developed surficial stone pavement, they equalled those of a Pleistocene alluvial terrace (6 mm). Due to the silty-sandy soil underneath the final infiltration rate was increased (10 mm hr^{-1}).

- *Terrain type 12* may be described as dissected Campanian flint plateau. It is found in the neighbourhood of terrain type 11 covering 7.6 % of the total catchment. Similar to terrain type 2 it is a combination of two different surface units: The upper headwater area is covered by small areas of flint plateaus which are dissected by deeply entrenched channels uncovering marly-sandy material. This material is soft and uncompacted, no stable crusts evolve due to the high percentage of sand. Hence, compared to terrain type 11, infiltration parameters have to be increased accounting for infiltration losses into the marly-sandy slopes. Also scale transition is two-fold,

since slope- and channel losses have to be regarded. Model parameters for this terrain type were 8 mm of initial loss and 20 mm hr^{-1} of final infiltration rate.

- *Terrain type 13* is made of uniform marly-clayish material mainly found inside the Zin Valley making up 4.4 % of the whole catchment. Under arid conditions this lithology is very resistant to erosion forming plains and slopes almost without any debris cover. Due to the clay content desiccation cracks are prominent in the surficial crust enhancing infiltration losses. Underneath the soil profile is very uniform with almost no layering. Still accentuated rill erosion on the slopes indicates considerable overland flow generation during storm events. Because of the desiccation cracks the initial losses were increased compared to the stable silty crust of terrain type 5, whereas the final infiltration rate was left unchanged. A value of 9.5 mm was assigned to initial loss (including channel losses), 15 mm hr^{-1} to final infiltration rate.

- *Terrain type 14* is represented by outcrops of the Lisan Marls in the Arava Rift Valley covering 0.6 % of the total catchment. The Lisan marls contain less clay than the marly sediments of the Zin Valley (terrain type 13). Although the whole formation is soft and susceptible to erosion with deeply incised channels, more surface runoff is generated than in the Zin Valley because of the more stable, silty surface crust. The advanced channel erosion in very small local catchments confirms this observation. For the model 7.5 mm of initial loss and 12 mm hr^{-1} for final infiltration rate were assigned to this terrain type.

- *Terrain type 15* consists of the same lithology as terrain type 14 above, however the marly sediments are covered by a stony pavement in 0.2 % of the catchment. The surface is plugged by the silty Lisan material limiting vertical infiltration by a stable surficial crust. The pavement, the crust and a vesicular horizon underneath are very well developed. Overall infiltration is considerably reduced, similar to a stable Pleistocene terrace (terrain type 8). Hence the model parameters could be transferred, resulting in 6 mm of initial loss and 8 mm hr^{-1} of final infiltration rate.

- *Terrain type 16* consists of the geologically oldest lithology, marine Jurassic sediments exposed in the cores of the Makhteshim, especially in Makhtesh Gadol, covering 0.9 % of the catchment. Smooth plain surfaces originating from marly-clayisch sediments alternate with limestone outcrops. These bare rocky surfaces reduce initial loss and final infiltration rate compared to the marly sediments in the Zin Valley. For the model 7.5 mm of initial loss and 10 mm hr^{-1} of final infiltration rate resulted.

- *Terrain type 17* is made of recent, active alluvium. Permanent erosion and deposition processes by ephemeral floods inhibit stable surface sealing. Along the upper channels of the Avdat Plateau a dense vegetation cover in a hilly terrain increases interception, detention and infiltration losses of a loessial alluvial fill. Downstream of the Avdat waterfall the channel alluvium consists of coarse fluvial deposits and embedded sandy and silty layers. In total 4.4 % of the catchment is covered by these active alluvial channel reaches. Their infiltration characteristics are decisive for the channel routing component and are treated in detail in Chapter 6.3. For runoff generation they were assumed to be inactive.

- *Terrain type 18* consists of agricultural areas covering 0.3 % of the catchment. Frequent ploughing and the construction of micro-catchment systems (SHANAN & TADMOR 1979) inhibit runoff generation. Similar hydrological characteristics prevail in 2.6 % of the catchment making up t*errain type 19*. Here the surface is totally destroyed by heavy machinery. Mining of phosphorite or quartzite sand churns the surface and leaves loose slag heaps behind. Thereby large areas in the Oron and Zin synclines are excluded from runoff generation. Also desert towns are included into this terrain type. Inside Nahal Zin the only extensive settlement is represented by the town of Mitzpe Ramon. Here two main effects affect the quantity of runoff generation: While some areas are absolutely impermeable (e.g. roofs or paved roads), in others the natural terrain is largely destroyed by construction activities and offroad vehicles. Moreover the drainage divide, made of by the steep cliffs of Makhtesh Ramon, is close, blurring the direction of artificial drainage. Hence excluding the town of Mitzpe Ramon from runoff generation seemed reasonable at the present large modelling scale.

- *Terrain type 20* is represented by marly badlands covering 0.6 % of the catchment. On soft erodible material intensive channel erosion has created a typical badland morphology. Due to the high percentage of clay desiccation cracks in the surface crusts are widespread and surface sealing is limited. Still runoff generation is a little bit enhanced compared to the steep active slopes of terrain type 3, since the material is more uniform and devoid of large boulders. YAIR et al. (1980) conducted sprinkling experiments on these badlands and discovered differences in the hydrological response linked to slope aspect. From these field experiments a mean value for the final infiltration rate of terrain type 20, amounting to 20 mm hr^{-1}, could be derived. Initial losses equal those of terrain type 13 (9.5 mm).

- *Terrain type 21* consists of outcrops of a resistant iron crust. This crust forms plain surfaces with a stable stony cover. Still considerable infiltration is possible, since the material underneath contains a high percentage of sand originating from weathered Cretaceous sandstone. As this layer marks the transition between Jurassic and Cretaceous it is limited to surroundings of Jurassic outcrops in the cores of the Makhteshim covering only 0.2 % of the total catchment. For the model the stable stony cover on sandy widely uncrusted material resulted in intermediate infiltration characteristics: 7 mm of initial loss and 20 mm hr^{-1} of final infiltration rate.

Initial infiltration rates were assigned uniformly for each terrain type. They were adjusted to the rain intensities used in the runoff plot experiments resulting in a representative mean value of 70 mm hr^{-1}. The temporal decay of infiltration did not follow a mathematical function but was directly derived from the experiments at a one minute time step. In general, infiltration rates decreased faster on rocky plateaus or slopes than on unconsolidated sediments; after 14 min the final rates of all terrain types were reached (Fig. 6.3). Together with the initial losses these time-functions of infiltration were attributed to the 21 terrain types yielding a catchment wide GIS data layer of infiltration characteristics.

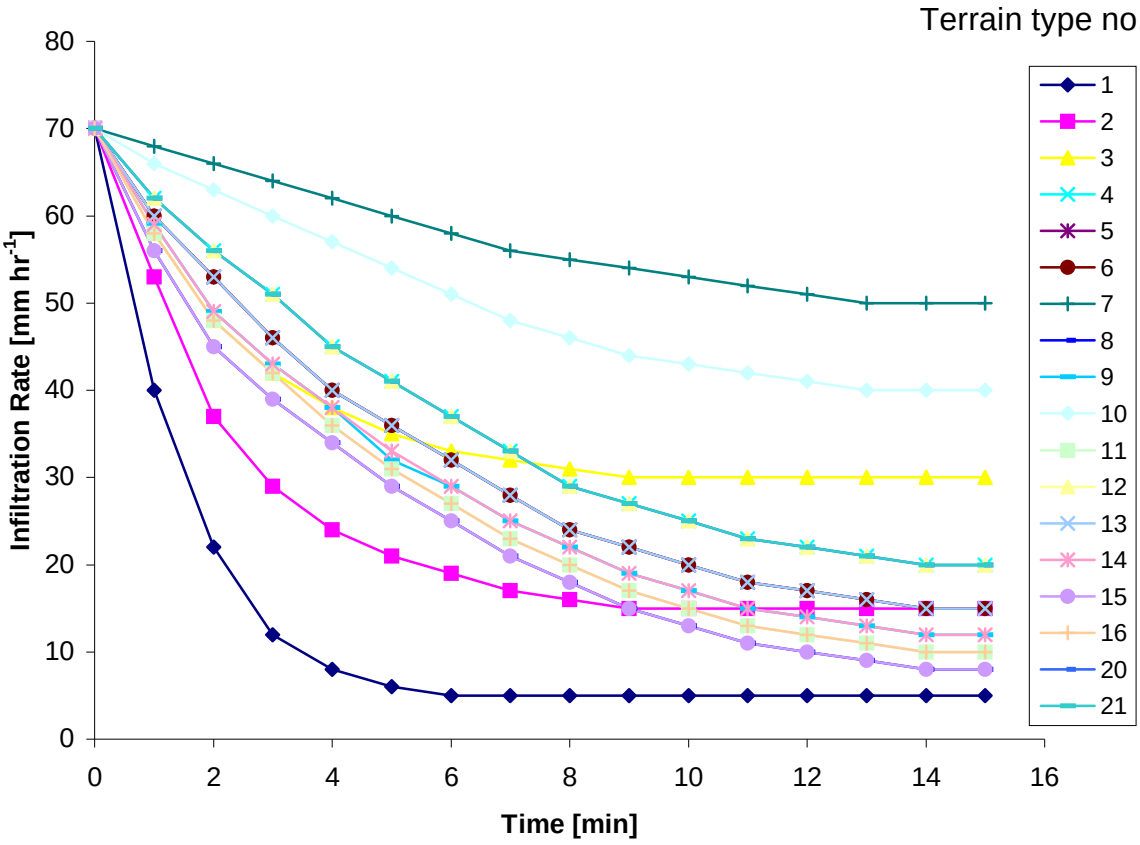

Fig. 6.3 Infiltration rates of the different terrain types

In combination with the temporal sequence of rain intensities these infiltration characteristics governed the model's Hortonian runoff generation: After enough rain had accumulated to satisfy the initial losses, runoff generation started when rainfall intensity exceeded the infiltration rate. Technically an Arc Macro Language (AML) Routines was used to carry out these steps. Using a 30 × 30 m grid the catchment-wide runoff generation was calculated every minute on a cell-by-cell basis. A listing of this routine is given in the annex (Listing A3).

6.2 Runoff concentration

6.2.1 Spatial disaggregation

Since only surface processes are responsible for the generation of arid zone high magnitude floods, the spatial concentration of runoff is governed by surface morphology. Hence the spatial sub-units for parameter determination of runoff generation were represented by sub-catchments delineated according to surface topography. For this purpose a complete coverage of high quality 1:50,000 topographical maps was available.

Spatial subdivision started at the channel network. Accounting for major junctions, channel nodes were placed along the course of the main channels (Fig. 6.4).

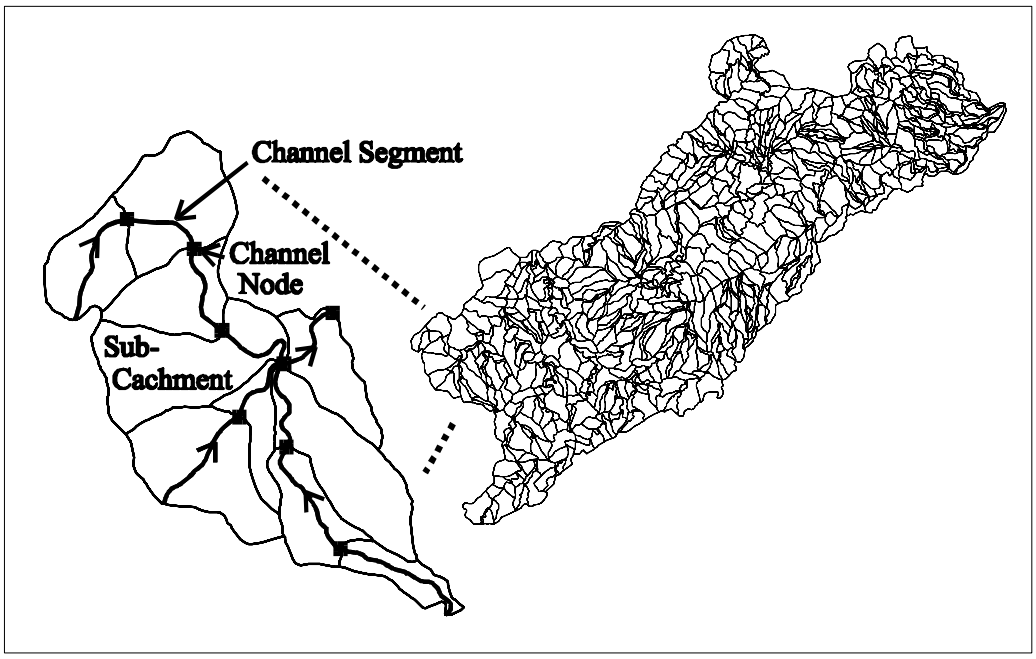

Fig. 6.4 Spatial subdivision of the Zin catchment

As a rough guideline for the distance steps between the single channel nodes, the Courant Condition (COURANT & FRIEDRICHS 1948) for explicit numerical solution schemes of the Saint-Venant equations for open channel flow was used:

$$\Delta t \leq \Delta x / v_k \qquad (6.1)$$

where Δt is the time step used, Δx the distance step and v_k the kinematic wave celerity. If in explicit schemes this condition is not satisfied, there is, in effect, an accumulation or spilling up of water (CHOW et al. 1988).

The time step to be used in the entire model was constant (1 min). For flow velocity the maximum measured velocity of floodwaves (about 6.8 m s^{-1}; Chapter 7) was used. Following (6.1) and (5.7) a lower boundary value of about 680 m for Δx resulted. The average length of the channel segments inside the Zin catchment was about 2 km. Caused by consecutive channel junctions six channel segments fell slightly below the Courant boundary. As all were located in flat tributaries with reduced flow velocities, a violation of the Courant Condition is very unlikely. The average area of the contributing sub-tributaries on both sides of the channel segments was about 1.6 km^2, this compared reasonably with the 1 km^2 REA-scale of catchment runoff (WOOD et al. 1988).

6.2.2 Parametrization

To obtain the necessary model parameters the data record of the experimental catchment Nahal Yael, southern Negev, Israel was used. This 2 km-long ephemeral stream drains 0.6 km^2 of bare rocky desert terrain with a mean annual rainfall of 31 mm (SCHICK & LEKACH 1993). Since 1966 a great number of rainfall and runoff gauging stations have been installed monitoring 24 events until 1994. During eleven years there was no flow at all. Data of 20 events were available for the determination of the hydrological time lag (Tab. 6.2).

Tab. 6.2 Determination of the hydrological timelag using event data from the Nahal Yael data base

Event	No. of rain-gauges	Onset of rain, mean	Onset of rain, standard deviation [min]	02 Flood arrival/ **timelag** [min]	03 Flood arrival/ **timelag** [min]	04 Flood arrival/ **timelag** [min]	05 Flood arrival/ **timelag** [min]
3	8	11:47	11.59		11:43 / **-4.8**	17:46 / **358.2**	
4	10	15:19	5.04	15:33 / **13.7**		15:31 / **11.7**	
6	10	17:02	4.96	17:36 / **33.7**	17:14 / **11.7**	17:06 / **3.7**	15:46 / **-76.3**
7A	7	13:44	2.85	13:57 / **12.9**	13:51 / **6.9**	13:49 / **4.9**	13:07 / **-37.1**
7B	8	17:29	11.66	17:29 / **0.0**	15:54 / **-95.0**	18:00 / **31.0**	
8	10	15:03	7.09			15:15 / **11.9**	15:18 / **14.9**
9	4	20:14	12.52		22:00 / **105.8**	20:03 / **-11.3**	21:27 / **72.8**
12	3	20:00	10.66	19:28 / **-32.7**	09:12 / **-648.7**		09:04 / **-656.7**
13	6	16:38	5.53			16:47 / **8.7**	17:00 / **21.7**
14	5	14:49	4.10			15:00 / **11.0**	15:00 / **11.0**
15	3	16:09	26.28	16:45 / **35.3**	16:39 / **29.3**	12:19 / **-230.7**	16:19 / **9.3**
16	4	18:23	2.49	18:03 / **-20.8**	18:30 / **6.3**		18:38 / **14.3**
17	4	15:49	15.51	15:36 / **-13.3**	15:54 / **4.7**	16:39 / **49.7**	15:42 / **-7.3**
19A	3	19:37	2.36		20:15 / **37.3**		20:05 / **27.3**
19B	2	15:34	3.00		15:11 / **-23.0**		15:52 / **18.0**
20	1	17:27	0.00			17:44 / **17.0**	17:41 / **14.0**
21	4	20:12	1.09	20:19 / **6.7**	20:20 / **7.7**	20:20 / **7.7**	20:19 / **6.7**
22	4	12:30	1.48	12:41 / **10.8**	12:45 / **14.8**	12:43 / **12.8**	12:46 / **15.8**
23	2	21:47	0.00	22:08 / **21.0**		21:58 / **11.0**	
24	4	15:51	0.83	15:59 / **7.7**	16:04 / **12.7**	16:02 / **10.8**	15:58 / **6.7**
drainage area [km^2]				0.5	0.12	0.10	0.05
mean timelag*				**15.2**	**13.9**	**9.4**	**15.2**

event excluded from analysis due to high standard deviation in the onset of rain

* negative timelags excluded

If there was no clear high intensity rain spell in the records, a lower boundary intensity of 20 mm hr^{-1} served as criterion for rainfall onset at a specific rainfall recorder. Problems arose establishing a mean value for rainfall onset even in this small catchment. Since up to event 19 analogue clock driven recorders had been used, problems in time synchronization resulted in large deviations of rainfall onset at the different stations. To exclude errors of this source, events were excluded where the standard deviation exceeded ten minutes or

where only one rainfall record was available. These events also contained the most significant deviations of hydrological timelags. Still four negative values remained. They were attributed to a false timing of the runoff gauges and also were excluded. The resulting mean hydrological timelags for the stations did not increase with drainage area: the smallest catchment (05) reacted as quick as the largest one (02). Finally a mean hydrological timelag of 13 min was calculated using all the four stations.

The extreme climatic conditions (long periods with no flow, accentuated sediment dynamics) made an accurate recording of entire event hydrographs difficult. After each event the rating curves changed and floats clogged frequently. Hence high quality records of only 14 flow hydrographs measured at the stations 02, 03 and 04 were available to study the shape of hydrological response. Five double-peak hydrographs were split increasing the number of recorded hydrographs from 14 to 19. Then these hydrographs were standardized and plotted as cumulative functions (Fig. 6.5).

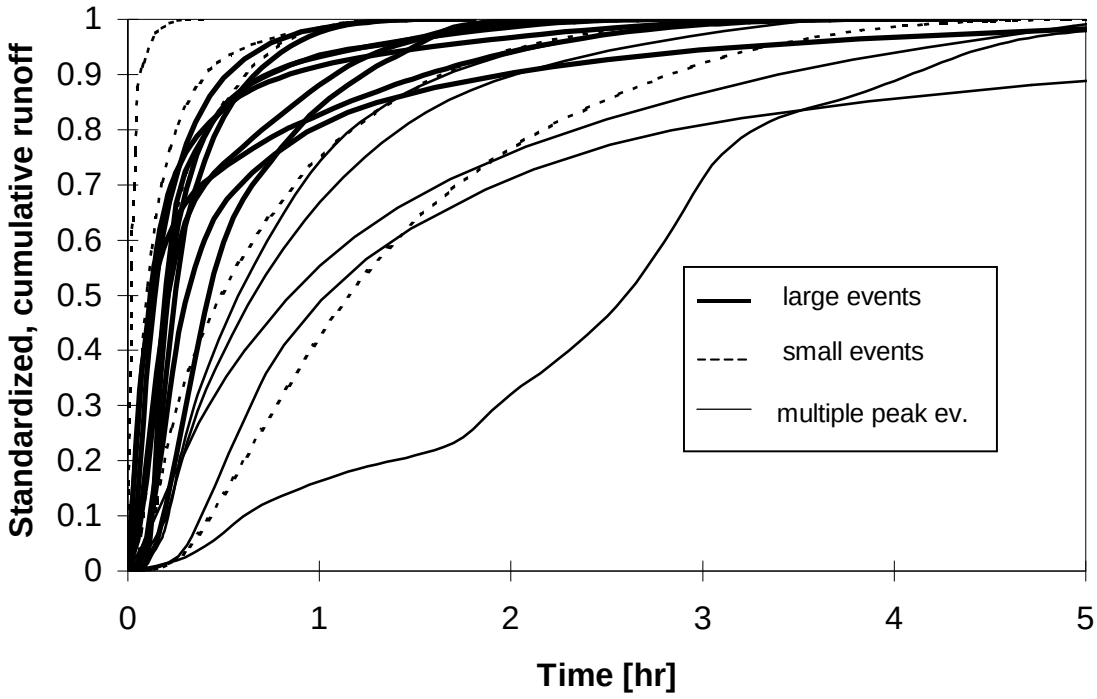

Fig. 6.5 Cumulative, standardized hydrographs of Nahal Yael

For two double-peak hydrographs (event 7 A, B recorded at the stations 02 and 04) the second peak arrived before the recession of the first peak was finished. Another hydrograph included several peaks (event 12 recorded at station 02). These five cumulative functions were characterized as multiple peak events and excluded from further analysis. The remaining functions were grouped according to runoff volume. Small events showed volumes less than 500 m^3, large events exceeded this value. It appeared that the standardized cumulative functions of the large events concentrated in a rather narrow range facilitating the calculation of a meaningful average. At a one-minute time step arithmetic mean values of the nine large event responses were calculated. Non-cumulatively and combined with the hydrological timelag of 13 min, the resulting

standardized hydrograph represented the mean response function of the Nahal Yael catchment (Fig. 6.6). This function was applied to the sub-catchments of the Zin-model. Multiplied by the volume of generated overland flow the lateral input to the channel segments could be calculated every minute.

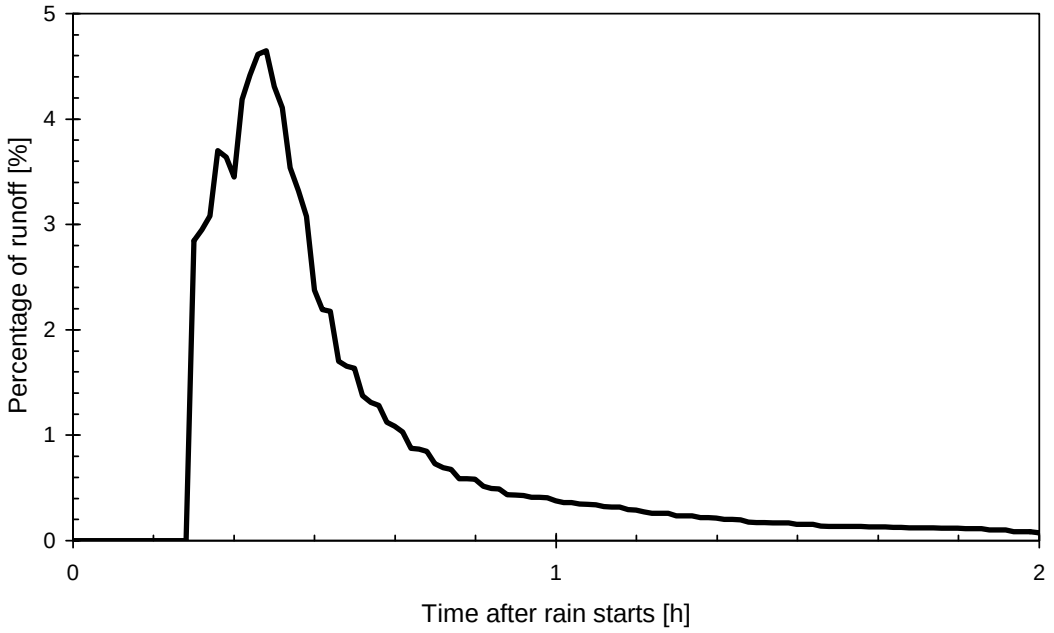

Fig. 6.6 Mean response function of runoff concentration

6.3 Channel flow and transmission losses

6.3.1 Spatial disaggregation

The spatial disaggregation of the channel network had already been performed for runoff concentration (Chapter 6.2.1). For each of the 419 channel segments seven model parameters had to be determined resulting in 2933 different parameter values. However, in a thorough field survey clear similarities between single channel reaches appeared. A classification into different channel types seemed reasonable reducing the number of independent parameters to be determined. The idea of grouping channels into types of similar morphological characteristics is not new. Straight, meandering and braided stream patterns were firstly described by LEOPOLD & WOLMAN (1957). SCHUMM (1977) tried to classify rivers using sediment transport, channel stability and measured channel dimensions. Recently, ROSGEN (1994) distinguished seven major stream type categories

differing in entrenchment, gradient, width/depth ratio and sinuosity. These categories were further subdivided according to the dominant channel materials. He claimed that regionalization of site-specific data was possible extrapolating data to channel reaches of the same type. MILLER & RITTER (1996) called the general applicability of this classification attempt into question. They thought that, among other deficiencies, the special character of arid-climate rivers was not properly accounted for. For the Zin channels a new, rather simple classification scheme was adapted to the model parameters to be regionalized. It was based on local field experience using classification criteria apparent in the field and on aerial photographs. Examples of the different channel types are given in the annex (Fig. A14-A17).

Channel type 1 is represented by channels flowing on flat loessial valley fills. A dense vegetation cover and limited channel incision are characteristic. Channels of this type are found in the upper Avdat Plateau where aeolian loess is widely distributed. Rather small catchment areas and low relief limit stream power and channel incision.

Channel type 2 is represented by a single clearly definable main channel. Linear channel erosion has lead to pronounced entrenchment. The channels may be straight or meandering with a rather coarse riverbed alluvium. Vegetation is limited to banks and high bars where flow velocities during ephemeral floods are reduced. Channels are further subdivided (types 2a and 2b) according to the underlying strata. In general hard rocks (e.g. limestones and dolomites) limit channel incision and vertical extent of the channel alluvium, while thicker alluvial reaches form on soft sediments (e.g. marls and conglomerates).

Channel type 3 consists of a braided channel system. Total cross-sectional width may exceed 500 m. This channel type is found at the Massos-Aqrabim reach with pronounced transmission losses.

Channel type 4 is limited to steep headwaters and are characterized by waterfalls and rocky reaches. Most alluvial deposits have been removed and flow obstacles by large boulders are prominent.

6.3.2 Parametrization

Topographical maps yielded parameter values for flow length and slope independently for each channel segment. For channel width, however, a representative average was needed not sufficiently represented by a single cross-section. Remotely sensed information from airphotos were used for this purpose. The area of active channel alluvium between two channel nodes was digitized and divided by the respective flow length (Fig 6.7). All steps were easily performed inside the GIS. The GIS-derived channel routing parameters are listed in the annex (Tab. A3). For the remaining model parameters the used channel classification scheme reduced the number of independently determined parameter values from 419 (for each channel segment) to five (for each channel type). Values are summarized in Tab. (6.3).

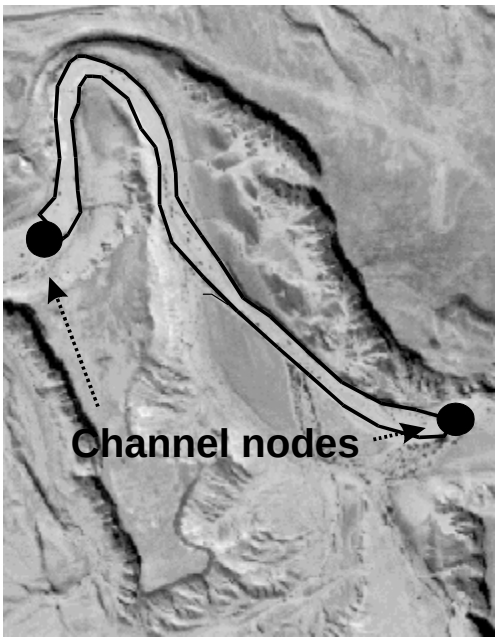

Fig. 6.7 Determination of a spatially averaged channel width

Tab. 6.3 Characteristics of the different channel types

Type	Description	Manning n	Infiltration rate		Depth of the active alluvium [m]	Percentage covered by inner channels [%]
			Channels [mm hr^{-1}]	Bars [mm hr^{-1}]		
1	Channel on loessial alluvium, vegetation in channel	0.05	44	44	2	20
2a	Confined channel entrenched into hard rocks	0.03	420	110	1	45
2b	Confined channel entrenched into soft sedimentary rocks	0.03	420	110	2	45
3	Wide braided channel system	0.045	420	110	2	20
4	Rocky channel, waterfalls and boulders in channel	0.07	0	0	0	100

Channel roughness was assessed accounting for bed material, flow obstructions and vegetation cover. CHOW et al. (1988) and JARRETT (1985) provided extensive quantitative data for Manning channel roughness also applicable for the Zin channels. Type-1 channels are characterized by an accentuated micro-relief and a dense vegetation cover. This increases channel roughness decisively despite the silty uniform bed material. A Manning n of 0.05 resulted. Independent from the underlying strata type-2 channels are

characterized by the lowest channel roughness. Channels are straight or follow large meanders. Usually the riverbed alluvium consists of a cemented mixture of gravels and fines forming a smooth surface. Also sandy reaches are found and no vegetation there to reduce flow velocities. A Manning n of 0.03 resulted. In type-3 channels diversion of flow to several sub-channels and vegetation on the channel bars decelerate overall flow velocity. Although the roughness of the sub-channels compares to that of the type-2 channels, the compound value of the entire type-3 section is therefore higher, amounting to 0.045. Flow obstructions by large boulders and waterfalls increase the roughness of type-4 channels. A Manning n of 0.07 was estimated as a representative average.

Infiltration rates of the channel alluvium were assigned studying the surface characteristics of the riverbed alluvium. Despite the vegetation cover the infiltration characteristics of type-1 channels were limited by a topsoil crust of the loessial/silty channel alluvium. SHANAN (1975) measured the depth of the wetting front after a two-hour flood under these conditions calculating an average infiltration rate of 44 mm hr^{-1}. This value was assigned to both the inner channels and the bars of type-1 channels, since surface properties were not markedly different. Type-4 channels did not contain significant riverbed alluvium. Infiltration losses into the rocky channel bed were therefore neglected. For the remaining channel types a distinction between inner channels and bars was important, as the silt content differed considerably. In the lower Zin KÜLLS et al. (1995) carried out two infiltration tests; one on a bar covered by a thin silty layer and one on a gravelly channel surface. The results were fitted to analytical infiltration models. At both sites a constant infiltration rate was reached quite soon (after approximately five minutes), the magnitude of this rate, however, was very different. While a double-ring infiltrometer on the silty bar yielded about 110 mm hr^{-1}, the infiltration on the gravely channel surface measured by a single-ring infiltrometer approached almost 500 mm hr^{-1}. The latter infiltration rate had to be reduced to account for lateral spreading of the wetting front resulting in a mean value of about 420 mm hr^{-1}. Since surface characteristics of bars (covered by a silty crusted surface layer) and inner channels (mixture of gravels and fines) were similar throughout the drainage network on type-2 and type-3 channels, 110 mm hr^{-1} and 420 mm hr^{-1} were used as representative mean infiltration rates.

Only limited field data of the vertical extent of the Zin riverbed alluvium exist. Throughout the course of the main channel the rocky bedrock crops out frequently. In several pits KÜLLS et al. (1995) reached the underlying bedrock at about 1 m in the lower Nahal Zin. RODED (1983), reported minimum depths of 5 m and maximum depths exceeding 47 m in the Massos-Aqrabim reach. These values show great variability making an estimation of an active alluvial depth very difficult. However, field evidence of various sources points to the assumption that not the entire depth of an alluvial body is active for water losses during a flood event.

LEKACH (personal communication 1996) discovered a compacted layer at a certain depth within alluvial sediments in the southern Negev, the so called ‘Red Layer’. This layer might represent a base level for channel erosion and might impede vertical infiltration. In three trenches inside the channel alluvium of Nahal Yael the Red Layer was reached at shallow depths of only 50 cm (LANGE et al. 1996).

Fine sediments deposited during flood events in Namibia reduced infiltration losses considerably (CREAR et al. 1988). Field observations in Saudi Arabian wadis may confirm this process, as unsaturated conditions in the upper riverbed alluvium were observed during flood events (WHEATER personal communication 1997).

The perennial springs of Ein Aqrabim and Ein Zin are discharging all over the year originating from a local alluvial aquifer in the Massos-Aqrabim reach replenished by flood waters. Hence a saturated zone at the bottom of the riverbed alluvium survives the dry summer and limits the storage available for infiltration losses.

The active depth of the alluvium was assumed to be a function of the underlying strata. In channels incised into hard rocks (type 2a) a depth of 1 m was estimated, while in soft sediments (types 1, 2b, 3) this depth was doubled. Type-4 channels did not contain any channel alluvium.

To quantify the percentage covered by inner channels, 74 cross-sections were measured and analysed. The complete data are given in the annex (Tab. A2). Where a main channel was clearly defined (channel types 2a,b), it, on average, covered 45 % of the entire cross section. In braided channel sections (channel type 3) and on loessial valley fills (channel type 1) this value was considerably lower (approximately 20 %). Type-4 channels covered the entire cross section. The bankfull stage was rather constant throughout the drainage network. Respecting the elevation of the channel bars a representative value of 1.5 m for all channels was assigned.

7 Flash flood simulation at Nahal Shahmon

7.1 Site and experiment

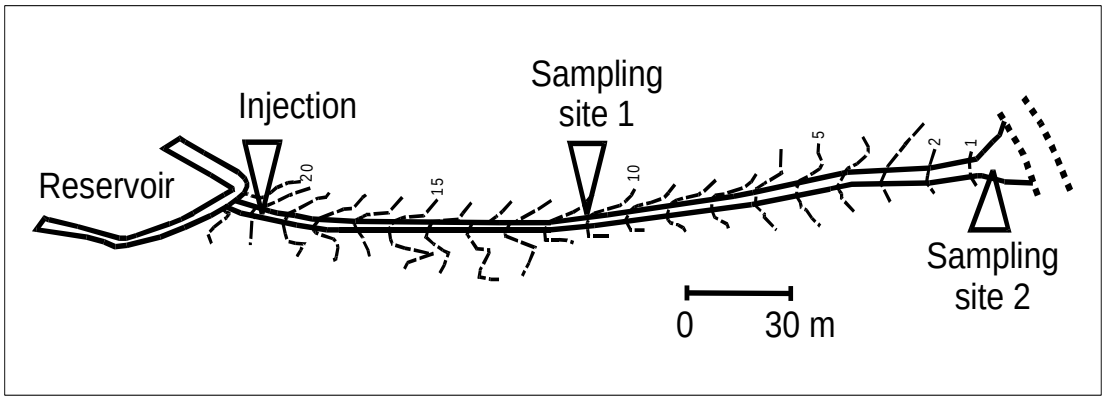

Fig. 7.1 Experimental setup

Nahal Shahmon, a small ephemeral stream channel in the southern Negev, drains an area of about 4 km^2 towards the town of Eilat into the Red Sea. Bare outcrops of magmatic and metamorphic rocks dominate the catchment. The climate is hyperarid with mean annual rainfall below 50 mm. Upon exiting the mountains, the channel is confined for about 250 m with a steep slope (Fig. 7.1). This section has been used as a dirt road and was chosen for an artificial flood experiment (SCHICK et al. 1996). A reservoir was built, filled with water (550 m^3) and breached artificially. When the first water spilled over the reservoir, an acoustic signal by a gunshot facilitated clock synchronization. Then the outflow was determined measuring the falling water level inside the reservoir. After about 2.5 min the water table dropped below the pressure sensor and an exponential function was fitted to reconstruct the remaining outflow (Fig. 7.2).

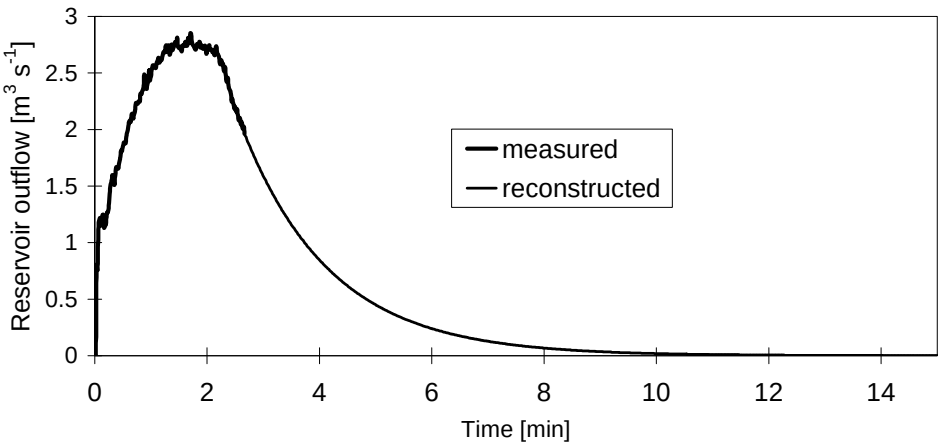

Fig. 7.2 Measured and reconstructed reservoir outflow

At different times three artificial tracers were injected about 10 m downstream the breach (LANGE et al. 1998). Approximately five seconds after the breach the flood passed the site of injection and Sulforhodamine (SRB, 400 g) was injected directly into the wave front. Uranine (UR, 400 g) was injected 45 s later and salt (NaCl, 15 kg) was injected close to peak discharge after another 50 s.

Surface water samples were taken at two locations (Fig. 7.1). Sampling site 1 was located about 120 m downstream the dam near the left bank. Sampling site 2 was located about 240 m downstream of the dam. Here the location of sampling was close to the right bank. The infiltrating water was sampled directly within the unsaturated zone. This was done by *fluocapteurs* placed about 20 cm beneath the channel surface at several locations. Within two trenches depths up to 1.5 m were reached. Fluocapteurs consist of small steel mesh bags containing approximately 10 g of adsorptive charcoal. The fluorescence tracers in the infiltrating water were adsorbed by the charcoal and kept inside the samples. After the event the fluocapteurs were recovered and analysed for the adsorbed tracers.

At sampling site 1 (Fig. 7.3) the initial background concentration of NaCl was very high as the flood water dissolved natural salt deposits in the channel. The measured concentration of salt declined exponentially and the signal from the injected 15 kg of salt can be seen as a small peak on this recession. The natural salt background below this peak was approximated by hand assuming a constant value of 1 g l^{-1}. SRB showed very high concentrations at the beginning with exponential decline. During the experiment it was observed that this tracer concentrated near the left bank. Being injected at the very beginning of the flood, it proceeded along with the front. At this site UR generally showed low concentrations. Already during the experiment it was noticed that at higher stage, when UR was injected, the flood travelled near the right bank.

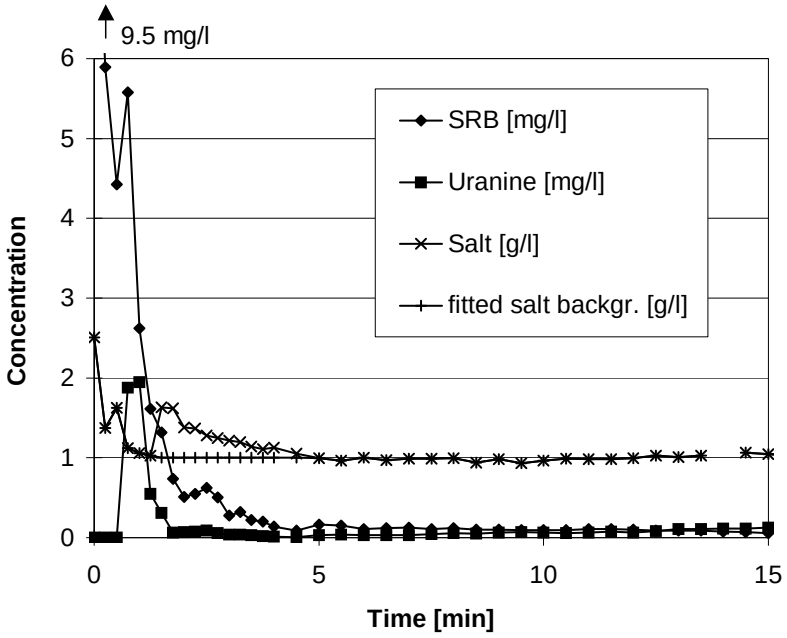

Fig. 7.3 Breakthrough curves at sampling site 1 (LANGE et al., 1998, modified)

Also at sampling site 2 (Fig. 7.4) the initial salt background was enormous. The signal caused by the salt injection spread out over small peaks on the overall NaCl recession. Similar to sampling site 1 the natural salt background below the NaCl-peaks was approximated by hand. This time the exponential decline was extended. Even the first water sample collected from the flood front contained traces of UR (0.05 mg l^{-1}), although this tracer was injected 50 s after the front had passed the site of injection. Hence an estimate of a maximum flow velocity was possible. Since the majority of UR travelled close to the right bank, a distinct breakthrough curve was recorded. The concentration of SRB showed characteristics similar to site 1. The peak, however, was significantly reduced, since the majority of SRB passed the site close to the opposite bank.

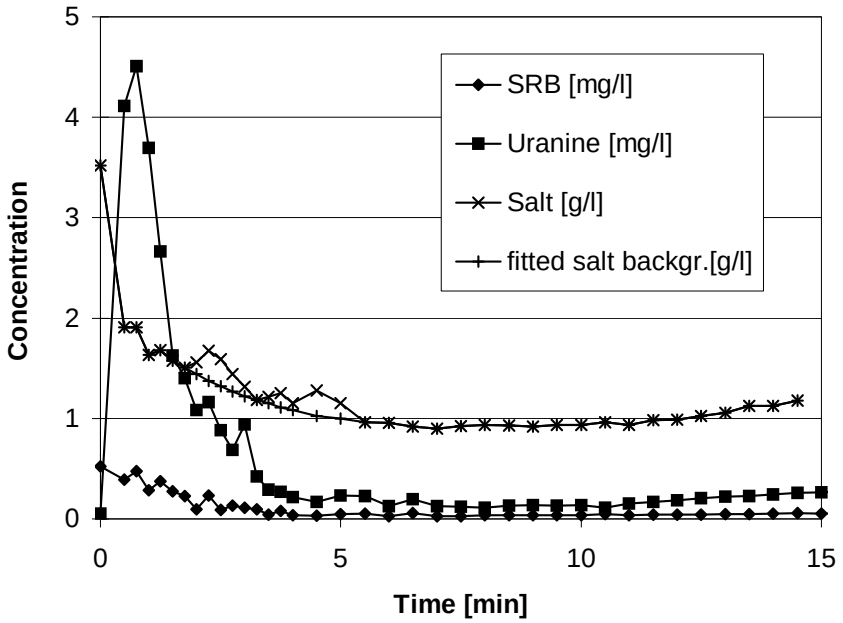

Fig. 7.4 Breakthrough curves at sampling site 2 (LANGE et al., 1998, modified)

7.2 Flow velocity and Manning n

To obtain tracer load and recovery, measured tracer concentrations at the sampling sites had to be combined with measured discharges from the reservoir outflow (Fig 7.2) representing the only available information on the pronounced temporal discharge fluctuations. The results of the calculated tracer recovery were poor, because of three main reasons:

(a) compared to the short breakthrough, the sampling interval (30 s) was rather long,

(b) the lateral mixing was markedly incomplete, obvious in the different flow paths of UR (right bank) and SRB (left bank),

(c) calculating tracer load using concentration and discharge values not determined at the same location introduces errors when the hydrograph shape changes downstream.

Due to the high salt background, which had to be manually fitted and then subtracted from the tracer breakthrough, NaCl should be considered with even more caution than UR and SRB. This is confirmed by completely unrealistic salt recoveries (Tab. 7.1).

Tab. 7.1 Travel velocities and calculated channel roughness values of the Nahal Shahmon flash flood simulation

		Distance [m]	Recovery [%]	t_1 [s]	t_{med} [s]	v_{max} [m s^{-1}]	v_{med} [m s^{-1}]	Manning n v_{max}	Manning n v_{med}
Site 1	flood front	120	-	50		2.4		0.033	
	SRB	110	137	45	120	2.4	0.9	0.033	0.088
	UR		53	40	70	2.8	1.6	0.029	0.049
	NaCl		720	35	65	3.1	1.7	0.025	0.046
Site 2	flood front	240	-	89		2.7		0.029	
	SRB	230	31	84	159	2.7	1.4	0.029	0.056
	UR		211	**34**	109	**6.8**	2.1	**0.012**	0.038
	NaCl		260	105	149	2.2	1.5	0.036	0.053

Still the travel times (t_1, t_{med}) determined by the three tracers allowed insights into the flow process in addition to the travel time of the advancing flood front which had been accurately measured at the two sampling sites. Starting from the dam (flood front) and the injection point (SRB, UR, NaCl) distances were measured down to the two sampling sites. Based on a topographical survey mean values for channel width (10 m) and channel slope (0.082) were determined. Estimating a flow depth of 0.15 m during the main phase of the flood, 0.145 m resulted for the hydraulic radius. With these data measured travel velocities could be translated into values of channel roughness applying the Manning equation:

$$n = (R_0^{2/3} S_0^{1/2}) / v \qquad (7.1)$$

where n is Manning roughness coefficient for the 240 m channel reach, R_0 the hydraulic radius, S_o is the channel slope and v is the flow velocity. Results are presented in Tab. 7.1, where t_1 is the time (after injection) when the first traces of tracer arrived at the site, t_{med} is the time when 50 % of the tracer load have passed; v_{max} and v_{med} are the respective velocities.

The maximum concentration of SRB, injected into the wave front, kept travelling with the front and only retarding components were responsible for longitudinal dispersion. Hence

v_{max} equalled the wave front velocity, while v_{med} was underestimated. At the sampling site 2 the high salt background blurred a clear breakthrough curve and results have to be treated with caution. In general the Manning n values grouped around 0.03. The outstanding v_{max} of UR at sampling site 2 (6.8 m s^{-1}) is an indication of the very high flow velocities possible in steep arid channels. Similar high values had already been reported by SCHICK (1968) and COSTA (1987).

7.3 Mean infiltration rate

Two fluocapteurs exposed at greater depths, 40 and 60 cm, had small traces of UR. Due to the higher sorptivity on SRB this tracer could not be found. Both samples were located close to the right bank. This was the main route UR travelled downstream. Although two samples are not sufficient to describe the spatial extent of the infiltration within the whole wadi, they provide the maximum depth of the wetting front at two specific points. This information may be used to estimate the magnitude of infiltration during a real flood event.

A model of time-dependent infiltration based on exfiltrating water from the alluvium proved that infiltration was not constant in time (LANGE et al. 1998). Still a mean infiltration rate was calculated since it was needed for the model and adequately described riverbed infiltration elsewhere (e.g. KÜLLS et al. 1995):

$$I = (d_w \, stor_{al}) / t_f \qquad (7.2)$$

where I is the mean infiltration rate, d_w is the depth of the wetting front, $stor_{al}$ is the available storage for losses in the channel alluvium governed by the porosity, and t_f the duration of the main flood.

During infiltration tests KÜLLS et al. (1995) found out that only about 16 % of the total volume of riverbed alluvium was available for water storage. This was attributed to entrapped air and silty layers. For the present estimate a value of 20 % was assigned for $stor_{al}$, since almost no silt was contained in the course alluvial sediment. The two charcoal samples were located beneath the main travel path of the flood. For t_f a value of 11 min was assigned after which flow had dropped below 10 l s^{-1}. With a mean value of 0.5 m for d_w approximately 550 mm hr^{-1} resulted for I.

7.4 Application of different routing schemes

The Shahmon flood experiment provided relevant data to test different physically based, distributed flow routing schemes. The outflow from the reservoir served as input into a

240 m straight channel reach. Due to the use as a dirt road cross-sectional geometry could be reasonably approximated by a simple rectangle. From the reservoir down to sampling site 2 the study reach was subdivided into eleven segments with independent parameters of width, slope and flow length each determined from a topographical map (scale 1:250) drawn by a surveying company. Following the above calculations a Manning n of 0.03 represented channel roughness and a constant value of transmission loss (550 mm h^{-1}) was subtracted from runoff at every channel segment.

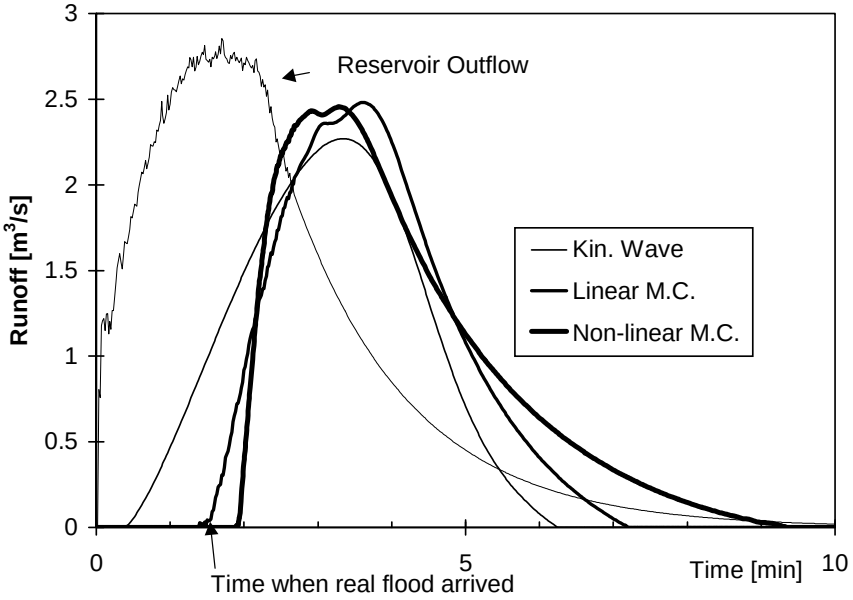

Fig. 7.5 Comparison of the different routing schemes

Using a time step of 1 s three different routing schemes were compared (Fig. 7.5). Solving Equations (5.1) - (5.8) two different modes of the Muskingum-Cunge technique were applied: in a linear mode a constant representative mean value of 1.5 $m^3 s^{-1}$ was assigned to the reference discharge Q_{REF}, while in a non-linear mode Q_{REF} was re-calculated for each time- and distance step using Equation (5.9). For a numerical solution of the kinematic wave a simple explicit scheme was used (CHOW et al. 1988). Therefore space- and time derivatives of the discharge were substituted by finite backward differences:

$$\partial Q/\partial x \approx (Q_{i+1,\,j} - Q_{i,\,j}) / \Delta x \qquad (7.3)$$

$$\partial Q/\partial t \approx (Q_{i+1,\,j} - Q_{i+1,\,j-1}) / \Delta t \qquad (7.4)$$

where Δt is the time step, Δx is distance between two nodes, $Q_{i+1,\,j}$ is the unknown discharge at the next node at the present time step, $Q_{i,\,j}$ is the discharge at the present node at the present time and $Q_{i+1,\,j-1}$ is the discharge at the next channel node at the last time step. As a result the unknown value of $Q_{i+1,\,j}$ could be computed as a single linear function of the two known values of Q ($Q_{i,\,j}$ and $Q_{i+1,\,j-1}$) (CHOW et al. 1988). For more details on

the different routing schemes the reader is referred to the listings in the annex (Listing A4/A5).

All simulations smoothed out the small discharge fluctuations recorded by the pressure sensor. The kinematic wave could not simulate the steep rise of the flood and completely overestimated the celerity of the flood front (Tab. 7.2). Shape and timing of the flood were better described by the Muskingum-Cunge technique. The linear mode only transferred the shape of the reservoir outflow downstream reducing the discharge values because of infiltration losses. The calculated flood arrival was nearly perfect, while the recession was aborted. The simulated non-linear flood arrived 25 s too late. Still only this hydrograph showed effects of flood front steepening and flow recession as predicted by theory. Peak discharges and flow volumes simulated by the three routing schemes were similar.

Tab. 7.2 Hydrograph characteristics of the simulated floods at sampling site 2

	Reservoir Outflow	Observed	Kinematic Wave	Linear M.C.	Non-linear M.C.
Flood arrival [s]		89	24	85	114
Front velocity [m s^{-1}]		2.7	10	2.8	2.1
Peak [m^3 s^{-1}]	2.85		2.27	2.48	2.45
Flow volume [m^3]	550		411	414	443

7.5 Discussion

The application of the artificial tracer technique allowed to study two parameters relevant for the Nahal Zin model in a real flood event travelling through a 240 m channel reach: Manning channel roughness and mean infiltration rate of the channel alluvium. The results have to be treated with caution mainly due to incomplete lateral mixing and the uncertain calculation of tracer load. Additional experiments in different ephemeral channels would be needed for more general statements. Still the evaluated mean values compare reasonably to parameters determined in other field studies. Except for the extreme v_{max} of UR at sampling site 2 and the generally retarded v_{med} for SRB, Manning n values fall within the ranges given for natural stream channels (CHOW et al. 1988, JARRETT 1985). The calculated mean infiltration rate was 30 % higher than that measured in the lower Nahal Zin (KÜLLS et al., 1995). This difference may be attributed to a lower silt and clay content in the alluvium, as in Nahal Shahmon channel sediments originate from entirely magmatic and metamorphic lithology. In general studying transmission losses by the present technique seems promising. Using several fluocapteurs at different locations and depths may help to overcome the problem of transferring results from ‘artificial’ point scale measurements (infiltration tests) to real floods covering entire channel reaches.

Often distributed routing schemes have been tested by purely constructed problems, i.e. the THOMAS (1934) classical problem where a sinusoidal flood wave with a 96 hr period is routed through a prismatic channel 500 miles long (PONCE & CHAGANTI 1994). Also statistical distribution functions, i.e. a four parameter Pearson type-III function (PERUMAL 1992) were used to represent natural flow hydrographs. In humid streams natural flood waves were successfully simulated by distributed flow routing schemes. Examples are given in the British Flood Studies Report (NATURAL ENVIRONMENT RESEARCH COUNCIL 1975) or by FREAD (1985, 1993). In arid streams the problem of transmission losses has limited the use of flow routing schemes to hydrological/lumped approaches with calibrated parameters. Often only the volume and the peak discharge are described (e.g. LANE 1985), a complete hydrograph may then be approximated by a triangular shape (SHARMA et al. 1994, 1998). KNIGHTON & NANSON (1994) calibrated the conventional three parameter Muskingum procedure to flow events in arid Australia.

Although no discharge measurements downstream of the reservoir were available for a more thorough check, this experiment provided an excellent framework to study real flood events in the scale of small arid channels. By measurements of the reservoir outflow the inflow hydrograph into the reach was quite exactly known, although flow recession had to be reconstructed. Measurement problems with unstable cross-sections due to scour and fill were circumvented. The existing geomorphological survey showed that channel geometry could be reasonably approximated by rectangular cross-sections. Due to the use as a dirt road the 240 m study reach consisted of a singular, straight and clearly defined channel with almost vertical banks.

Under these circumstances the simple explicit solution of the kinematic wave performed poorly and did not prove to be applicable for the fast rising hydrograph of the Nahal Shahmon flash flood simulation. These findings correspond to recommendations of FREAD (1993) stating not to use kinematic wave models for channel routing when hydrographs are fast rising and attenuation is pronounced. In contrast the Muskingum-Cunge technique provided better results, while only the non-linear mode could predict wave steepening as observed during the experiment. Moreover, the linear mode required an a-priori estimation of a constant reference discharge Q_{REF}. In arid ephemeral channels with accentuated transmission losses this seems an impossible task making only the non-linear mode applicable. For all three routing schemes the simulated volume losses (approx.: 110-140 m^3) were considerably smaller than those (approx.: 250 m^3) calculated for 11 min flood on a 240 × 10 m channel reach with a constant infiltration rate of 550 mm hr^{-1}. A part of this underestimation derived from a decreasing flow duration caused by transmission losses (the non-linear Muskingum-Cunge technique simulated only 7 min at the lower end of the reach). Still it seems that distributed routing schemes more accurately predict the peak of arid zone flash floods than their volume.

8 The October 1991 event

8.1 Event characteristics and available data

As part of a widespread rainstorm system on 13/10/1991, a major thunderstorm was active in the Sinai, Negev and southern Jordanian mountains (GREENBAUM et al. 1998). The storm advanced from south to north producing large floods in the neighbouring wadis of Nahal Zin. In the southern vicinity Nahal Paran (3,350 km^2) peaked at 248 $m^3 s^{-1}$ and Nahal Neqarot (697 km^2) at 104 $m^3 s^{-1}$. In the north, Nahal Beer-Sheva (1,220 km^2) flooded several neighbourhoods in the town of Beer-Sheva with a peak discharge of 247 $m^3 s^{-1}$. Inside Nahal Zin already during the preceding night small thunderstorms had occurred producing only a few millimetres of pre-rain. They were negligible compared to the severe weather of the main storm event. At ground stations a sudden weather deterioration was observed with thunder, hail and an abrupt 8°C fall in temperature causing debris flows and severe damage to the town of Mitzpe Ramon.

A rainfall radar located at Ben Gurion Airport, Tel Aviv, was in operation, about 130 km north of the centre of the Nahal Zin catchment (Fig. 4.3). Every 5 min a radar scan of the complete catchment was made using a wave length of 5.4 cm and a 1.5 degree beam resulting in a cell size of about 3 km^2. Even at a distance of more than 150 km recorded radar echoes exceeded 50 dBZ indicating very high rain intensities. This detailed information showed that a huge single raincell entered the southern margins of Nahal Zin (Fig. 8.1). Then a curved squall line developed and crossed the catchment from south to north. Into this main convective rain system three inner core cells were embedded. Two of them hit the centre of the catchment leaving its northern tributaries at about 18:00, while a third, isolated one entered at about this time the western headwaters.

No completely gauged hydrographs were available, since all gauging stations went out of operation during this high magnitude flood. Therefore the ISRAEL HYDROLOGICAL SERVICE (IHS) determined the peaks by the indirect slope-area method (DALRYMPLE & BENSON 1967); 550 $m^3 s^{-1}$ was assessed at Mapal, 530 $m^3 s^{-1}$ at Massos. KIRBY (1985) estimated a root mean square error (RMSE) of 25 % for these evaluations. At a site 4.7 km downstream of the Aqrabim station results from a detailed paleoflood analysis were available (GREENBAUM et al. 1998). In this study high water marks of organic material, surveyed three days after the flood, were used to determine the October 1991 peaks. Then the hydraulic step-backwater model HEC-2 (HYDROLOGIC ENGINEERING CENTER 1982) was employed to determine water surface profiles and paleodischarges resulting in a peak of 550 $m^3 s^{-1}$. O'CONNOR & WEBB (1988) estimated the precision of estimated discharges by hydraulic modelling on the order of ± 10 %.

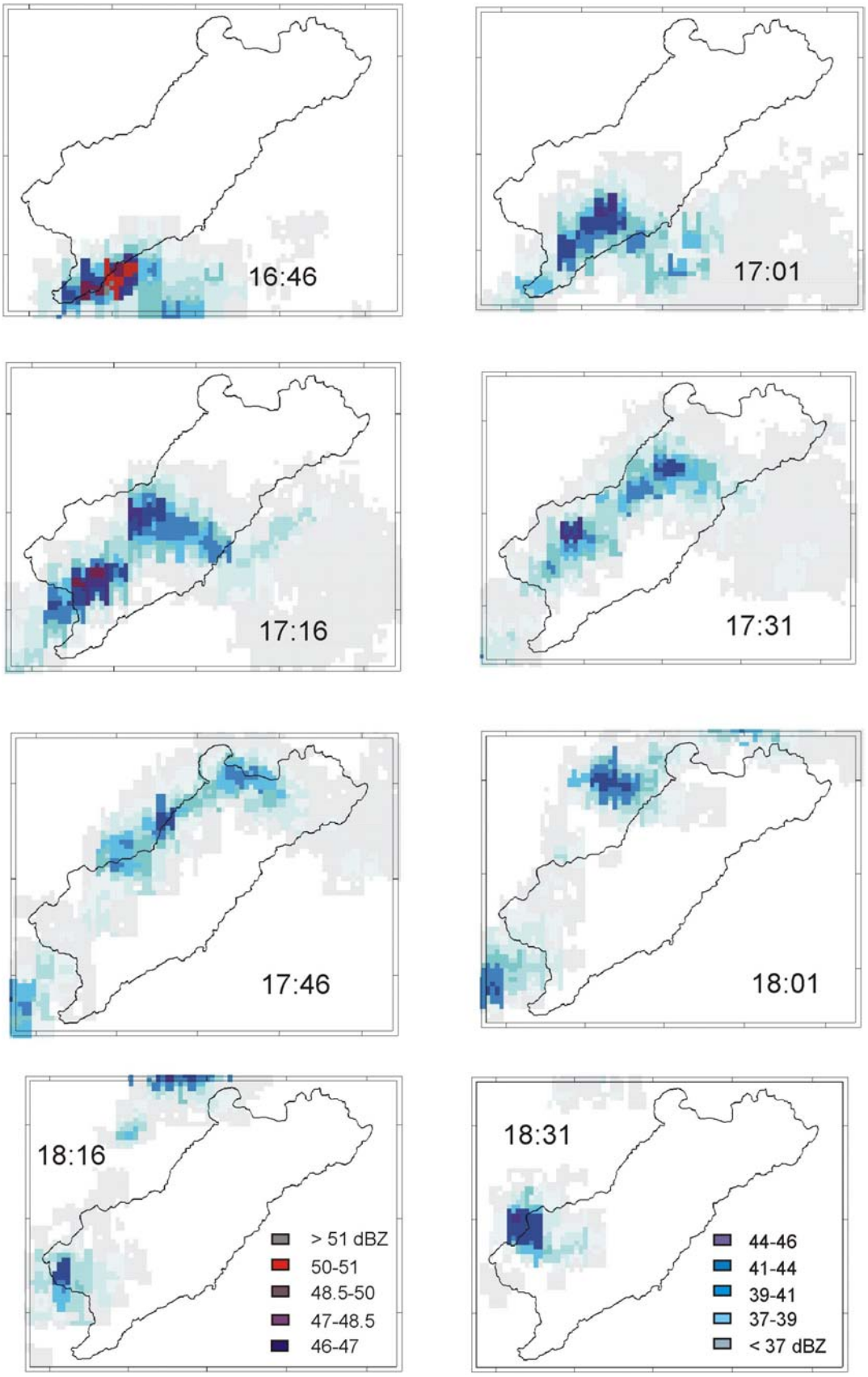

Fig. 8.1 Recorded refectivity values during 13/10/1991

8.2 Raingauge adjustment of the radar

The distance between radar location and precipitation over the Nahal Zin catchment ranged between 104 and 157 km. Still, typically for the limited data availability in the arid zone, no information was available to account for changes in the vertical reflectivity profile or in the Z-R relationship. Therefore a one-step raingauge adjustment of radar reflectivity was made. Data of six rainfall recorders were available (GREENBAUM et al. 1998).

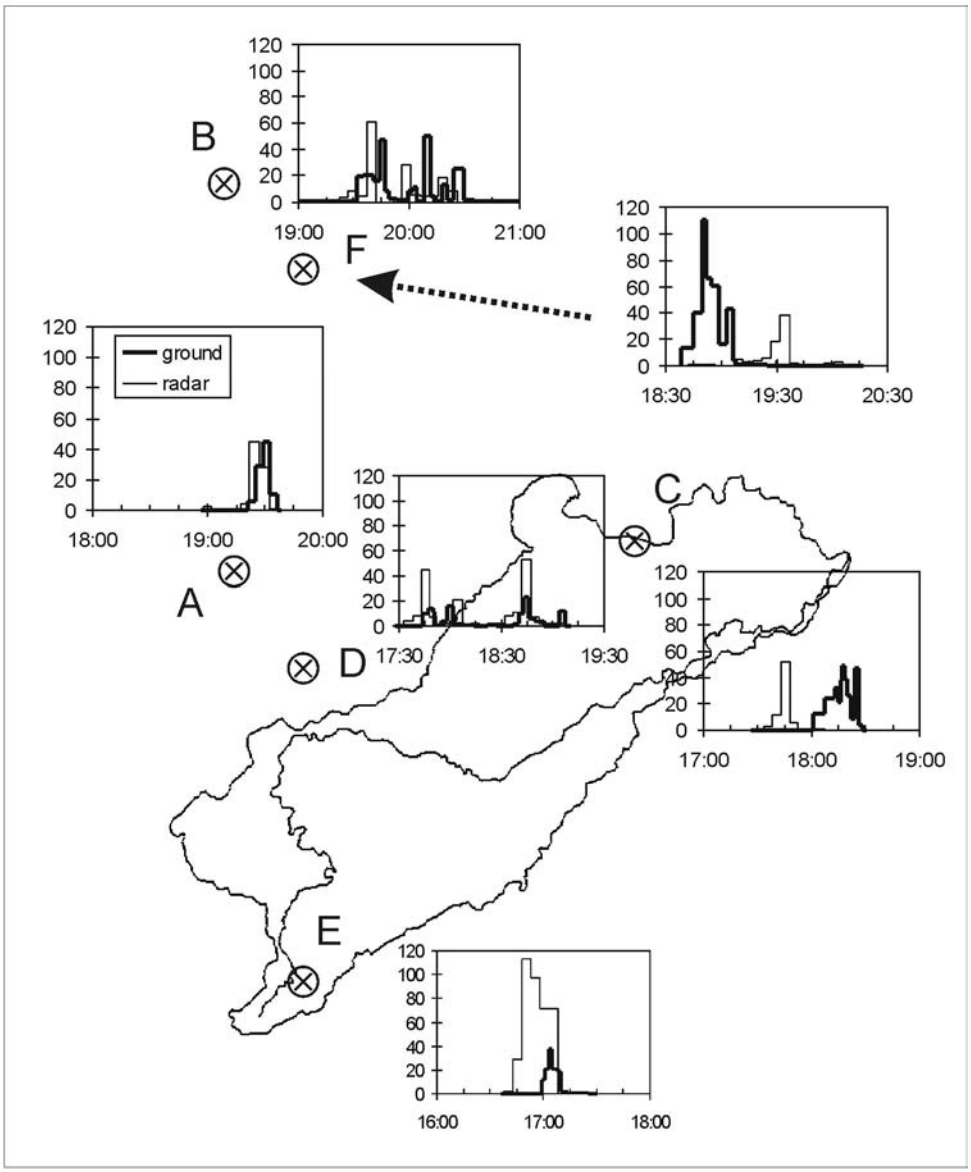

Fig. 8.2 Calibration of the rainfall radar, 13/10/1991

To translate measured reflectivity values of the radar (Z) into pre-adjusted rainfall intensities (R), a commonly used relation for thunderstorms, based on extensive measurements of sensitive rainfall recorders, was applied (SCHROTH 1995):

$$Z = 500\ R^{1.5} \qquad (8.1)$$

Then the magnitude of underestimation of the rainfall intensity caused by the long distance between the radar location and the sampling volumes was determined. At the six rainfall recorders the time distribution of ground rainfall and reflectivity measurements of the closest radar pixel were compared. The station with the best time correspondence was selected (Station A) and the maximum values of pre-adjusted rainfall intensities and ground measurements were fitted. As a result a value of 9.8 dBZ was added to the raw reflectivity data.

The different stations reflected the problems inherent with the one-step adjustment of rainfall radar with station data (Fig. 8.2, Table 8.1). Not a single radar pixel was centred directly above a ground station. However, the goodness of fit between ground station and calibrated radar did not depend on the distance between pixel centre and gauge location. Besides the adjusted maximum intensities, Station A revealed the best fit in timing and rain amount. Also the results of Stations B, C and D were satisfactory, although Station C showed a 30 min time shift. At Stations E and F the correspondence of calibrated radar and ground measurements was poor. Besides measurement errors of the ground gauges, the question arose how representative point measurements at these locations were compared to the spatial (about 3 km^2) and temporal (5 min) average value of the closest radar pixel.

Tab. 8.1 Radar calibration at the different stations

Station	A*	B	C	D	E	F
Location [Israeli Grid]	123.7 044.2	130.0 073.0	162.0 046.0	131.0 034.0	130.7 006.6	139.5 069.5
Centre of closest radar pixel [Israeli Grid]	124.4 044.2	130.8 073.6	162.8 046.2	132.0 034.3	130.0 006.4	138.9 070.0
Distance (Station/radar pixel) [m]	720	1040	860	1080	760	800
Maximum intensity measured at the ground [mm/h]	45	50	50	24	38	110
Maximum intensity derived by calibrated radar [mm/h]	45	61	53	52	113	39
Rain amount collected at the ground [mm]	5.3	15.7	10.7	6.6	4.2	19.5
Rain amount derived by calibrated radar [mm]	6.7	12.8	6.2	16.0	32.0	7.0

* used for calibration

To test the radar calibration, the maximum rainfall intensities of the radar pixels inside the Nahal Zin catchment were analysed. This was done for the original radar calibration described above and for two alternative runs using Station E and F as reference station, respectively.

(a) The original radar calibration (using Station A with the best timing) resulted in maximum values of 210 mm hr^{-1} corresponding well with extreme rainfall intensities measured elsewhere in the Negev, e.g. 200 mm hr^{-1} in the Nahal Yael experimental catchment (SCHICK 1988) or 224 mm hr^{-1} at Mitzpe Ramon.

(b) If Station E were used for radar calibration, radar and ground intensities could be aligned only adding 2.6 dBZ to the raw reflectivity data. Then maximum intensities inside the entire Zin catchment did not exceed 69 mm hr^{-1}, much too small to generate the high magnitude flood witnessed.

(c) If Station F were used, 16.6 dBZ had to be added to the raw reflectivity data. Then the maximum intensities of radar pixels inside the upper Nahal Zin exceeded 590 mm hr^{-1}. This value was more than 2.5 times higher than the maximum intensity ever measured in the Negev desert and seems completely exaggerated.

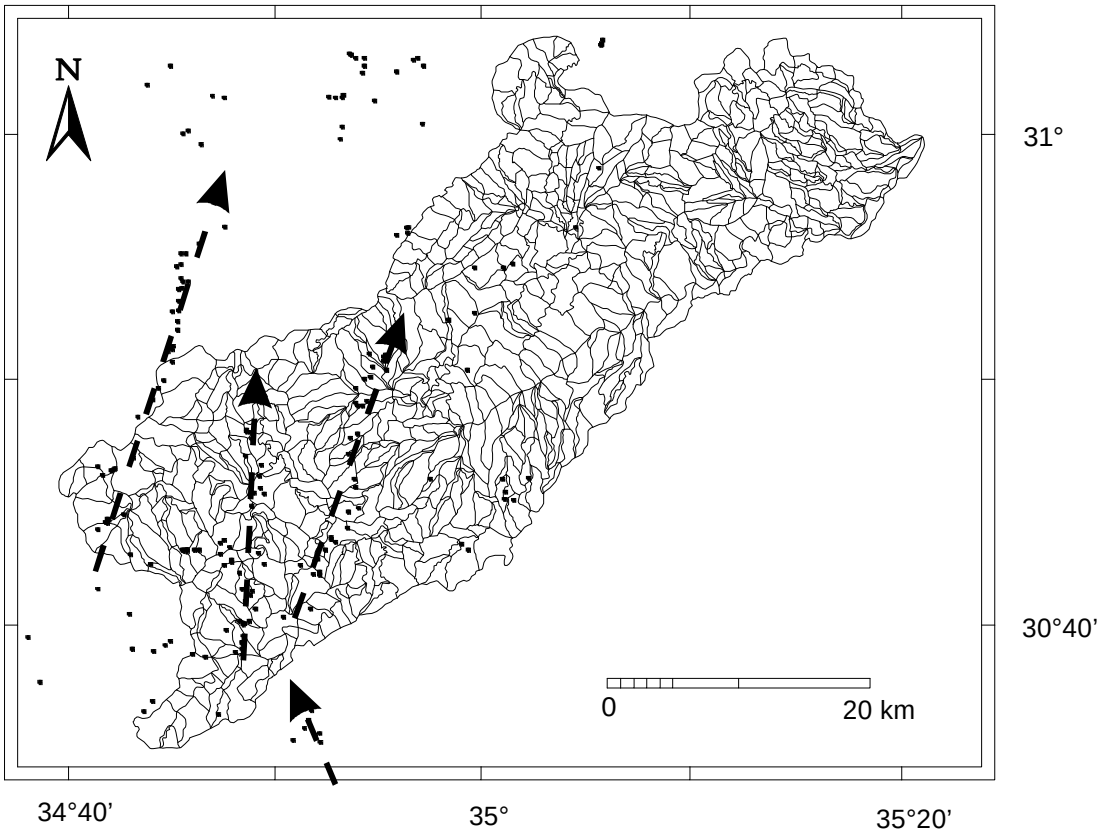

Fig. 8.3 Centres of areas exceeding 80 mm hr^{-1} rain intensity and main cell trajectories

The original radar calibration was incorporated as raster data sets into the GIS. Then it was possible to calculate intermediate spatial rainfall intensity distributions by linear averaging. Both steps were facilitated by AML-routines listed in the annex (Listings A1/A2). The original time step of 5 min by the radar was reduced to 1 min required for the model. To illustrate the spatial and temporal rain distribution, the centres of areas, in which the calibrated intensity exceeded 80 mm hr^{-1}, were marked every minute. Trajectories of the inner cells and their life times became visible (Fig. 8.3).

For the whole catchment a very uneven rain distribution resulted (Fig. 8.4). Rain was mainly concentrated in the upper part of the catchment reflecting the area of major cell activity. There peak amounts of total rain on a single gridcell exceeded 60 mm. This complex spatial pattern of fallen rain could not have been detected by a typically available number of conventional ground based rain gauges.

8.3 Model validation

The very detailed information on the rainfall input, provided by the calibrated rainfall radar, served as input to run all model components in succession. Compared to the rainfall the calculated spatially distributed Hortonian overland flow was considerably reduced but similar in pattern (Fig. 8.4). Only highly infiltrating surfaces (e.g. active channel alluvium) modified this pattern visibly. After the model routines of runoff concentration and channel routing were passed, simulated hydrographs could be obtained at any node of the distributed channel network. This enabled validation of the model structure with all its 'non-calibrated' parameters, using available field data at Mapal, Massos and the Paleoflood Site including runoff peaks and their uncertainty (Fig. 8.5). At Mapal the field peak was underestimated by 24 %. More downstream, at Massos and at the Paleoflood Site, a good agreement between simulation and field data was reached (deviation both below 10 %). In general, all simulated peaks were within the uncertainty ranges of the field data. The flow volumes increased from station to station, amounting to 3.6×10^6 m^3 at Mapal, 7.3×10^6 m^3 at Massos and 8.5×10^6 m^3 at the Paleoflood Site.

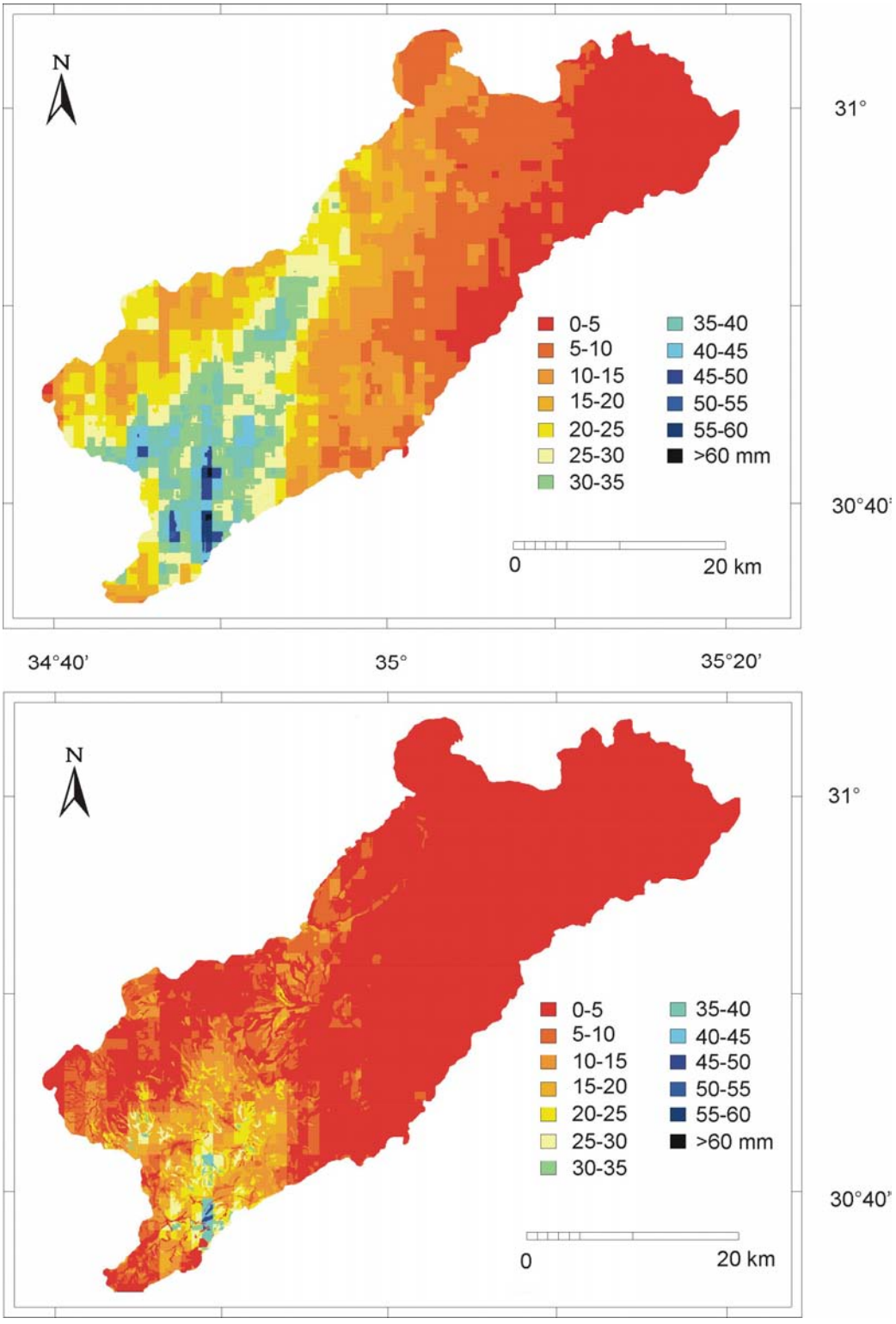

Fig. 8.4 Upper part: total rain, lower part: generated overland flow, 13/10/1991

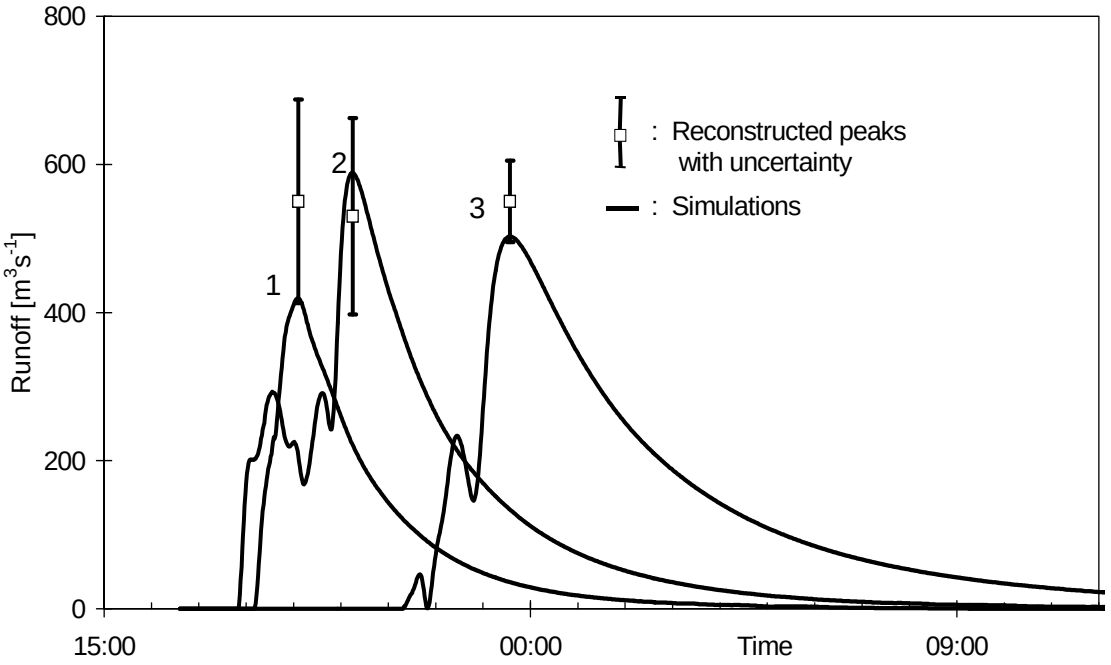

Fig. 8.5 October 1991: Model validation with reconstructed peak discharges, uncertainties of field peaks are given in brackets:
(1) Mapal (25%) (2) Massos (25%) (3) Paleoflood Site (10%)

8.4 Tributary input and flood generation

The spatially distributed structure of the non-calibrated model provided insight into processes active during the high magnitude flood of October 1991. Hydrographs obtained upstream and downstream of major confluences were compared to analyse the role the different major tributaries (Fig. 4.9) played for flood generation. Results indicated that the tributaries acted differently (Fig. 8.6). The most upstream tributary Nahal Avdat produced a large flood arriving simultaneously with the peak in the main channel. Downstream of the confluence the peak was significantly sharpened. Nahal Aqev and Nahal Hava responded much quicker and generated flood peaks arriving long before the main flood. Downstream of the confluence they travelled as preceding peaks in front of the main flood wave. Also the small peak of Nahal Hatira had a larger effect on these preceding peaks than on the following main one.

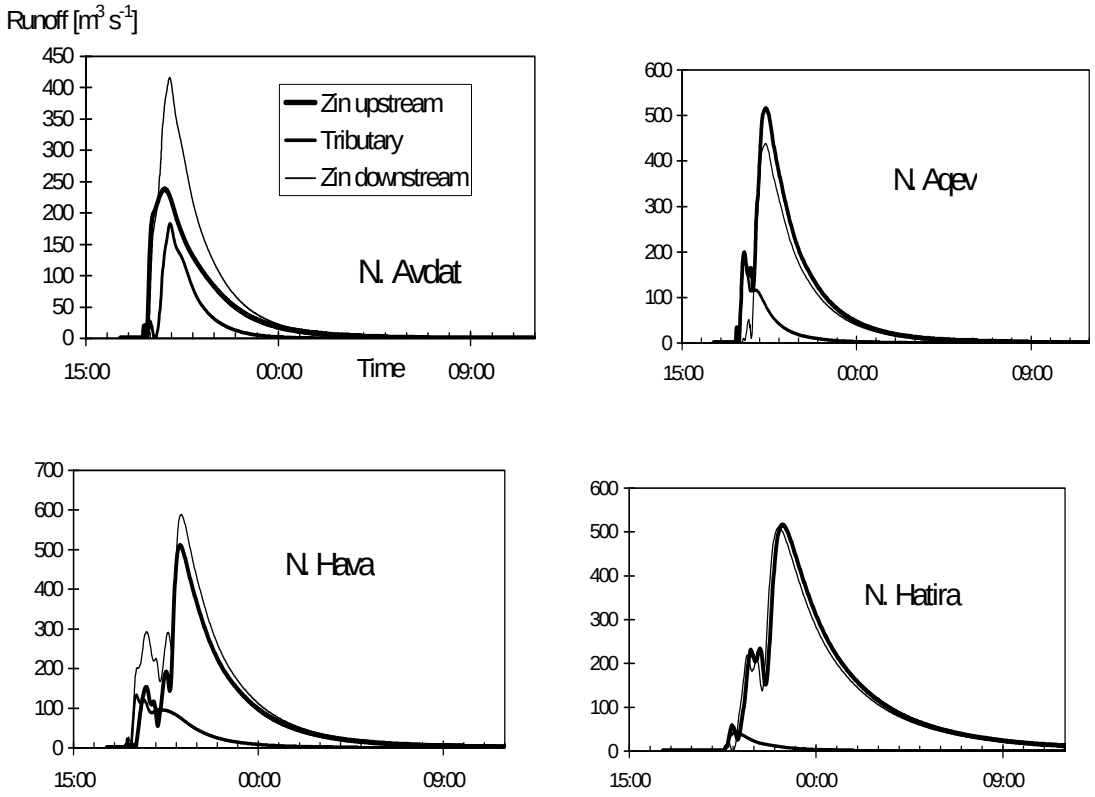

Fig. 8.6 Tributary response, October 1991

The marked time difference in the tributary response was the reason for a closer look at catchment characteristics and flood arrival times (Tab. 8.2). Despite its short main channel Nahal Avdat responded later than Nahal Aqev and Nahal Hava. Hence this delay had to be attributed to the time of beginning runoff generation rather than to a longer travel time in the channel network. The spatial pattern of runoff onset confirmed this assumption (Fig. 8.7). The westernmost parts of the Zin catchment, which contain the Nahal Avdat tributary, generated runoff only after 18:00, although the main curved squall line had already left the catchment by this time (Fig. 8.1). Hence the isolated cell that only touched the western margins of the Zin catchment (evident in the last three pictures of Fig. 8.1) had a decisive effect on the magnitude of the October 1991 flood. It postponed runoff response of the western headwaters to the time of high flow in the main channel and almost doubled the runoff peak.

Tab. 8.2 Channel length and flood arrival, October 1991

Tributary	Nahal Avdat	Nahal Aqev	Nahal Hava	Nahal Hatira
Length of the main channel [km]	19.9	30.5	38.7	36.5
Simulated flood arrival at the tributary mouth	18:55	18:12	18:03	20:06

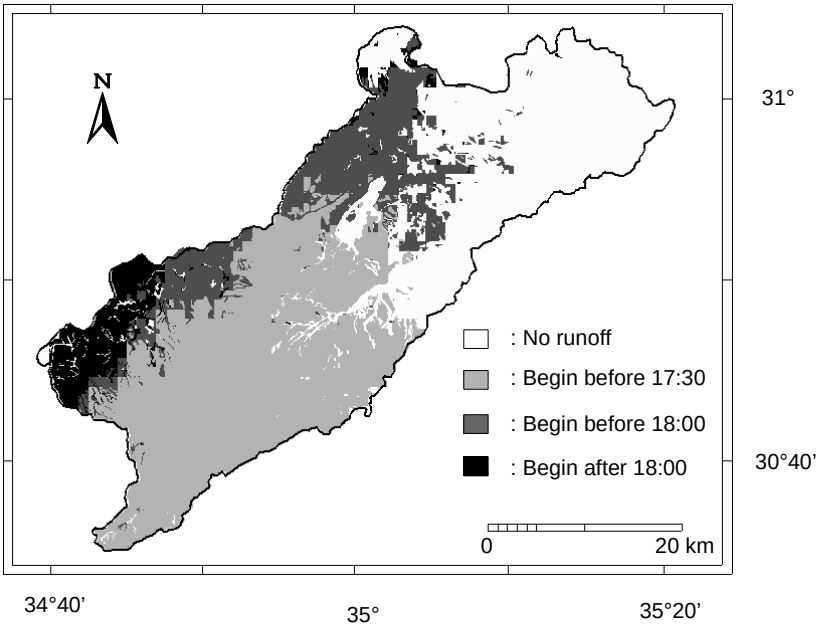

Fig. 8.7 Onset of runoff, October 1991

The influence of the remaining tributaries on the peak of the main flood was indirect. They wetted or even saturated the channel alluvium before the main peak arrived. Consequently the main flood wave rushed over a wet channel and was not further reduced on its way downstream. This fact can be noticed also in Fig (8.5). At Mapal only a single peak hydrograph was simulated. At Massos upstream entering tributaries (Nahal Aqev and Hava) were evident in an obvious preceding peak. At the Paleoflood Site 30 km downstream, most of this peak had infiltrated into the channel alluvium, while the main flood peak only reduced from 588 to 502 $m^3 s^{-1}$.

8.5 The following day

For the second day of the October 1991 event (14/10/1991) the radar showed a small rain cell hitting the catchment of Nahal Hatira (Fig. 8.8). A runoff peak of 300 $m^3 s^{-1}$ was reconstructed for this flood (GREENBAUM et al. 1998). As Nahal Hatira had already produced a small flood the day before, it was assumed that both the terrain and the channels were completely saturated. On the terrain types initial losses were neglected and the infiltration rates were set to their final value. Moreover, no transmission losses were incorporated into the simulation. However no data from ground stations were available to re-calibrate the radar data and the reflectivity-intensity-correlation from the preceding day had to be transferred. As a result, the simulated flood peaked at only 8 $m^3 s^{-1}$ and did not nearly reach the field-reconstructed value (Figure 8.9).

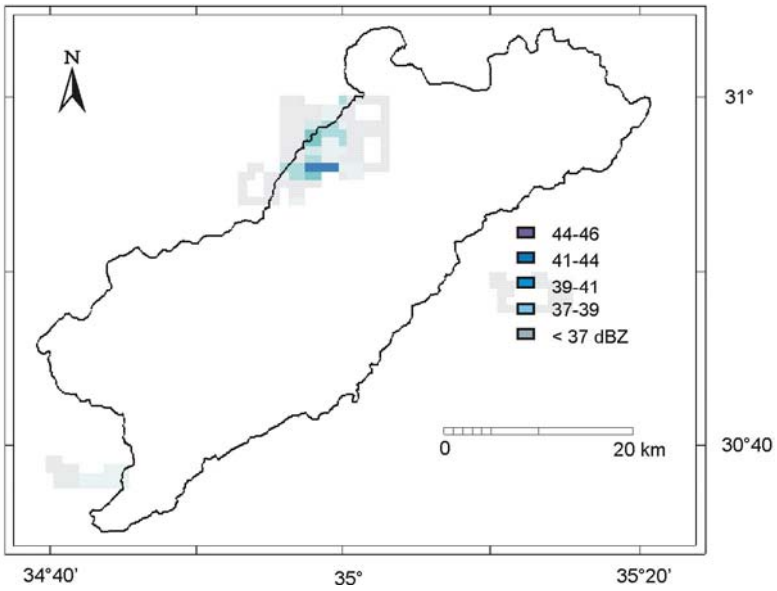

Fig. 8.8 A small raincell hitting the Hatira tributary, 14/10/1991

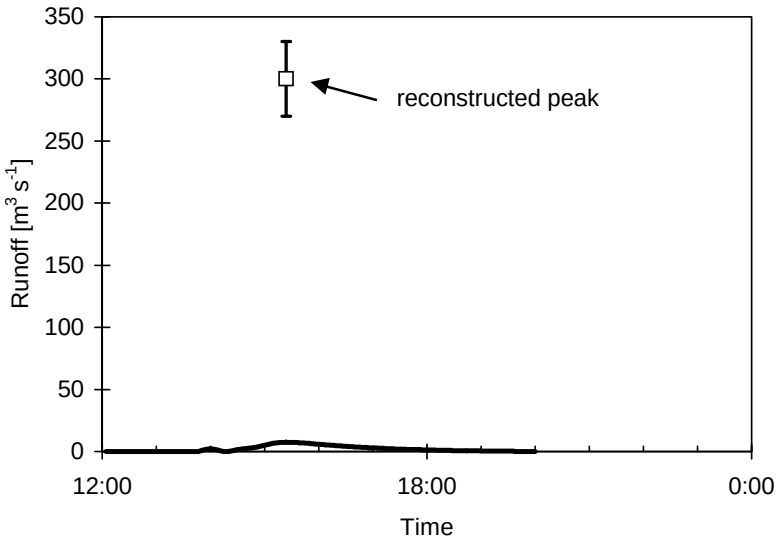

Fig. 8.9 Model failure, 14/10/1991

8.6 Discussion

The majority of large floods in the arid zone are generated, as a rule, by high intensity rainstorms of a limited spatial extent which are difficult to measure. Conventional ground measurements may be effective in very small catchments in which a reasonable gauge

density may be achieved. In larger catchments the number of gauges needed to evaluate the spatial variability exceeds reasonable numbers. Here the use of rainfall radar is an appropriate solution. However, considerable care is needed when adjusting radar measurements to ground rainfall, as shown by the two consecutive days in October 1991.

On 13/10/1991 six rainfall recorders were available for raingauge adjustment. Large differences between ground and radar intensities during the calibration procedure already pointed to problems of measurement errors and inadequate representativity of the ground gauges. However, over- and underestimates were balanced and a reasonable one step adjustment was possible for this day even without additional information on Z-R-relations or on vertical reflectivity profiles. Still, the high quality information on rainfall intensity of the six rain recorders was indispensable. On 14/10/1991 a small, isolated cell reached the catchment and disappeared after only 30 min. To translate the comparatively small reflectivity values into correct intensity estimates, measured ground data would have been required also for this day, but they were not available because the trajectory of the small cell moved entirely between existing raingauges. A transfer of the reflectivity-intensity-correlation from the preceding day resulted in a huge underestimate of rainfall intensities and simulated runoff. This demonstrates how problematic the transfer of results of raingauge adjustment from one storm to another may be, if both show different characteristics. If only reflectivity values are available, reasonable radar estimates of rainfall require at least one reliable ground station recording high rain intensities near a storm centre. Hence the use of rainfall radar does not fully replace a ground based gauging network. It only reduces the needed density from 25 (MICHAUD & SOOROOSHIAN 1994b) to roughly one gauge per 100 km^2.

The soundly calibrated rainfall radar of 13/10/1991 facilitated a complete model run which will be used in all following analyses. The simulated peak discharges fell within the uncertainties of the field measurements. For the flow volume of the entire flood, including the 14/10/1991-Nahal-Hatira peak, GREENBAUM et al. (1998) estimated 7×10^6 m^3. This estimate was possible analysing data of inundated salt evaporation pans located downstream of the Zin alluvial fan. Including only the main flood peak of 13/10/1991, the model simulated a flow volume of 8.5×10^6 m^3 at the Paleoflood Site. Hence the flow volume was a bit overestimated but still in a correct order of magnitude.

By its distributed structure the model served as a tool to analyze flood generation. The spatial pattern of generated overland flow generally compared to that of the rainfall input (Fig. 8.4). Hence almost the entire catchment was active, most runoff was generated in areas of major cell activity in upper parts of the catchment. An isolated cell postponed the response of the Nahal Avdat tributary. Downstream the main flood peak was sharpened which was responsible for the high magnitude flood at Mapal. Lower tributaries (Nahal Aqev, Hava and Hatira) produced preceding flood peaks causing an initial wetting of the alluvium. The following main flood crossed over a nearly saturated channel alluvium with a high flow velocity. Hence the effect of transmission losses on flood peaks may be limited when additional parts of a catchment are active.

9 The October 1979 event

9.1 Event characteristics and available data

In October 1979 one rainfall station located in the upper catchment at Mitzpe Ramon recorded the highest rain intensity (224 mm hr^{-1}) ever measured by a ground station in the Negev (Fig. 9.1). The hyetograph was characterized by a clear single peak with an almost sudden onset of rain. Data from other Negev stations were totally missing for this day. This points to a highly localized convective storm represented by a single supercell storm directly hitting Mitzpe Ramon.

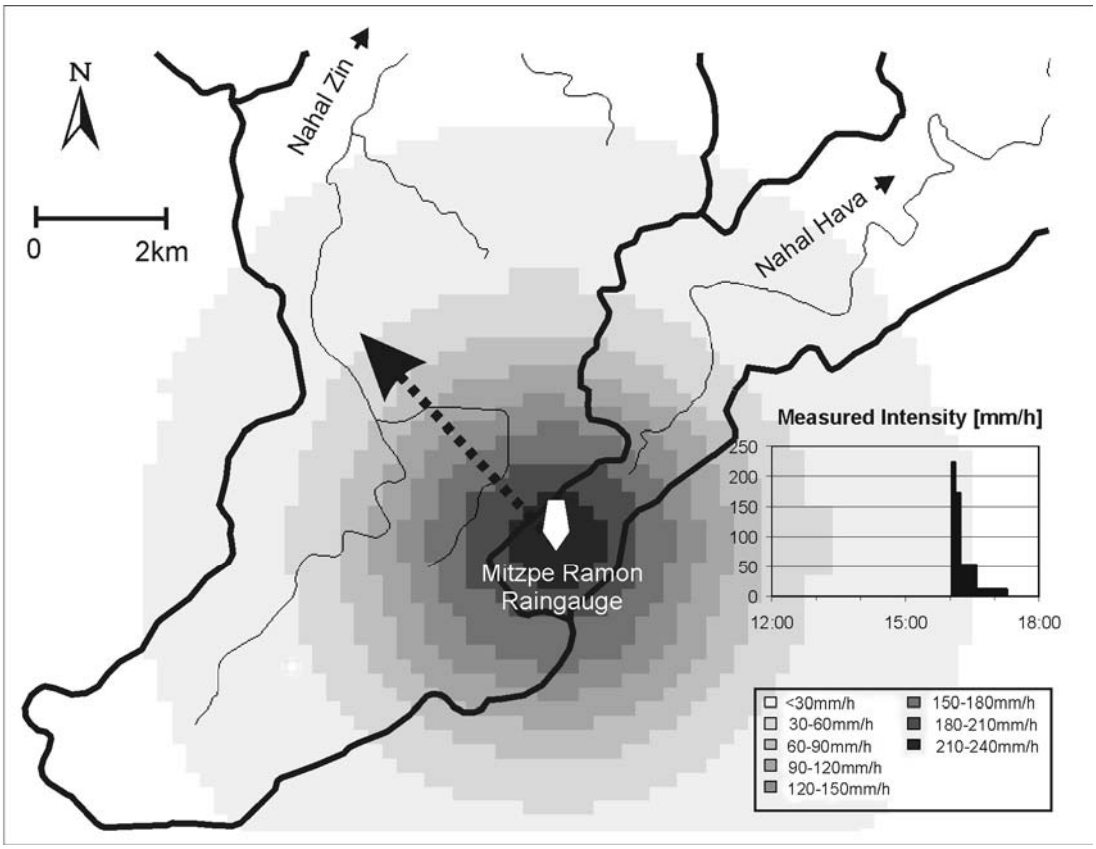

Fig. 9.1 Measured rain intensity at the Mitzpe Ramon Meteorological station and schematic representation of the spatial rainfall structure by a symmetrical cell

This assumption is confirmed by the runoff data available. Hydrographs from all the Zin stations exist, whereas Nahal Mamshit, a lower tributary, did not flow. Moreover, no preceding peaks were measured in the main channel and flood peaks and volumes

constantly decreased from station to station due to channel transmission losses (Fig. 9.2): Mapal: 324 $m^3 s^{-1}$, 2.04×10^6 m^3; Massos: 210 $m^3 s^{-1}$, 1.60×10^6 m^3; Aqrabim: 42 $m^3 s^{-1}$, 0.95×10^6 m^3. Hence runoff generation took place only in the uppermost Zin headwaters and no measurable tributary input occurred in the entire catchment. The water stage was recorded continuously making the unofficial rating scale of the Israel Hydrological Service (Chapter 4.5) applicable to estimate the uncertainty of the field peaks.

9.2 Validation of the routing component

In absence of tributary inflows the October 1979 hydrometric data provided an excellent framework to separately validate the routing component. The most upstream hydrograph at Mapal served as input and validation of the distributed routing procedure, containing only field derived input parameters, was done for Massos and Aqrabim (Fig. 9.2).

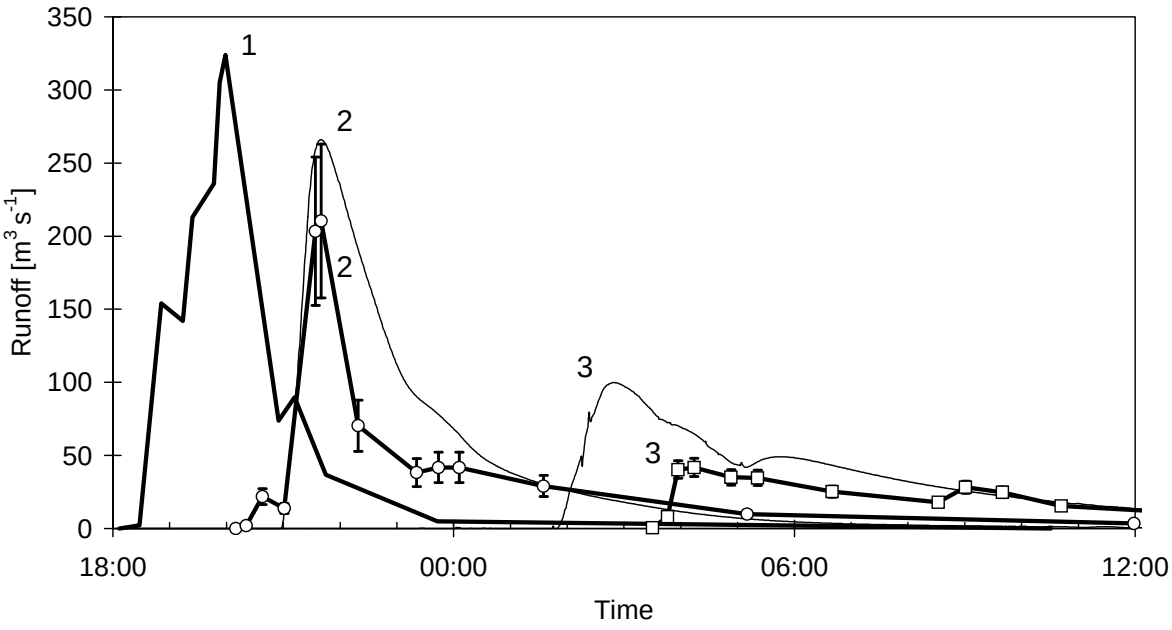

Fig. 9.2 Validation of the routing component, gauged hydrographs with uncertainties (in brackets)
fine: simulations, bold: gauged hydrographs
(1) Mapal (input), (2) Massos (25%), (3) Aqrabim (15%)

At Massos the simulated peak was 266 $m^3 s^{-1}$ (= 56 $m^3 s^{-1}$ or 27 % too high) and just exceeded the uncertainty of the field peak, while the timing was nearly perfect. At Aqrabim the simulated flood arrived 85 min too early and was 100 $m^3 s^{-1}$ (= 57 $m^3 s^{-1}$ or 135 % too high). Due to the same absolute overestimation the relative model error was

smaller for the large flood at Massos than for the diminished one at Aqrabim. The simulated flow volume increased slightly from Mapal (2.04×10^6 m^3) down to Massos (2.12×10^6 m^3) despite the presence of transmission losses. Only at Aqrabim (1.73×10^6 m^3) infiltration losses could be felt in the simulation. Modelled flow volumes exceeded those measured in the field by 32 % (Massos) and 83 % (Aqrabim). This implies that the distributed, non-calibrated routing scheme did not accurately conserve mass as already suspected during the flash flood simulation at Nahal Shahmon.

9.3 Tracing back the rainfall input

The database of the October 1979 event (high quality runoff data at three gauging stations but rainfall data at only one point) suggested an unorthodox use of the Nahal Zin model. It was used as a 'runoff-rainfall model' to reconstruct the input rainfall on the basis of known runoff hydrographs. Thereby a physically-related description of convective raincells was designed following the ideas of WAYMIRE et al. (1984). These authors represented the space-time field of ground level rainfall intensity by three component stochastic point processes. In space and time a system of circular raincells was embedded within clusters which, in turn, were embedded into storms. Their mathematical construction contained stochastic parameters (e.g. frequencies of cell arrival or birth) and physically based ones (e.g. cell's diameter or speed relative to the ground). ISLAM et al. (1988) used the method of moments to estimate parameters of such a 'physically based stochastic rainfall model' from station data of the Walnut Gulch experimental catchment. The model came out with a set of realistic parameters which satisfactorily reproduced historical data on cumulative rainfall.

In these models stormcells are assumed to be circular with an exponential symmetrical decay of rainfall intensity (i) around the cell centre:

$$i(r) = i_o \, EXP(-r^2/x) \qquad (9.1)$$

where i_o is the rainfall intensity at the centre, r the distance from the centre and x a measure of the cell's spatial extent. The Mitzpe Ramon hyetograph provided data on the maximum rain intensity during the October 1979 storm (approx. 224 mm hr^{-1}). Following relevant literature on the characteristics of convective stormcells (e.g. BURGES & LEMON 1977, DWD 1995) a cell diameter of 15 km, typical for supercells, was assigned. Assuming that the rain intensity dropped down from 224 mm hr^{-1} in the centre to 1 mm hr^{-1} at the cell's margin, 10.35 km^2 resulted for x (Fig. 9.1).

The results of four different model scenarios were compared with the measured hydrographs at the three gauging stations Mapal, Massos and Aqrabim (Fig. 9.3). First, a stationary cell was constructed decaying in time as recorded at the ground station. The resulting flood was too small and totally disappeared at Aqrabim (Scenario 1). Moreover, the hydrograph at Massos arrived earlier than at the uppermost station, Mapal, and was dominated by the fast-responding, steep and rocky tributary Nahal Hava. To improve the

simulations it was assumed that the ground measured intensity decay at Mitzpe Ramon was not caused by a temporal decay, but by a spatial displacement of the stormcell. The moving velocity was determined using (9.1) and the time spans until the rain intensity dropped from the recorded maximum (224 mm hr^{-1}) to the values of 172, 54 and 12 mm hr^{-1}. The resulting mean velocity (1.87 m s^{-1}) indicated a slow moving system. As most high intensity storms in the Negev originate from the Red Sea Trough in the south (BAR-LAVY et al., 1977) and as Nahal Hava was obviously inactive, the trajectory of the storm cell was set to move from SE to NW. Due to its low velocity the high intensity stormcell needed approximately four hours to cross the entire catchment. The resulting hydrographs were much too high (Scenario 2). Then it was assumed that, additionally to the spatial displacement, the cell decayed completely after 34 min (Scenario 3). At this point the measured rain intensity at Mitzpe Ramon had dropped down to 12 mm hr^{-1}. Still the catchment response was exaggerated. Finally a cell lifetime of 24 min reproduced the gauged hydrographs in a correct order of magnitude (Scenario 4). This reconstructed, or 'calibrated' rainfall input, was used for all the following analyses.

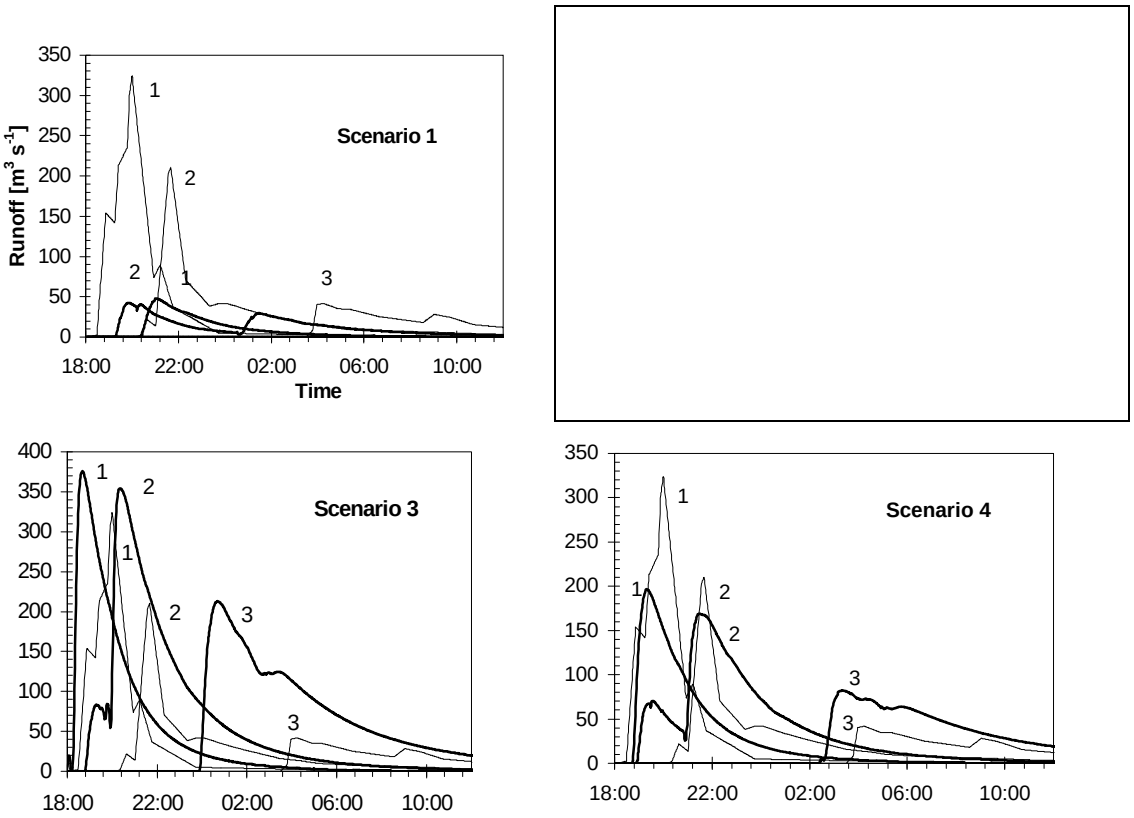

Fig. 9.3 Model scenarios to trace back the rainfall input
bold: simulation, fine: gauged hydrographs
(1) Mapal, (2) Massos, (3) Aqrabim

9.4 Discussion

The physical basis of the non-calibrated model provided the flexibility to include entirely different sources of information. Since for October 1979 data of three different runoff stations but only one single rainfall station were available, the runoff information was used to trace back the rainfall input. Size and geometry of a moving cell were determined using general knowledge. The recorded rain intensity helped to estimate maximum intensity, velocity and temporal decay. However, information of only one rainfall station was not enough to fully describe temporal decay and spatial displacement of a moving stormcell. The missing information was obtained comparing simulated and gauged runoff hydrographs. As a result, the spatial pattern and the quantity of rainfall could be reconstructed. If additional information on rainfall characteristics had been available (e.g. eyewitnesses of the event or additional ground measurements), the physically based description of the convective rainfall might have been used to simulate the catchment response in a 'non-calibrated way', like during the validation event of October 1991 when a rainfall radar station had already been in operation.

The runoff simulation using a reconstructed rainfall input could not accurately describe all details of this specific event. At Mapal the extreme rise was under- and the recession overestimated. More downstream at Massos the main peak arrived in time but the response of Nahal Hava was exaggerated. At Aqrabim the simulated hydrograph arrived too early and was too high. However, it should be recalled that considerable error may also be possible for measured hydrographs (Fig. 9.2), that not a single model parameter was fitted by calibration and that the rainfall input was described applying rather simple geometrical rules. Calibration of the model parameters, e.g. changing the infiltration rate of the alluvium at specific locations, could have produced a perfect fit between measured and simulated hydrographs at all stations. However, then these parameters would have been only valid for this specific event and the potential to make more general statements would have been lost.

10 Sensitivity analysis and uncertainty assessments

10.1 General aspects

An estimate of the reliability of rainfall-runoff models comparing observed and predicted discharges by measures of goodness-of-fit may be misleading. Sometimes a high model accuracy is pretended, since good model fits may be possible with completely unrealistic parameter values or process descriptions (e.g. MEIN & BROWN 1978, GRAYSON et al. 1992). MELCHING (1995) distinguished four principle sources of model uncertainty:

(a) *natural uncertainties* include the random fluctuations inherent in the natural, hydrological processes,

(b) *data uncertainties* are a measure for systematic and random errors during measurement and spatial averaging of input data,

(c) *parameter uncertainties* describe how accurate model parameters are identified by model calibration or measured data,

(d) *model structure uncertainties* address the inability to truly represent the physical runoff process by a mathematical model.

In the present model the spatial pattern of parameters was determined by measured field characteristics with assessable ranges of uncertainty. These ranges included the first three sources of model errors listed above: natural, data and parameter uncertainties. As follows they are treated uniformly as '*model parameter error*'. Model structure uncertainties can only be determined by validating model simulations with gauged data where distributed data provide best judgements. They will be discussed separately in Chapter 12. For the model parameter error a rather simple, 'field based' analysis was employed. The Aqrabim station (October 1979) and the Paleoflood Site (October 1991) offered the most reliable field data of the two investigated high magnitude events. These locations were chosen to study the sensitivity of the four parameter groups (runoff generation, runoff concentration, channel routing, transmission losses) containing 12 different model parameters. Within different model runs one parameter was varied over its maximum range of uncertainty, while the others were kept constant. The effects on the simulated flood, i.e. deviations in peak, volume and timing, were analyzed and compared (Tab. 10.1 and Tab. 10.2). Then in a worst-case scenario, all parameters were set to the boundary values of their maximum uncertainty range. For October 1979 the reconstructed rainfall served as model input; for October 1991 the calibrated rainfall radar was used.

10.2 Parameter uncertainty ranges

The maximum range of uncertainty for each parameter was estimated based on experience gained during parameter assessment. Following RIEDL (1995) and JOSS (1995) an

uncertainty range of ± 1 dBZ was estimated for the rainfall radar on October 1991. This corresponded to ± 16 % in rain intensity for the uncertainty range of the model input. For the infiltration characteristics of the different terrain units the results of GREENBAUM (1986) were analysed, who conducted independent of rainfall simulator experiments on various lithologies (Annex, Tab. A1). For the initial losses an average RMSE of approximately 1 mm resulted. Accounting for scale transition this value was increased to an uncertainty range of ± 2.5 mm for the initial losses of the Zin model. For the final infiltration rates a percentage uncertainty range ± 20 % was estimated. Comparing the hydrological timelags of the four different stations inside Nahal Yael (Tab. 6.2) an uncertainty range of ± 5 min was assigned to this parameter. To keep up mass conservation, a balanced change in the hydrograph shape was made, raising the first part and lowering the second part of the response function by 20 %. The length of the channel segments was determined digitizing 1:50,000 topographical maps. A digitizing error of ± 3 mm resulted in an uncertainty range of ± 150 m. For the slope and for the channel width, evaluated from topographical maps and airphoto analysis respectively, percentage uncertainty ranges of ± 20 % were estimated. For Manning channel roughness an uncertainty range of ± 0.01 was assigned following the range given by CHOW et al. (1988) from gravel bottoms (0.02) to clean winding streams (0.04).

Tab. 10.1 Model parameter error, October 1979

Input Parameter (Identification number)	Parameter uncertainty range	Resulting uncertainty for the simulated peak		Resulting uncertainty for the simulated flood arrival		Resulting uncertainty for the simulated volume	
		$m^3 s^{-1}$	**%**	min	**%**	$10^6 m^3$	**%**
Characteristics of the terrain units:							
Initial loss (1) (incl. scale transition)	± 2.5 mm	± 13	**± 15.9**	± 36	**± 5.3**	± 0.27	**± 13.9**
Infiltration rate (2)	± 20 %	± 5	**± 6.1**	± 17	**± 2.5**	± 0.13	**± 6.7**
Runoff concentration:							
Hydrologic timelag (3)	± 5 min	± 0	**± 0**	± 5	**± 0.7**	± 0	**± 0**
Hydrograph shape (4)	± 20 %	± 16	**± 19.5**	± 42	**± 6.2**	± 0.31	**± 15.9**
Routing parameters:							
Channel length (5)	± 150 m	± 11	**± 13.4**	± 81	**± 11.9**	± 0.02	**± 1.0**
Channel slope (6)	± 20 %	± 12	**± 14.6**	± 89	**± 13.1**	± 0.10	**± 5.1**
Channel width (7)	± 20 %	± 18	**± 22.0**	± 91	**± 13.4**	± 0.20	**± 10.3**
Manning n (8)	± 0.01	± 32	**± 39.0**	± 154	**± 22.6**	± 0.01	**± 0.5**
Bankfull stage (9)	± 0.5 m	± 18	**± 22.0**	± 55	**± 8.1**	± 0.16	**± 8.2**
Percentage occupied by inner channels (10)	± 20 %	± 1	**± 1.2**	± 29	**± 4.3**	± 0.04	**± 2.1**
Transmission losses:							
Depth of the active alluvium (11)	± 2 m	+ 121*	**+ 147.6***	-112*	**-16.5***	+ 1.94*	**+ 100.0***
Infiltration rate of the alluvium (12)	± 200 mm hr^{-1}	+ 98*	**+ 119.5***	-86*	**-12.6***	+ 1.45*	**+ 74.6***
Worst Case total model parameter error		+ 268*	**+ 327.8***	-347*	**-51.0***	+ 2.1*	**+ 108.0***

* minimum flood totally infiltrated

The uncertainty for the bankfull stage was estimated during the field evaluations (± 0.5 m) as was the uncertainty for the percentage covered by inner channels (± 20 %). The depth of the active alluvium during the floods could not be measured directly and consequently was accorded a large error. The estimated range of uncertainty (± 2 m) corresponded to a relative error of up to ± 200 %. For the infiltration rate of the alluvium field measurements were available (SHANAN, 1974; KÜLLS et al., 1995). Still no information existed on the process of infiltration during flood events. Therefore the estimated uncertainty range was considerably high (± 200 mm hr^{-1}) corresponding to a relative error up to ± 450 %. The parameter uncertainty ranges are summarized in Tab. (10.1) and Tab. (10.2).

Tab. 10.2 Model parameter error, October 1991

Input Parameter (Identification number)	Parameter uncertainty range	Resulting uncertainty for the simulated peak		Resulting uncertainty for the simulated flood arrival		Resulting uncertainty for the simulated volume	
		$m^3 s^{-1}$	**%**	min	**%**	$10^6 m^3$	**%**
Model input error:							
Radar calibration	± 1 dBZ	± 181	**± 36.1**	± 45	**± 10.8**	± 2.68	**± 31.5**
Characteristics of the terrain units:							
Initial loss (1) (incl. scale transition)	± 2.5 mm	± 90	**± 17.9**	± 25	**± 6.0**	± 1.61	**± 18.8**
Infiltration rate (2)	± 20 %	± 80	**± 15.9**	± 18	**± 4.3**	± 1.3	**± 15.2**
Runoff concentration:							
Hydrologic timelag (3)	± 5 min	± 0	**± 0**	± 5	**± 1.2**	± 0	**± 0**
Hydrograph shape (4)	± 20 %	± 40	**± 8.0**	± 14	**± 3.3**	± 0.53	**± 6.2**
Routing parameters:							
Channel length (5)	± 150 m	± 26	**± 5.2**	± 44	**± 10.5**	± 0.35	**± 4.1**
Channel slope (6)	± 20 %	± 35	**± 7.0**	± 34	**± 8.1**	± 0.08	**± 0.94**
Channel width (7)	± 20 %	± 18	**± 3.6**	± 29	**± 6.9**	± 0.18	**± 2.1**
Manning n (8)	± 0.01	± 56	**± 11.2**	± 79	**± 18.9**	± 0.67	**± 7.8**
Bankfull stage (9)	± 0.5 m	± 16	**± 3.2**	± 16	**± 3.8**	± 0.11	**± 1.3**
Percentage occupied by inner channels (10)	± 20 %	± 2	**± 0.4**	± 3	**± 0.7**	± 0.06	**± 0.7**
Transmission losses:							
Depth of the active alluvium (11)	± 2 m	± 99	**± 19.7**	± 17	**± 4.1**	± 1.77	**± 20.7**
Infiltration rate of the alluvium (12)	± 200 mm hr^{-1}	± 40	**± 8.0**	± 6	**± 1.4**	± 0.47	**± 5.5**
Worst Case (including model input error)		± 681	**± 135.6**	± 313	**± 74.9**	± 6.00	**± 59.3**
Worst Case (total model parameter error without rainfall)		± 455	**± 90.7**	± 248	**± 59.3**	± 3.64	**± 42.6**

10.3 Results

In contrast to October 1979, where the simplified physically based description of the rainfall input did not allow an estimate of the input uncertainty range (Tab. 10.1), for October 1991 the uncertainty of the rainfall input (model input error) was included (Tab. 10.2). By this error source the uncertainty of the peak discharge was enhanced by more than 36 %, effects on timing (10.8 %) and flood volume (31.5 %) were less obvious. For a comparison of the relative importance of the single model parameter errors during the two events (Fig. 10.1) the model input error was excluded, because of two reasons: first, as the rainfall should be regarded as model input rather than as a model parameter, its uncertainty does not contribute to the true model parameter error and second, an input error range was only available for the October 1991 event.

(a) The *runoff generation parameters* (parameters 1 and 2) caused 34 % of the peak uncertainty during 1991 and even 41 % of the volume uncertainty. For flood arrival of 1991 they were less important (15 %); during 1979 runoff generation parameters generally were of minor importance (5 % uncertainty on the peak, 9 % on the flow volume and 7 % on the flood arrival).

(b) The model uncertainty originating from the *runoff concentration parameters* (parameters 3 and 4) was minor throughout the analysis only ranging between 5 and 8 %; the hydrological timelag (parameter 3) even did not show any effect on peak discharge and flow volume.

(c) The *routing parameters* (parameters 5 - 10) had a much more accentuated influence on the flood arrival (62 % for 1979 and 69 % for 1991) than on the peak (25 % for 1979 and 30 % for 1991) and volume (10 % for 1979 and 21 % for 1991); Except for the volume of 1979 Manning n (parameter 8) was most important.

(d) During 1979 the *transmission loss parameters* (parameters 11 and 12) clearly dominated the uncertainty of the peak (65 %) and volume (74 %), during 1991 they were less important than those of runoff generation (28 % for the peak and 31% for volume); for the flood arrival they came second to those of the routing during both events (25 % for 1979 and 8 % for 1991).

The maximum total model parameter error is illustrated in two worst case scenarios (Fig. 10.2). During October 1979 the maximum flood rushed 5.8 hr (+ 51 %) ahead and peaked 268 $m^3 s^{-1}$ (328 %) higher than the simulated one; the flow volume was 2.1×10^6 m^3 (109 %) higher. The minimum flood totally infiltrated into the channel alluvium. During October 1991, both ‘worst-case floods’ arrived. The maximum uncertainty ranges were smaller than during October 1979 but still considerable: ± 455 $m^3 s^{-1}$ (± 91 %) for the peak, ± 4.0×10^6 m^3 (± 48 %) for the volume and ± 4.1 hr (± 59 %) for the peak arrival.

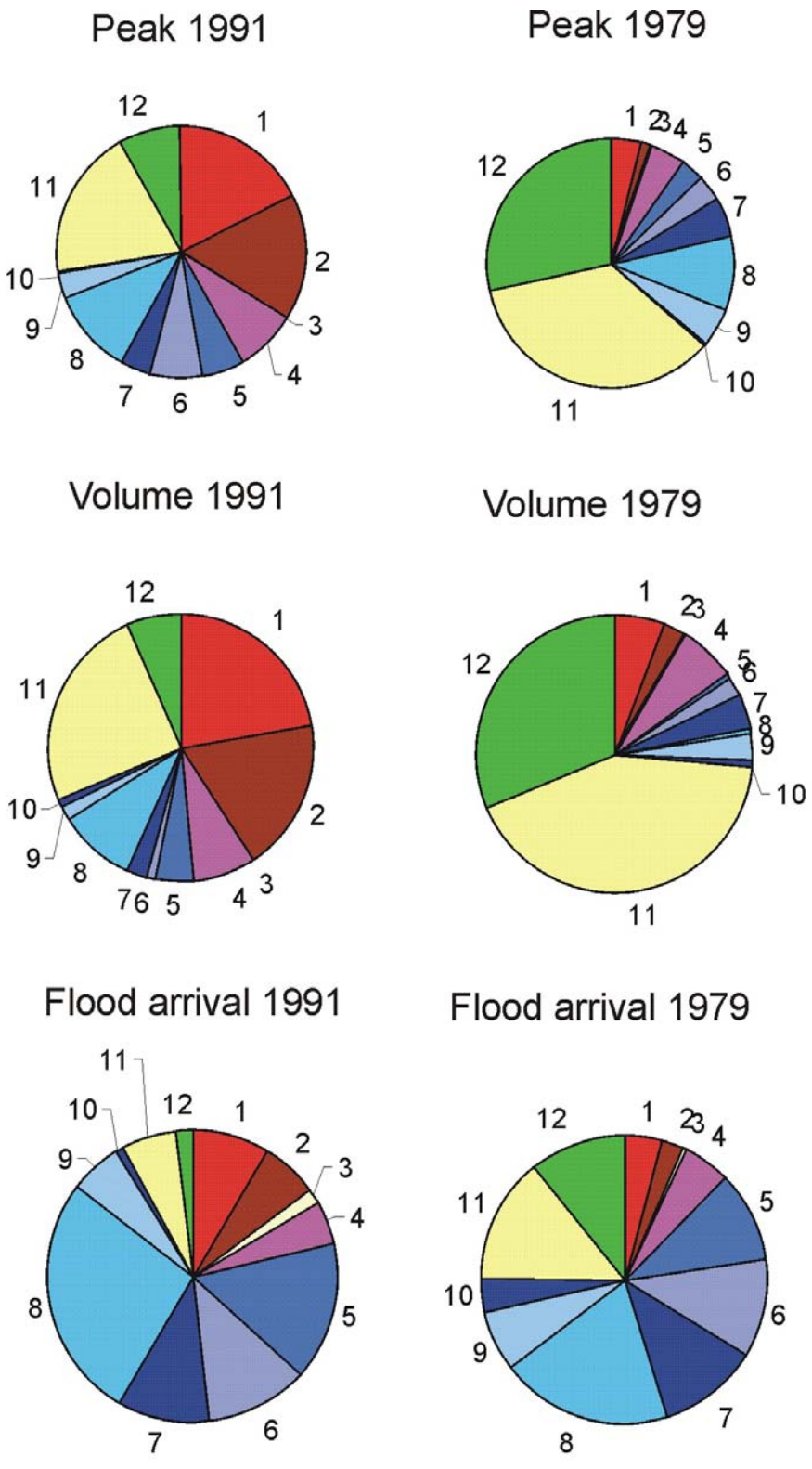

Fig. 10.1 The relative importance of the single model parameter errors, numbers refer to the identification numbers in Tab. (10.1) and Tab. (10.2)

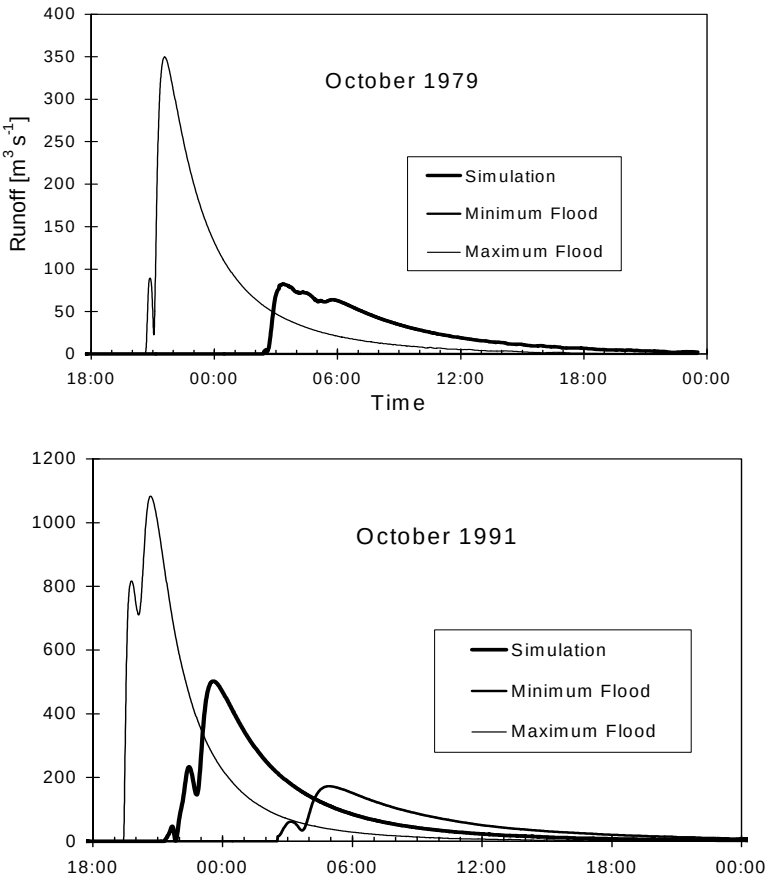

Fig. 10.2 Worst case scenarios of the two high magnitude events

10.4 Discussion

The model uncertainty caused by the rainfall input could only be studied by the calibrated rainfall radar during October 1991. During this event it considerably increased overall model uncertainty. In the analysis of the true model parameter error (excluding the rainfall input) the channel routing appeared to be decisive for the correct timing of a flood making up approximately two thirds of the error. Parameters for runoff concentration generally were in the background. Within the remaining two parameter groups striking differences between the two high magnitude events appeared.

(a) The October 1979 flood was generated in a small area in the uppermost Zin headwaters, no major tributary was active. Therefore it constantly decreased on its long way downstream owing to channel transmission losses. Both model parameters for this process (infiltration rate and depth of the active alluvium) were inherent with a large maximum error resulting in a large uncertainty range for the simulated peak discharge. Meanwhile parameters of runoff generation lost their importance.

(b) During October 1991 runoff was generated by almost the entire catchment. This was documented by a larger sensitivity of the runoff generation parameters. Compared to October 1979 the travelling distance of the flood was the same, however preceding peaks by tributary inflows and a higher main peak limited the effect of transmission losses; the resulting total model error was smaller.

Hence model uncertainty considerably varies from event to event and should be re-evaluated for each flood. Subjectivity was involved in assessing the maximum uncertainty ranges of some input parameters. Still the resulting uncertainty bounds may help to judge model reliability and may guide future efforts to enhance model accuracy.

(a) For a correct timing the flood routing parameters play a primary role. The flood magnitude, however, is governed be different parameters:

(b) For large floods generated on a large area, runoff generation and transmission loss parameters are of almost the same importance.

(c) For smaller floods, generated on small parts of a catchment and travelling for long distances on dry channels, transmission loss parameters totally dominate model parameter error. For these floods more field information on infiltration processes active during real flood events would decisively reduce model uncertainty.

In general, the sensitivity of the different parameter groups corresponds to expected values. This may be regarded as a proof of a correct model structure which cannot be taken for granted. In a multi-scale application of the conceptual HBV-model (BERGSTRÖM 1992), for instance, the parameter MAXBAS describing channel routing remained very sensitive even in the smallest (0.093 km^2) catchment (UHLENBROOK et al. 1998).

The calculated maximum ranges of model parameter error must be regarded as uppermost boundaries. It is very unlikely that, in a particular model run, all parameters are at the boundary of their uncertainty range. Moreover, most parameters were assessed independently for different terrain types, channel segments and channel types. Thus single mistakes in the data input tend to cancel each other out. This effect is difficult to quantify but most pronounced, where the number of independently derived parameter values is highest (e.g. for the routing parameters length, slope and width determined independently for each of the 419 channel segments). Hence reasonable model outputs are possible, as shown by the simulated peaks of October 1991 (Fig. 8.5). If future efforts concentrate on the most apparent sources of error (i.e. raingauge adjustment of arid rainfall radar, detailed field based studies of runoff generation at the catchment scale and infiltration losses during flood events), the accuracy of non-calibrated model simulations may be further increased.

11 Hydrological analyses

11.1 Flow characteristics

The distributed model enabled to simulate hydrographs at the ungauged apex of the Zin alluvial fan. There the three main flow characteristics of the catchment responses during the two high magnitude events of October 1979 and October 1991 were analysed (Fig. 11.1). The October 1991 flood simulation was characterized by a peak of 495 $m^3 s^{-1}$, a flow duration of 37 hr and a volume of 8.9×10^6 m^3. In 1979 these values amounted to 61 $m^3 s^{-1}$, 27 hr and 1.9×10^6 m^3, respectively.

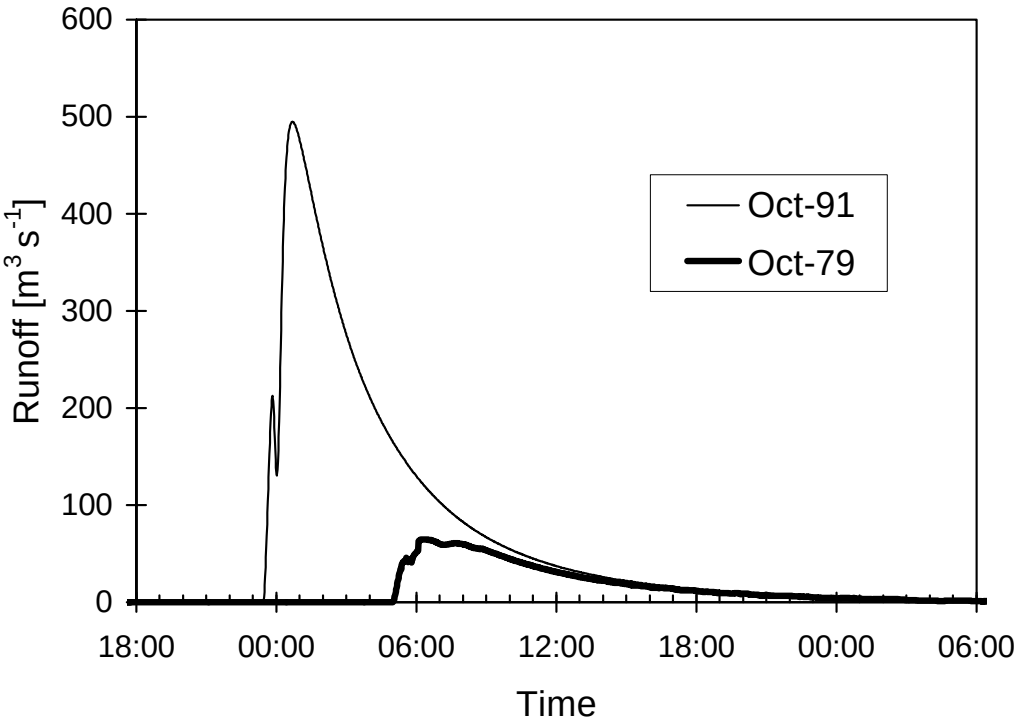

Fig. 11.1 Simulated hydrographs at the Zin alluvial fan for the two high magnitude events

For an analysis of catchment-wide flood generation these parameters were compared with those at the three gauging stations Mapal, Massos and Aqrabim (Fig. 11.2). To judge model parameter error at each location, the results of the minimum and maximum floods of the worst case scenarios were added to the simulations as error bars representing maximum model parameter error. Not part of the true model parameter error, the input error stemming from the rainfall was not included. Also the field data was added for comparison; there errors could only be quantified for peak discharges.

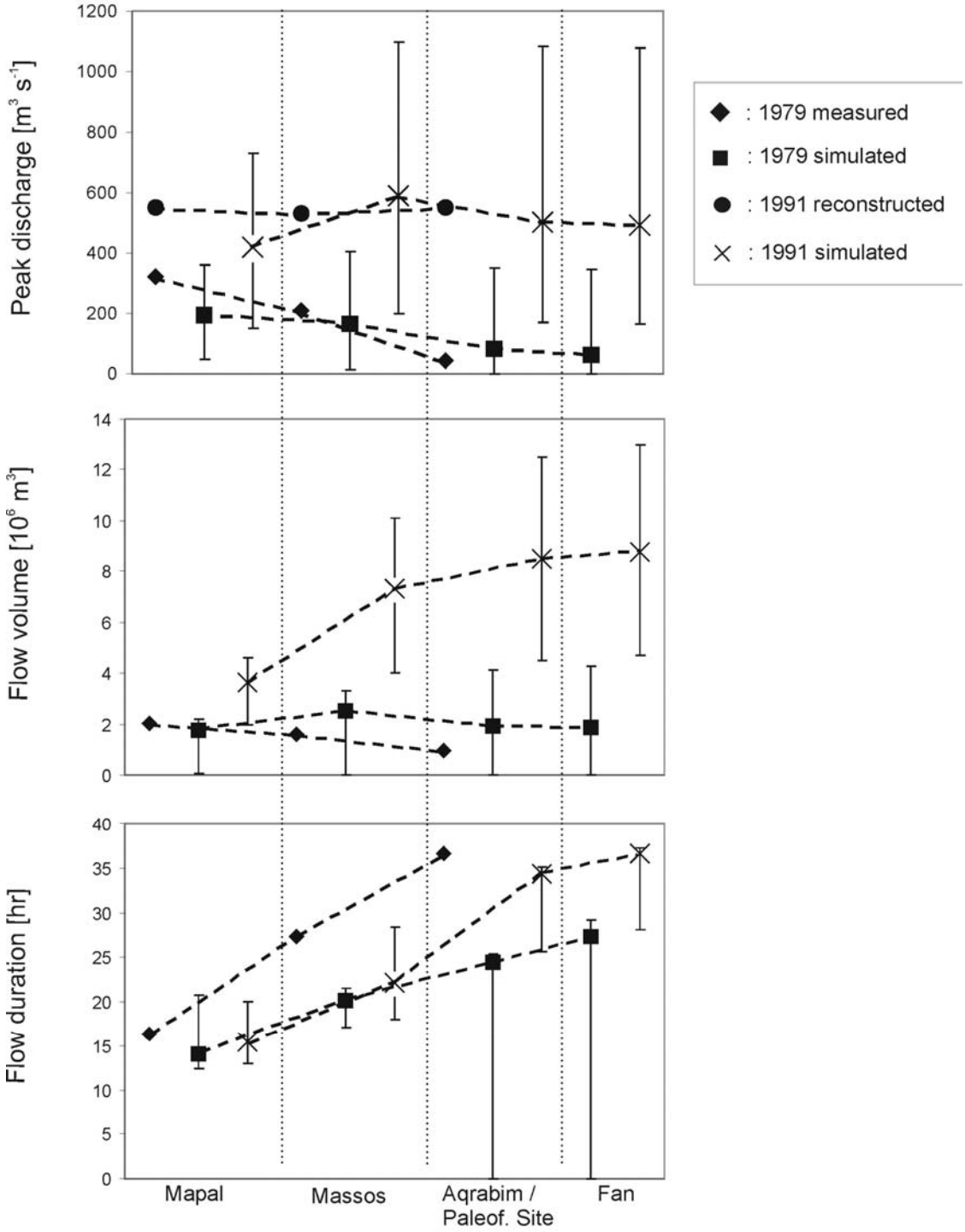

Fig. 11.2 Downstream development of flow characteristics during the two high magnitude events

During the October 1991 event the calibrated rainfall radar provided a catchment-wide model input, whereas only the flood peaks could be validated with field values. As already shown in Fig. (8.5) the model underestimated the peak at Mapal, while at the two lower stations a closer fit was reached. Simulated flow volumes and durations constantly increased downstream. In a similar way model simulations became more and more uncertain with increasing flow distance. Model parameter error was largest for peak discharge and considerably smaller for volume and duration of flow.

For the October 1979 event the model run with the reconstructed rainfall input was used. The decreasing trend of peak flow was correctly simulated although the intensity of this development was underestimated. Also flow durations were underestimated, still they increased downstream like those measured in the field. The generally decreasing tendency of the field runoff volumes was correctly simulated only downstream of Massos despite a close fit at Mapal. The overestimation at Massos was intensified by a simulated response of Nahal Hava not evident in the field hydrograph. At Aqrabim and at the Paleoflood Site the minimum scenario flood totally disappeared into the alluvium increasing the errors of flow volume and duration.

11.2 Runoff concentration times and maximum flow velocities

The analyses of runoff concentration times using historic runoff events is often inherent with large errors due to clock malfunctions and inadequate time-synchronisation of conventional rain and streamflow gauges. LAURENSON & O'DONNELL (1969) found out that synchronization errors by far dominated the uncertainty in unit hydrograph derivation. Due to extreme climatic conditions these problems are even accentuated in the arid zone. As gauged hydrographs are not needed in the present non-calibrated model, it may provide information on runoff concentration inside a large arid catchment from an independent, field-based source.

Flow velocities may be measured directly at gauging stations (e.g. using current meters) or applying tracers along channel reaches. However, especially for high magnitude floods in arid channels, only little direct evidence exists mainly due to their rare occurrence and measurement problems. The flash flood simulation at Nahal Shahmon and findings of SCHICK (1968, 1988) are examples indicating that maximum peak flow velocities may exceed 5 m s^{-1}. Flow velocities may also be assessed indirectly studying travel times of runoff crests along channel reaches. This analysis requires hydrographs of the same event peak at two gauging stations upstream and downstream a channel reach imposing errors inside large arid channels, when tributary inflows and disappearing peaks by the influence of transmission losses impede the interpretation.

BEN-ZVI et al. (1991) included reaches of Nahal Zin into a study of that kind. Regression analysis yielded two parameters (a,b) of a simple power function relating travel time (t) to peak discharge (Q_{peak}):

$$t = a \times Q_{peak}^{b} \qquad (11.1)$$

Since the peak discharges differed considerably between the upstream and downstream stations, two independent parameter sets were evaluated for each reach. The findings of this study were applied to the October 1991 event at the reaches Mapal-Massos and Massos-Aqrabim, where almost a constant peak discharge of 530 - 550 m^3 s^{-1} was reconstructed (GREENBAUM et al. 1998). Although discharges were nearly constant, the results indicated an enormous variation in travel times and flow velocities (Tab. 11.1).

Tab. 11.1 Application of the regression relation by BEN-ZVI et al. (1991) to the October 1991 event

Reach	Q_{peak} used for regression analysis	Q_{peak} [m^3 s^{-1}] *	a [hr (m^3 s^{-1})$^{-b}$] **	b [-] **	r^2 [-] **	Travel time [hr] ***	Reach length [km] **	Velocity [m s^{-1}] ***
Mapal-Massos	upstream	550	2.64	-0.358	0.3	0.15	20.2	**37.9**
	downstream	530	3.24	-0.291	0.08	0.23	20.2	**24.7**
Massos-Aqrabim	upstream	530	536	-1.323	0.76	1.02	27.1	**7.4**
	downstream	550	5390	-1.843	0.87	67.1	27.1	**0.1**

* October 1991 discharges

** Values by BEN-ZVI et al. (1991)

*** Calculated values for the October 1991 discharges

For the Mapal-Massos reach calculated flow velocities were about one order of magnitude too high. Using the downstream peak discharge for the Massos-Aqrabim reach BEN-ZVI et al. (1991) had determined a close correlation between discharge and travel time (r^2 = 0.87). Yet the application of relation to the October 1991 event yielded a much too slow velocity.

Strictly speaking a validation of the realistic time-simulation of the present non-calibrated rainfall-runoff model was only possible during October 1979. Only this event provided hydrometric data at three gauging stations. As the fit in timing was rather close (Fig. 9.3), it may be assumed that also the model results of October 1991 may be used for a realistic look into runoff concentration times and flow velocities (Tab. 11.2).

For the distances between the stations the digitized length of the channel segments in between were added up. The very short concentration times during the October 1991 event show that even large rocky arid catchments may react within a few hours on high intensity rainfall. The quick flood arrival at Massos was caused by the short-cut of the steep Nahal Hava. During both events the flood front was only a little bit slower than the peak. Values exceeding 6 m s^{-1} during the October 1991 event document the extreme danger inherent in high magnitude flash floods.

Tab. 11.2 Runoff concentration and travel times during the two high magnitude events, maximum uncertainty range defined by the worst case scenarios given in brackets
(bold: field measurements during October 1979)

Station	Mapal	Massos	Aqrabim	Paleoflood site
Drainage area [km^2]	233	660	1130	1140
Timelag of flood arrival 1979 [hr]	2.7 / **2.1** (1.6 - 4.8)	2.9* / **4.1** (1.8 - 12.9)	10.4 / **11.5** (4.6 - **)	-
Timelag of peak arrival 1979 [hr]	3.3 / **4.0** (2.0 - 7.0)	5.5 / **5.6** (3.1 - 15.5)	11.4 / **12.2** (5.6 - **)	-
Timelag of flood arrival 1991 [hr]	1.6 (1.2 - 1.9)	1.3* (0.9 - 1.8)	-	4.8 (2.8 - 9.9)
Timelag of peak arrival 1991 [hr]	2.5 (1.7 - 3.7)	3.7 (2.4 - 6.1)	-	7.0 (4.1 - 12.3)

Reach	Mapal-Massos	Massos-Aqrabim	Massos-Paleoflood site
Distance [km]	27.9	24.3	29.0
Flow velocity 1979, flood front [m s^{-1}]	* / **3.7** (* - *)	0.9 / **0.9** (2.4 - **)	-
Flow velocity 1979, flood peak [m s^{-1}]	3.6 / **4.6** (7.3 - 0.9)	1.1 / **1.0** (2.6 - **)	-
Flow velocity 1991, flood front [m s^{-1}]	* (* - *)	-	2.3 (4.2 - 1.0)
Flow velocity 1991, flood peak [m s^{-1}]	6.8 (11.1 - 3.2)	-	2.4 (4.8 - 1.3)

* preceding peak by Nahal Hava
** flood infiltrated completely

11.3 Scenarios

11.3.1 A high magnitude flood in Nahal Hazera

Nahal Hazera, a 55 km^2 tributary in the lower Nahal Zin, is known to produce large floods. The channels are characterized by steep slope and only negligible alluvium, while the catchment has an almost circular shape. In recent years a large flood breached several reservoirs and completely destroyed the road through the entrance of Makhtesh Katan. As the tributary entrance into Nahal Zin is located downstream the Massos-Aqrabim reach,

the influence of transmission losses is limited and large floods of Nahal Hazera may reach the alluvial fan of Nahal Zin with only minor attenuation. To illustrate this fact the circular raincell used to simulate the October 1979 event (15 km diameter, 224 mm hr^{-1} maximum rain intensity), was transferred to the centre of the Hazera catchment. There it travelled for 24 min in a north-western direction (Fig. 11.3).

Only 30 min after rainfall onset, a large flash flood was simulated at the mouth of Nahal Hazera with a single peak of 440 $m^3 s^{-1}$ and a flow volume of 1.3×10^6 m^3 (Fig. 11.4). Other tributaries responded only weakly. Upstream the Hazera inflow a 3 $m^3 s^{-1}$, 3×10^3 m^3 flood was simulated in the main channel and except for Nahal Zafit (0.2 $m^3 s^{-1}$, 60 m^3) large tributaries downstream of Nahal Hazera did not flow. Hence the simulated flood peak was diminished at the alluvial fan (345 $m^3 s^{-1}$). Nevertheless the simulated flow volume increased (1.7×10^6 m^3).

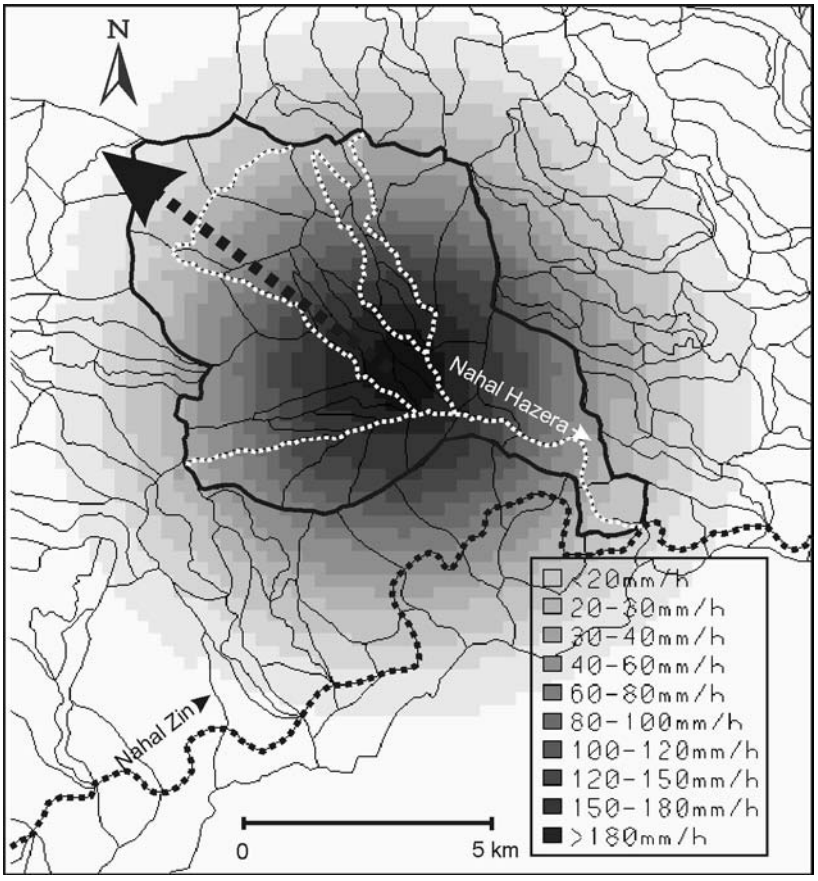

Fig. 11.3 Rainfall input used for the Hazera flood scenario

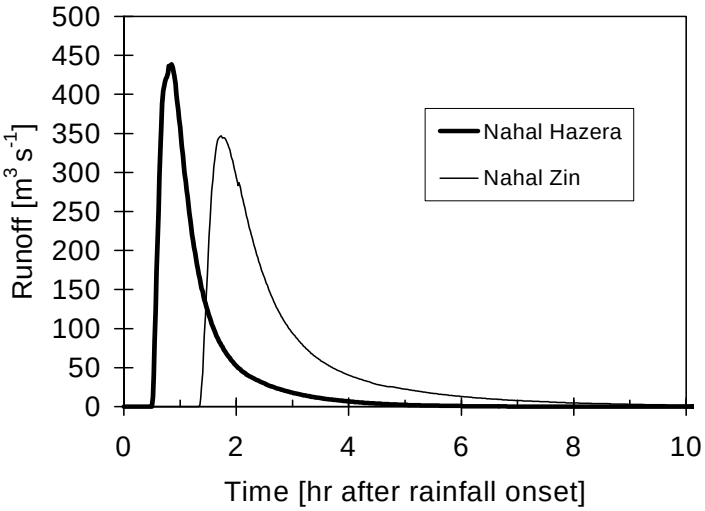

Fig. 11.4 The Hazera flood scenario at the tributary mouth (bold) and at the Zin alluvial fan (fine)

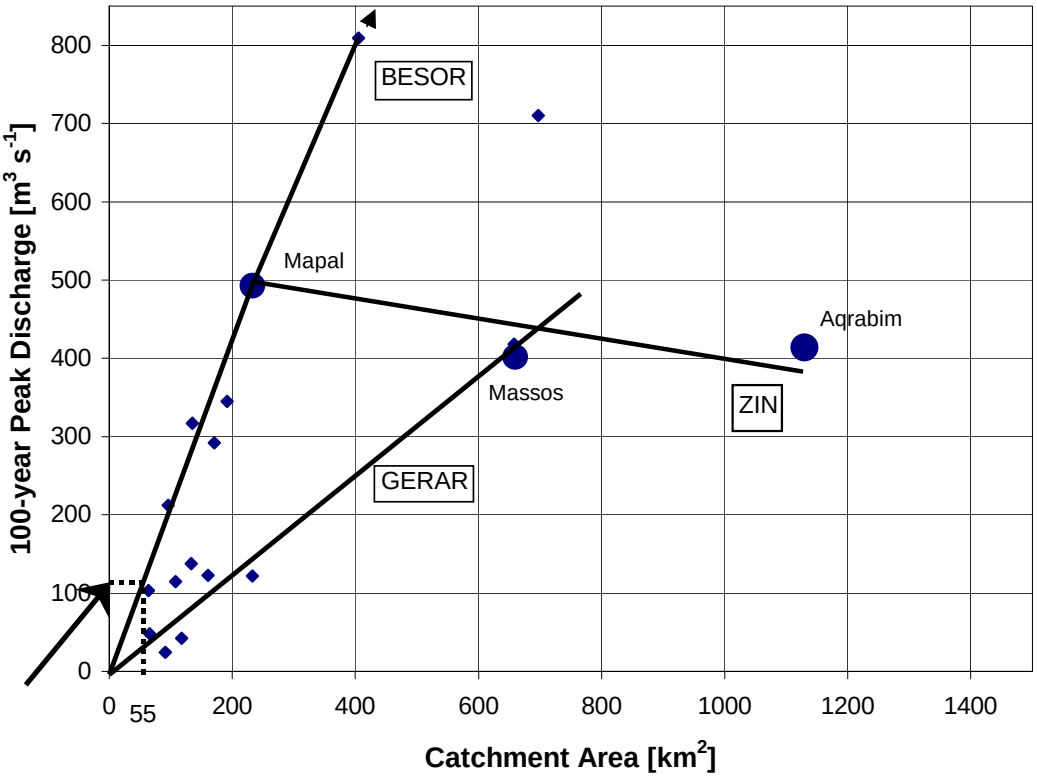

Fig. 11.5 Regional discharge-area relations for the channel systems in the Negev including the three Zin stations (large dots); arrow: Nahal Hazera (MEIROVICH et al. 1998, modified)

For rare discharges in the Negev regionalized statistical models exist, fitting probability distribution functions to observed discharges. SHENTSIS et al. (1997) fitted the log Pearson type- III distribution to annual maximum series of peak discharges for 67 hydrometric stations all over Israel. The entire Negev was delineated into three homogeneous regions for which extreme discharges were related to drainage area. For the region containing the Nahal Zin catchment a 100-year peak discharge in a 55 km^2 catchment did not exceed approximately 130 $m^3 s^{-1}$. MEIROVICH et al. (1998) concentrated their analysis on the arid parts of Israel and selected large events, rather than annual series, for a fit of probability distribution functions to gauged data. Thereby more stations could be included and discharge-area relationships were determined independently for each stream system (Fig. 11.5). Up to a catchment area of 250 km^2 the 100-year peak discharge increased almost linearly with drainage area and the Zin relationship was the most extreme one. Still the value of approximately 130 $m^3 s^{-1}$, given by SHENTSIS et al. (1997) for a 55 km^2 catchment, was not exceeded.

In the Negev also maximum observed discharges have been analysed. YANOVICH et al. (1996) combined maximum observed discharges including 55 hydrometric stations and 109 occasional sites all over the Negev and Sinai deserts. On the unified enveloping polygon for the complete area a maximum runoff peak of approximately 500 $m^3 s^{-1}$ could be expected from a 55 km^2 desert catchment (Fig. 11.6).

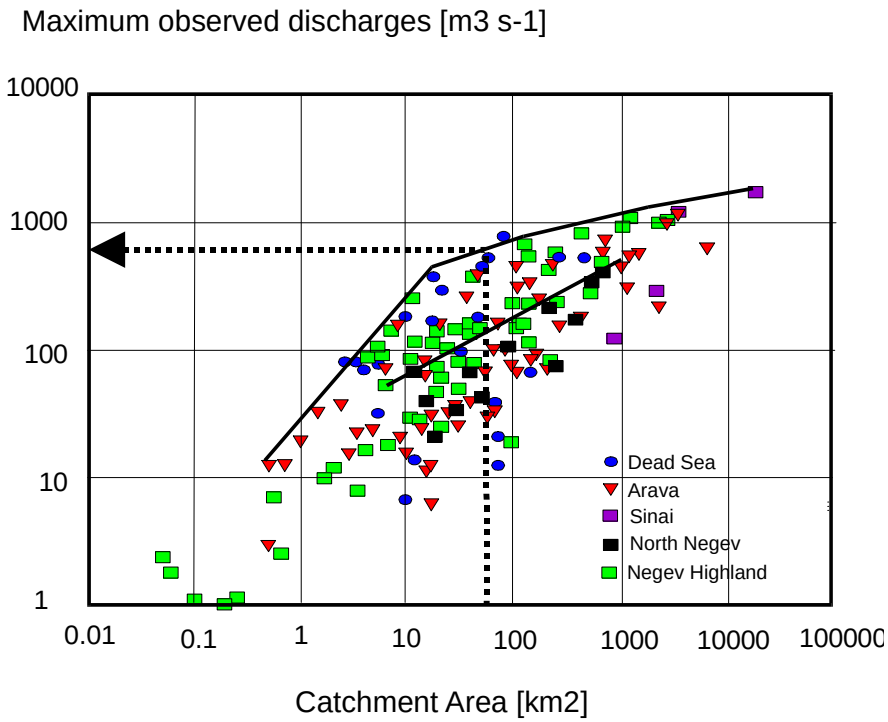

Fig. 11.6 Maximum observed discharges in the Negev and in Sinai; arrow: Nahal Hazera (YANOVICH et al. 1996, modified)

According to MEIROVICH et al. (1998) the enveloping curve of the maximum observed flow volumes (V_{max}; 10^6 m^3) in the Negev may be related to catchment area (A; km^2) by the following power function:

$$V_{max} = 0.17 \times A^{0.71} \quad (11.2)$$

For a 55 km^2 catchment a maximum volume of 2.9×10^6 m^3 results. Hence both the peak discharge (440 m^3 s^{-1}) and the flow volume (1.3×10^6 m^3) of the Nahal Hazera scenario are within the range of maximum values observed in desert environments.

11.3.2 Climatic change

It is now commonly accepted in the scientific community that unabated growth of anthropogenic greenhouse gas emissions into the atmosphere over the next century could induce a global warming and affect global climate (e.g. HOUGHTON et al. 1996). When the world as a whole warms up due to this 'greenhouse effect', the higher latitudes warm up more than the lower ones reducing the difference in temperature between the poles and the equator (VERHOOG 1987). This modifies global circulation as simulated by General Circulation Models (GCM's). However, two main issues limit the use of GCM-outputs as direct inputs for hydrological catchment-scale models: (a) the degree of uncertainty in the accuracy of the simulated meteorological parameters, and (b) the discordant scales of GCM's (10^4 - 10^5 km^2) and hydrological catchment-scale models (10^{-1} - 10^3 km^2) (LEAVESLEY & HAY 1998). Hence, in most climatic change scenarios, only rough expectations of future temperature and precipitation changes are incorporated into hydrological models. If calibrated approaches are used for this purpose, most model parameters optimised to fit the historical runoff data remain unchanged and existing parameter intercorrelations have to be neglected (e.g. CHIEW et al. 1995). It is assumed that under the scenarios the catchments will continue to behave as they do at present, which may be misleading especially in the arid zone, like the northern Negev. Several researchers (e.g. YAIR 1987, 1994, ISSAR et al. 1984, GERSON 1982) found evidence that a shift to wetter climatic conditions in the past was followed by a considerable change in surface properties. During pluvial periods loess penetration buried the rocky landscape increasing infiltration and decreasing runoff and erosion energy. As follows an attempt is made to use these historic findings for a future climatic change scenario.

Inside Nahal Zin the hydrological characteristics of loessial terrain, representing a remnant of a Pleistocene wetter climate, may still be studied today. It is found throughout the Avdat Plateau (terrain types 4 and 5) and along the upper channel network (channel type 1). Terrain type 5 represents a loessial plateau surface with fine material and stable crust. For a scenario of a wet future climate this material was assumed to settle on the high uniform limestone plateaus. Steep active slopes and badlands were left unchanged, while the rest of the catchment was assumed to be covered by terrain type 4 representing a Pleistocene valley fill. The entire channel network of the scenario consisted of type-1 channels flowing on a flat loessial valley fill. Rainfall input was left unchanged for the

two events of 1991 (rainfall radar) and 1979 (moving circular raincell). Similar to the evaluations of parameter sensitivity and uncertainty, results were highly event-dependent (Fig. 11.7). The 1979 flood scenario peaked a little bit higher than the original simulation, while in 1991 the clear opposite was observed.

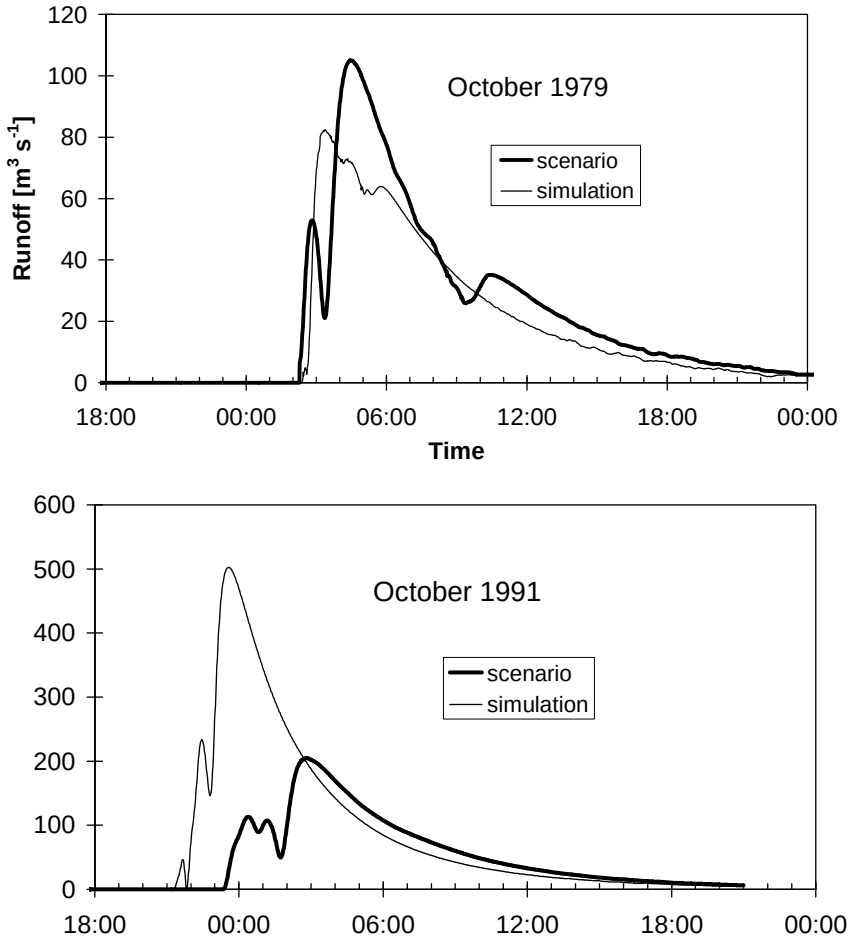

Fig. 11.7 Climatic change scenarios for the October 1979/1991 rainfall

11.4 Discussion

Despite a considerable model parameter error, the present non-calibrated, field based rainfall-runoff model proved to be an *appropriate tool to analyse flow characteristics* of the two completely different high magnitude events inside Nahal Zin. On the one hand, during October 1991, flood peaks increased or almost remained constant on their way

downstream due to flow additions from tributaries. During October 1979, on the other hand, runoff peaks significantly decreased with increasing flow distance. Irrespective of a downstream gain or loss in runoff, flows got longer from station to station. This seems to be a widespread phenomenon for arid floods, also confirmed by gauged Zin hydrographs during October 1979. As a main drawback the model could not correctly reproduce volumes of flow. Already apparent in the separate test of the routing component during October 1979, runoff volumes increased downstream despite the presence of transmission losses. During the Nahal Hazera flood scenario the runoff volume increased on the way from Nahal Hazera down to the Zin alluvial fan, although contributions from other tributaries were minor. Hence the model in its present form should not be used for an accurate analysis of the downstream development of flow volumes.

The present non-calibrated, field based approach was clearly superior to an existing calibrated stochastic alternative in analysing flow velocities of high magnitude floods. The regression model by BEN-ZVI et al. (1991), determined by calibration using small to medium flows, could not be extrapolated to high magnitude floods as represented by the October 1991 event. This documents a common dilemma of calibrated hydrological models: Once calibrated to a range of conditions given in historic data, predictions for conditions outside this range are inherent with large uncertainties difficult to assess. Here non-calibrated field-based models are more appropriate.

The simulated high magnitude flood in Nahal Hazera has implications for maximum possible floods and flood control at Nahal Hazera but also at the mouth of Nahal Zin. It documents that the same rainstorm, dependent on its location over the catchment, may produce high magnitude floods as well as almost disappearing ones. The long travel distance on dry channels during October 1979 buffered most of the flow, while the almost circular tributary Nahal Hazera generated an extreme flash flood with only minor attenuation on its way downstream. This flood may be seen as a field-based estimate of a rare high magnitude flash flood generated in Nahal Hazera under the present day climatic configuration. If such an extreme tributary response arrives simultaneously with a high flow in the main channel, very high flood peaks are to be expected also at the mouth of Nahal Zin, exceeding by far the largest flood on record (550 $m^3 s^{-1}$).

The high runoff peak of the Nahal Hazera flood scenario is very close to the envelope line of YANOVICH et al. (1996) describing the maximum discharges ever observed in the Negev and in Sinai. It may be assumed that the destructive discharges on this line originate from a fatal combination of catchment morphology and rain intensity. Hence the present model correctly translates favourable catchment characteristics (the almost circular shape of the catchment, the accentuated relief and the limited extent of the channel alluvium) into a quick and accentuated flood generation. Nahal Hazera is an ungauged extreme inside Nahal Zin not contributing to the existing data record. As a consequence, this tributary hardly fits into regional statistical models based on gauged data from more ‘normal’ catchments (i.e. more elongated catchments where channel transmission losses are more important). Ten years after the first hydrometric station had been installed on 13/05/1945, a high magnitude flood (550 $m^3 s^{-1}$) was recorded at the mouth of Nahal Zin (GREENBAUM et al. 1998). Then, within a time interval of only twelve years, two large rainstorms (1979 and 1991) were active in the catchment. Although only one affected Nahal Hazera in its margins, it seems reasonable that once in a hundred years

the centre of such a rainstorm may also cross Nahal Hazera inducing a high magnitude flood similar to that of the scenario. On this assumption the peak discharge of a 100-year flood in Nahal Hazera would equal the scenario flood and exceed those given by regional statistical models by the factor of three or even more.

For climatic change scenarios temperature parameter changes have the greatest impact when they occur around freezing temperatures (EYBERGEN & IMESON 1989), or when long-term water balances are investigated (increased evapotranspiration). Studying single events in arid catchments, they may be neglected as evapotranspiration is not relevant. In contrast, precipitation changes play a decisive role for the generation of high magnitude floods with rain intensity as the dominating factor. This is evident in the uncertainty evaluations of the 1991 rainfall radar, where a 16 % change of rainfall intensity induced a 36 % change of the runoff peak and a 31 % change of the runoff volume (Tab. 10.2). Thus statements on climatic-change-induced runoff changes are not very reliable, if they do not explicitly follow the effects of increased rainfall intensities.

The climatic change scenarios in this chapter only simulated changes in surface properties. It was assumed that an almost uniform layer of loess covered the entire catchment and that changes in vegetation are negligible. However, just desert and grassland ecosystems are very sensitive to climatic changes (VERHOOG 1987). Hence the present quantitative results should be interpreted with caution and only rough trends are reliable. Nevertheless these trends document that changes of catchment properties are not negligible for climatic change scenarios in arid zone catchments. Moreover, dependent on the spatial distribution of rainfall input, different events may produce contrasting results, predicting an increase (October 1979) or a decrease (October 1991) of runoff.

12 General discussion

On the one hand, records of high magnitude events in arid catchments are extremely rare. On the other hand, in contrast to humid areas with their important indirect subsurface runoff components, the development of large desert floods is governed by mainly two surficial processes:

(a) generation and spatial concentration of Hortonian overland flow and

(b) channel transmission losses.

These special features make it necessary and possible to *refrain from calibration* in arid zone rainfall-runoff modelling. The structure of the present model was kept as simple as possible, accounting solely for the two above mentioned processes. The resulting number of model parameters could be kept small, and none of them was determined by calibration (i.e. not a single model parameter was changed to reach a better fit between simulated and gauged streamflow). In this respect the spatial distribution of rain intensities is regarded as model input and not as a model parameter. The common determination of the Z-R-relation calibrating radar reflectivity with ground gauges did not change the non-calibrated model structure, as it did not affect the rainfall-runoff transformation.

To determine important model parameters (initial loss and infiltration parameters, scale transition, shape and hydrological timelag for runoff concentration) gauged rainfall and runoff information inside Nahal Zin or nearby was used. Still none of these parameters were part of hydrodynamic concepts containing mathematical relations that were calibrated by the best fit between simulated and observed data. Instead, all of them were determined evaluating measured field data directly (i.e. comparing runoff responses of plots and small catchments, averaging standardized hydrographs). Together with topographical parameters (e.g. channel dimensions and slopes) and a commonly used (empirical) roughness parameter (Manning n), they were incorporated into the present model and remained unchanged, although a better fit could have been reached by final calibration. Hence all model parameters quantify general hydrological processes in arid environments and are not bound to a specific hydrological model nor to calibration data sets.

Assuming that the rapid runoff concentration during large desert floods is similar, a *model application to ungauged arid catchments* seems reasonable even without long years of local field experiments. Inside the Nahal Zin catchment the infiltration characteristics were parameterized for a variety of typical arid terrain types, ranging from bare rock to sandy plains. In an ungauged catchment the mapping of these terrain types becomes an important/ responsible part of the model procedure and requires sound field experience. Topographical input can be quickly determined with the help of today's powerful GIS-systems. The flexibility of the present model enables the incorporation of any hydrological information available (e.g. local infiltration tests or gauged data from subcatchments), which should be fully exhausted in ungauged basins. For the rainfall input also general knowledge on the properties of arid zone rainfall (e.g. the spatial structure of raincells with their maximum dimensions) or observations of eyewitnesses on spatial extent and timing of high intensity rain may be incorporated.

All model parameters are effective parameters representing a balanced mean of internal variability in the units of spatial subdivision (terrain types, model elements, channel segments). Where possible, parameter estimation techniques were chosen to *assess these effective parameters directly in the modelling scale*. The accuracy of the spatial discretization used in Nahal Zin must be regarded as an uppermost boundary for a meaningful model parameterization. As this spatial subdivision was not rigid but, facilitated by the GIS, parameter dependent, the efficiency of parameterization was maximized.

To represent *scale transition* in the description of runoff generation from the plot/slope scale to 0.3 to 9 km^2 model elements, initial losses were increased to account for processes critical for the runoff response of larger areas. Runoff concentration was parameterized using data collected inside 0.05 to 0.5 km^2 tributaries of another Negev catchment. Errors originating from the variable size of the individual model elements, required for an adequate subdivision of the channel network, had to be disregarded in both catchment scale representations to maintain a field based model structure. Model parameters for channel routing and transmission losses were assigned to the scale of (on average) 2 km long channel segments. Because of the large number of independent segments special techniques for parameterization were needed. The definition of channel types with rather uniform characteristics made it easier to evaluate representative model parameters (e.g. mean cross sections represented by the area covered by inner channels and a bankful stage, mean channel roughness and infiltration rates). For channel width a representative mean value was determined dividing channel area by flow length.

The present evaluation of model uncertainty is limited to the model parameter error describing the variability/uncertainty of the estimated effective model parameters. As such it does not address *model structure uncertainties* originating from the use of simplified descriptions for occurring hydrological processes. These model structure uncertainties may only be analysed by the variations between measured and simulated discharge. They affect the prediction of different runoff features (e.g. peak discharge, flow duration, runoff volume, timing) in different ways and to different degrees (MELCHING 1995). For runoff generation, model structure uncertainties are mainly due to the simplified description of scale transition. For runoff concentration, the use of a single mean response function for 0.3 to 9 km^2 model elements, irrespectively of size and topography, may cause concern. The close model fit of the October 1991 peaks (Fig. 8.5) and the almost perfect timing in the upper catchment during the October 1979 event (Fig. 9.3) may justify the use of these simplifications for generation and concentration of runoff.

However, an *incomplete mass conservation* was apparent in the separate test of the routing component with the October 1979 hydrographs and in the Nahal Hazera flood scenario. This indicates that for flow routing and channel transmission losses considerable model structure uncertainties exists. They may stem from

(a) the one-dimensional representation of the flow process in occasionally braided channel reaches,

(b) the approximations in the Muskingum-Cunge technique describing unsteady open channel flow,

(c) the need to average model parameters to approximately 2 km channel reaches,

(d) the simplified description of cross-sectional geometry,

(e) a constant, stage-independent channel roughness,

(f) a constant infiltration rate for transmission losses, which are immediately stopped after the wetting front reaches the base of the active alluvial storage.

Mass conservation problems in distributed routing schemes have been reported before. PONCE & CHAGANTI (1994) studied mass conservation of different Muskingum-Cunge methods for a sinusoidal flood wave in a prismatic channel. Losses of mass were small but increased with flow distance. Even a numerical solution of the complete Saint-Venant equations was inherent with small mass inconsistencies, if a term for flow volume losses was implemented (JIN & FREAD 1996).

In the present application model structure uncertainties are particularly problematic for the simulation of small floods like the diminished one of October 1979 at Aqrabim. They affect the magnitude of a flood (volume and peak discharge) rather than its timing (flood arrival and flow duration). Additionally a huge model parameter error increases the uncertainty of simulations, exceeding in its maximum 300 % for the peak and 100 % for the volume. For large floods, as represented by the October 1991 event, model uncertainties are considerably smaller. Moreover, the uncertainty of gauged runoff data increases considerably because of measurement problems (e.g. accentuated sediment dynamics, cross-section instability and high flow velocities). If gauging stations are even destroyed as during October 1991, the analysis of paleostage indicators or slackwater deposits may provide the most accurate information on peak discharges but only vague estimations on flow volumes. Hence for large floods model uncertainties fall into similar ranges like those of field gaugings and model simulations may provide valuable information.

Still the main area of application for the present model is the *simulation* of high magnitude runoff responses and flow processes *in conditions or areas with limited field information*. Then the field-based model structure is superior to calibrated relationships that must be extrapolated or regionalized. Two examples discussed in the previous chapter may illustrate this statement:

- The use of regression analysis relating travel time to peak discharge (BEN-ZVI et al. 1991) yielded satisfactory results for small to medium floods in two reaches of Nahal Zin. For high magnitude floods, as represented by the October 1991 event, the results were unrealistic.
- According to the regional statistical models by SHENTSIS et al. (1997) and MEIROVICH et al. (1998), that are based on probability distributions fitted to gauged data, the 100-year peak discharge of Nahal Hazera should not exceed 130 $m^3 s^{-1}$. Although the recurrence interval of the present scenario (440 $m^3 s^{-1}$) could not be calculated directly, it is reasonable to assume that a rain event similar to that of the scenario may occur once in a hundred years. The obvious difference in 100-year flood peaks may be explained by the particular catchment characteristics of Nahal Hazera suitable for the generation of high magnitude floods. These characteristics can only be accounted for in a non-calibrated approach.

13 Conclusions

This study shows that, in principle, field based data on generation and losses of runoff may be incorporated into a distributed hydrologic model to *overcome calibration with the poor data records* of arid high magnitude events. Doing this, model parameters must be determined by techniques suitable for the large modelling scale. These techniques include an analysis of field measurements conducted at the point- and model element scale, the use of rainfall radar scans, a GIS-based interpretation of aerial photographs and a non-rigid spatial subdivision dependent on single model parameters.

In the Zin catchment neither of the two large floods used for model validation was completely documented. This is a typical example of the scarcity of hydrologic data in large arid catchments. During the October 1979 flood the rainfall radar had not yet been installed and only the routing component could be tested. For the October 1991 event data from six rainfall recorders and a rainfall radar were available, facilitating a complete model run. However, gauging stations were destroyed and peak discharges had to be reconstructed post-factum. The fit of the peak discharges was encouraging as simulations fell within the uncertainty range of reconstructed field values. The flow volume was a bit overestimated but still in a correct order of magnitude.

A calibrated rainfall radar, as used for model input during the October 1991 event, may adequately describe the rainfall input for the scale of 1400 km^2 catchments. It may regionalize rain intensities measured at single points on the ground to entire catchments with accurate spatial and temporal distribution. However, using reflectivity values alone, a renewed calibration is required for each event. Hence the use of rainfall radar does not fully replace a ground based gauging network. It only reduces the needed density from 25 (MICHAUD & SOOROOSHIAN 1994b) to roughly one gauge per 100 km^2. In the absence of this elegant tool a physically based rainfall model, as used during the October 1979 event, may describe the two-dimensional rainfall distribution in the catchment scale. As general knowledge may be incorporated, these models may serve as an input for the estimation of rare discharges in ungauged catchments, as shown by the Hazera flood scenario. Still these models mainly suffer from the required 'geometrical' simplification of the spatial rainfall structure and any rainfall radar data, if available, is preferable.

Overall model uncertainty constantly increased with flow length. Besides the downstream increasing model parameter error, particularly evident during the October 1979 event, considerable model structure uncertainties existed for the channel routing and transmission loss routines. Here future research is needed to improve the simulations. It should concentrate on well documented channel reaches including reach-scale field measurements of flow processes and transmission losses during real flood events. Still, in general, reasonable model outputs are possible, as shown by the model validation during October 1991. If future efforts concentrate on the most apparent sources of error (i.e. raingauge adjustment of arid rainfall radar, detailed field based studies of runoff generation at the catchment scale and infiltration losses during flood events), the accuracy of non-calibrated model simulations may be further increased.

The different event characteristics directly affected parameter sensitivity and model uncertainty. Maximum model parameter error of the diminished October 1979 peak was governed by transmission loss parameters and exceeded 300 %. During 1991 only 90 % was determined for this value and infiltration characteristics of the terrain were more relevant. Also scenarios on the hydrological effects of widespread loess deposition, induced by a possible climate change, produced completely opposite results dependent on the rainfall input used (October 1979 or October 1991). It may be concluded that in general the separate analysis of single events is crucial for a thorough understanding of high magnitude floods in arid catchments. Gross general statements may lead to wrong conclusions.

By its distributed structure the model served as a *tool to analyze flood generation* during the two high magnitude floods:

In the uppermost catchment a localized, convective rainstorm caused the high magnitude flood of October 1979. Areas of major cell activity and runoff generation could be reasonably reconstructed by a reversed use of the Zin model as a 'runoff-rainfall model'. Both simulated and gauged hydrographs showed that even large floods may totally disappear flowing on dry arid channels for long distances.

The October 1991 rainstorm flood was generated by a huge squall line. Runoff generation took place in almost the entire catchment, still the spatial pattern revealed the trajectories of the inner core rainfall cells. The postponed response of an upper tributary directly sharpened the main flood peak. Then the peak did not decrease significantly downstream. Preceding inflows from tributaries caused an initial wetting of the alluvium. The following main flood crossed over a nearly saturated channel alluvium with a high flow velocity. Hence the effect of transmission losses on flood peaks may be limited when additional parts of a catchment are active.

Especially during the October 1991 flood, runoff concentration was quick with high flow velocities. Only five hours after rainfall onset the simulated flood front arrived at the Paleoflood Site (draining a 1,130 km^2 catchment), followed by the peak after only two more hours (Tab. 11.1). Peak flow velocities exceeding 6 m s^{-1} during the October 1991 event document the extreme danger inherent in these high magnitude flash floods. Despite the entirely different character of the two events, simulated flow duration constantly increased downstream. This was confirmed by the field hydrographs during October 1979.

The comparison to existing calibrated or regionalized models showed that the present approach may be regarded as superior when runoff responses (e.g. rare high magnitude discharges) and flow processes (e.g. concentration times and flow velocities) are simulated in conditions or areas where no field data exist. Hence, as a main area of application in *water resources management*, the model may be reasonably applied to *ungauged* catchments simulating the dangers and benefits of desert floods:

(a) First, a more dependable flood control for rapidly growing desert towns is possible. Aerial photographs, topographical maps (digital elevation models) and field evaluations may provide the data necessary for a model run. A 'field based estimate' of extreme discharges and flood concentration times will be provided.

(b) Second, the present model may be used to estimate runoff volumes available for groundwater recharge at the mouth of large dryland rivers. This may contribute to the understanding of recharge mechanisms of local and regional aquifers important for a sustainable management of the rare water resources in arid environments.

Notation

A	catchment area
a,b	regression parameters
B	width of the water surface
d_w	depth of the wetting front
I	mean infiltration rate
i_o	rainfall intensity at the raincell centre,
K	storage constant having dimensions of time
n	Manning roughness coefficient
$Q_{i+1, j}$	discharge at the next channel node at the present time step
$Q_{i, j}$	discharge at the present channel node at the present time
$Q_{i+1, j-1}$	discharge at the next channel node at the last time step
$Q_{i, j-1}$	discharge at the present channel node at the last time step
Q_{peak}	peak discharge
Q_{REF}	reference discharge
R_0	hydraulic radius
R	pre-adjusted rainfall intensities
r	distance from the centre
r^2	coefficient of determination
S_0	energy/channel slope
$stor_{al}$	available storage for losses in the channel alluvium
t	travel time
Δt	time step
t_1	time (after injection) when the first traces of tracer arrive
t_f	duration of the main flood
t_{med}	time when 50 % of the tracer load have passed
V_{max}	maximum observed flow volume
v	flow velocity
v_k	kinematic wave velocity
v_{max}	maximum velocity (determined by tracer sampling)
v_{med}	median velocity (determined by tracer sampling)
X	weighting factor
x	measure of a raincell's spatial extent
Δx	distance step (between two nodes)
Z	reflectivity values of the radar

References

Abbott, M. B., Bathurst, J. C., Cunge, J. A., O'Connel, P. E. & Rasmussen, J. (1986a): An introduction to the European Hydrological System - Système Hydrologique Européen, „SHE", 1: History and philosophy of a physically-based, distributed modelling system. Journal of Hydrology, 87, 45-59.

Abbott, M. B., Bathurst, J. C., Cunge, J. A., O'Connel, P. E. & Rasmussen, J. (1986b): An introduction to the European Hydrological System - Système Hydrologique Européen, „SHE", 2: Structure of a physically-based, distributed modelling system. Journal of Hydrology, 87, 61-77.

Abdulrazzak, M. J., Sorman, A. U. & Alhamas, A. S. (1989): Water balance approach under extreme arid conditions - a case study of Tabalah Basin, Saudi Arabia. Hydrological Processes, 3, 107-122.

Agnew, C. & Anderson, E. (1992): Water resources in the arid realm. Routledge, London.

Allam, M. N. (1990): Case study evaluation of a geomorphologic rainfall-runoff model, incorporating linear infiltration expression. Hydrological Processes, 4, 71-84.

Amiran, D. H. (1950): Geomorphology of the central Negev Highlands. Israel Exploration Journal, 1, 107-120.

Amit, R. & Gerson, R. (1986): The evolution of Holocene Reg (gravelly) soils in deserts; an example from the Dead Sea region. Catena, 13, 59-79.

Al-Turbak, A. S. (1996): Geomorphoclimatic peak discharge model with a physically based infiltration component. Journal of Hydrology, 176, 1-12.

Bänziger, R. (1994): Abflussmessung in Mittellandbächen - mit Messflügel oder Salzverdünnung?. Wasser, Energie, Luft, 86, 321-323, 1994.

Baker, V. R. (1987): Paleoflood hydrology and extraordinary flood events. Journal of Hydrology, 96, 79-99.

Bar-Lavy, B., Margalit, A. & Sharon, D. (1977): Desert rainfall patterns associated with the Red Sea trough. Conf. on Meteorology of Semiarid Zones, Tel Aviv, Israel.

Becker, A. (1992): Methodische Aspekte der Regionalisierung. In: Regionalisierung in der Hydrologie. Ed. by H.- B. Kleeberg. DFG-Mitt. XI, VCH-Verl. Ges. Weinheim, 16- 33.

Ben-Zvi, A., Massoth, S. & Schick, A. P. (1991): Travel time of runoff crests in Israel. Journal of Hydrology, 122, 309-320.

Bentor, Y. K. & Vroman, A.(1960): The Geological Map of Israel, Sheet 16: Mount Sdom. Jerusalem, Israel.

Beven, K. (1996): A discussion of distributed modelling. In Distributed hydrological modelling. Ed. by M. B. Abbott & J. C. Refsgaard, 255-278, Kluwer Academic Publishers, Dordrecht, The Netherlands.

Beven, K. (1995): Linking parameters across scales: subgrid parameterization and scale dependent hydrological models. Hydrological Processes, 9, 507-525.

Beven, K. & Kirkby, M. J. (1979): A physically-based variable contributing area model of basin hydrology. Hydrological Science Bulletin, 24, 43-69.

Bergström, S. (1992): The HBV-model - its structure and applications. SMHI Hydrology, RH no.4, Norrköping.

Black Dog & Leventhal Publishers Inc. (1995): Webster's New Encyclopedic Dictionary. New York.

Blöschl, G. & Sivapalan, M. (1995): Scale issues in hydrological modelling: a review. Hydrological Processes, 9, 251-290.

Blöschl, G., Grayson, R. B. & Sivapalan, M. (1995): On the Representative Elementary Area (REA) concept and its utility for distributed rainfall-runoff modelling. Hydrological Processes, 9, 313-330.

Brakensiek, D. L. & Rawls, W. J. (1994): Soil containing rock fragments: effects on infiltration. Catena, 23, 99-110.

Bull, W. B. (1991): Geomorphic Responses to Climatic Change. Oxford University Press. New York.

Bull, W. B. (1997): Discontinuous ephemeral streams. Geomorphology, 19, 227-276.

Burgess, D. W. & Lemon, L. R. (1990): Severe thunderstorm detection by radar. In: Radar in Meteorology. Ed. by D. Atlas, 619-647. American Meteorol. Society. Boston.

Chiew, F. H. S., Whetton, P. H., McMahon, T. A. & Pittock, A. B. (1995): Simulation of the impact of climate change on runoff and soil moisture in Australian catchments. Journal of Hydrology, 167, 121-147.

Chow, V. T. (1959): Open-channel Hydraulics. McGraw-Hill. New York.

Chow, V. T., Maidment, D. R. & Mays, L. W. (1988): Applied Hydrology. McGraw-Hill. New York.

Collier, C. G. (1996): Weather radar precipitation data and their use in hydrological modelling. In: Distributed hydrological modelling. Ed. by M. B. Abbott & J. C. Refsgaard, 143-163, Kluwer Academic Publishers, Dordrecht, The Netherlands.

Cordery, I., Pilgrim, D. H. & Doran, D. G. (1983): Some hydrological characteristics of arid western New South Wales. In: Proc. Hydrology and Water Resources

Symposium. Institution of Engineers. Australia. Natl. Conf. Pub. No. 83/13, 287-292.

Costa, J. E. (1987): Hydraulics and basin morphometry of the largest flash floods in the conterminous United States. Journal of Hydrology, 93, 313-338.

Courant, R. & Friedrichs, K. O. (1948): Supersonic Flow and Shock Waves, Interscience Publishers, New York.

Crawford, N. H. & Linsley, R. K. (1966): Digital simulation in hydrology, Stanford watershed model. Tech. Rep. No. 39, Dep. Civ. Eng. Stanford University.

Crear, S., Fry, R. G. & Slater, G. (1988): An unexpected factor affecting recharge from ephemeral river flows in SWA/Namibia. In: Estimaton of natural groundwater recharge. Ed. by I. Simmers, 11-28. Reidel. Dordrecht. The Netherlands.

Cunge, J. A. (1969): On the subject of a flood propagation method (Muskingum method). Journal of Hydrological Research, 7, 205-230.

Dalrymple, T. & Benson, M. A. (1967): Measurements of peak discharges by the slope-area method. USGS Tech. Water Resour. Invest., 3, A2.

Dan, J., Yaalon, D. H., Moshe, R. & Nissim, S. (1982): Evolution of Reg soils in southern Israel and Sinai. Geoderma, 28, 173-202.

Dan, J. (1981): The northwestern part of the Negev hills and mountains. in Aridic Soils of Israel, Properties, Genesis and Management. Ed. by J. Dan, R. Gerson, H. Koyumdjisky & D. H. Yaloon, 223-238. Division of Scientific Publications. Bet Dagan. Israel.

Dooge, J. C. (1992): Hydrological models and climatic change. Journal of Geophysical Research, 97. D3, 2677-2683.

DWD (German Weather Service) Ed. (1995): Herbstschule Radarmeteorologie. Annalen der Meteorologie, 32. DWD. Offenbach.

Emmett, W. W. (1978): Overland Flow. In: Hillslope Hydrology, ed. by M. J. Kirkby, 145- 176. Wiley. New York.

Evenari, M., Yaalon, D. H. & Gutterman, Y. (1974): Note on soils with vesicular structure in deserts. Zeitschrift für Geomorphologie, 18(2), 162-172.

Evenari, M., Shanan, L. & Tadmor, N. (1982): The Negev, the Challange of a Desert. Harvard University Press. Cambridge. Massachusetts.

Eybergen, F. A. & Imeson, A. C. (1989): Geomorphical processes and climatic change, Catena, 16, 307-319.

Fan, Y. & Bras, R. L. (1995): On the concept of a Representative Elementary Area in catchment runoff. Hydrological Processes, 9, 821-832.

Fread, D. L. (1985): Channel Routing. In: Hydrological Forecasting. Ed. by M. G. Anderson & T. P. Burt, 437-503. Wiley. New York.

Fread, D. L. (1993): Flow Routing. In Handbook of Hydrology. Ed. by D. R. Maidment, 10.1-10.36. McGraw-Hill. New York.

Gerson, R. (1982): The Middle East, landforms of a planetary desert through environmental changes. In: The Geological Story of the World`s Deserts. Ed. by T. L. Smiley. Striae, 7, 52-78.

Gerson, R. & Amit, R. (1986): The Evolution of Holocene Reg (gravelly) soils in deserts - an example from the Dead Sea region. Catena, 13, 59-79.

Gerson, R., Amit, R. & Grossman, S. (1985): Dust availability in desert terrains. A study in the deserts of Israel and the Sinai. Institute of Earth Sciences. The Hebrew University of Jerusalem. Israel.

Goodfriend, G. A., Magaritz, M. & Carmi, I.(1986): A high stand of the Dead Sea at the end of the Neolithic Period: paleoclimatic and archeological implications. Climatic Change 9, 349-356.

Goodrich, D. C., Lane, L. J., Shillito, R. A., Miller, S. N., Syed, K. H. & Woolhiser, D. A. (1997): Linearity of basin response as a function of scale in a semi-arid watershed. Water Resources Research, 33, 2951-2965.

Graf, W. D. (1988): Fluvial processes in dryland rivers. Springer. Berlin.

Grayson, R. B., Moore, I. D. & McMahon, T. A. (1992): Physically based hydrologic modeling, 1. A terrain-based model for investigative purposes. Water Resources Research, 28, 2639-2658.

Greenbaum, N. (1986): Point runoff in an extremely arid region. Infiltration-runoff tests on small plots in the southern Arava and their hydrological and pedological implications, Msc. Thesis, Department of Physical Geography, The Hebrew University of Jerusalem, (In Hebrew).

Greenbaum, N., Margalit, A., Schick, A. P. , Sharon, D. & Baker, V. R. (1998): Reconstruction of a high magnitude rainstorm-flood in Nahal Zin - a large hyperarid catchment in the Negev Desert, Israel. Hydrological Processes, 12, 1-23.

Greenbaum, N., Schick, A. P. & Baker, V. R., The paleoflood record of Nahal Zin - a hyperarid catchment in the Negev Desert, Israel. Earth Surface Processes and Landforms. in press.

Gupta, V. K., Rodríguez-Iturbe, I. & Wood, E. F. (1986): Scale Problems in Hydrology. Reidel. Dordrecht.

Horton, R. E. (1933): The role of infiltration in the hydrological cycle. EOS. American Geophysical Union Transactions, 14, 446-460.

Houghton, J., Filho, B., Callendar, N., Harris, N., Kattenburg, A. & Maskell, K. (1996): Climatic Change 1995: The Science of Climatic Change. Cambridge University Press. New York.

Hughes, D. A. & Sami, K. (1994): A semi-distributed, variable time interval model of catchment hydrology - structure and parameter estimation procedures. Journal of Hydrology, 155, 265-291.

Hughes, D. A. (1997): Southern African „FRIEND"- The Application of Rainfall-Runoff Models in the SADC Region, WRC Report No. 235/1/97, Grahamstown, South Africa.

Hydrological Engineering Center (1982): HEC-2 Water Surface Profiles: Program User's Manual. US Army corps of Engineers. Davis.

Islam, S., Bras, R. L. & Rodriguez-Iturbe, I. (1988): Multidimensional modeling of cumulative rainfall: parameter estimation and model adequacy through a continuum of scales. Water Resources Research, 24, 985-992.

Issar, A. (1983): Emerging groundwater, a triggering factor in the formation of the Makhteshim (erosion cirques) in the Negev and Sinai. Israel Journal of Earth Sciences, 32, 53-61.

Issar, A., Karnieli, A., Bruins, H. J. & Gilead, I. (1984): The Quarternary geology and hydrology of Sede Zin, Negev, Israel. Israel Journal of Earth Sciences, 33, 34-42.

Jarrett, R. D. (1985): Determination of roughness coefficients for streams in Colorado. Water resources invest. report No. 85-4004. Lakewood. Colorado.

Jin, M. & Fread, D. L. (1996): Channel routing with flow losses. Journal of Hydraulic Engineering ASCE, 580-582.

Joss, J. (1995): Radar als Hilfsmittel für quantitative Niederschlagsmessung. In: Herbstschule Radarmeteorologie. Ed. by DWD. Annalen der Meteorologie, 32.

Joss, J. & Waldvogel, D. (1990): Precipitation measurement and hydrology. In: Radar in Meteorology. Ed. by D. Atlas, 577-606. American Meteorol. Society. Boston.

Karnieli, A. M., Diskin, M. H. & Lane, L. J. (1994): CELMOD5 - a semi-distributed model for conversion of rainfall into runoff in semi-arid watersheds. Journal of Hydrology, 157, 61-85.

Kelway, P. S. & Herbert, S. I.(1969): Short term rainfall analysis. Weather, 24, 342-354.

Kirby, W. (1985): Statistical error analysis of the slope-area method of indirect discharge determination. EOS, 66, AGU.

Klemes, V. (1983): Conceptualisation and scale in hydrology. Journal of Hydrology, 65, 1-23.

Klemes, V. (1988): A hydrological perspective. Journal of Hydrology, 100, 3-28.

Knighton, D. A. & Nanson, G. C. (1994): Flow transmission along an arid zone anastomosing river, Cooper Creek, Australia. Hydrological Processes, 8, 137-154.

Kochel, R. C. & Baker, V. R.(1988): Paleoflood analysis using slackwater deposits. In: Flood Geomorphology. Ed. by V. R. Baker R. C. Kochel & P. C. Patton, 357-376. Wiley. New York.

Kotwicki, V. (1987): On the future of rainfall-runoff modelling in arid areas - Lake Eyre case study. IAHS-Publ. no. 164, 341-351.

Külls, C., Leibundgut, Ch., Schwartz, U. & Schick, A. P. (1995): Channel infiltration study using dye tracers, IAHS-Publ. no 232, 429-436.

Kutiel, H. & Sharon, D. (1980): Diurnal variation of rainfall in Israel. Archives for Meteorology, Geophysics and Bioclimatology, 29, 387-395, 1980.

Lane, L. J. (1982): Distributed model for semiarid watersheds. Journal of the Hydraulics Division, ASCE 108 (HY10), 1114-1131.

Lane, L. J. (1985): Transmission losses. In: National Engineering Handbook. Ed. by SCS. chapt. 19, 1-21.

Lange, J., Leibundgut, Ch., Lekach, J., Grodek, T. & Schick, A. P. (1996): A study on infiltration characteristics of the channel alluvium in Nahal Yael using dye tracers. Proc. of the Third IGRG Conference, Eilat, Israel, 86-87.

Lange, J., Leibundgut, Ch., Grodek, T., Lekach, J. & Schick, A. P. (1998): Using artificial tracers to study water losses of ephemeral floods in small arid streams. IAHS-Publ. no. 247, 31-40.

Laurenson, E. M. & O'Donnel, T. (1969): Data errors in Unit Hydrograph derivation. Journal of the Hydraulics Division, ASCE 95, HY6, 1899-1917.

Laurenson, E. M. & Mein, R. G.: (1983): RORB Version 3 - User Manual. Monash University, Melbourne, Australia.

Lavee, H.(1986): A deterministic simulation model for the rainfall-runoff relationship on arid hillslopes. Zeitschrift für Geomorphologie, Suppl. 58, 35-46.

Leavesley, G. H. (1994): Modelling the effects of climatic change on water resources - a review. Climatic Change, 28, 159-177.

Leavesley, G. H. & Hay L. (1998): The use of coupled atmospheric and hydrological models for water-resources management in headwater basins. IAHS-Publ. no. 248, 259-265.

Leopold, L. B. & Wolman, M. G. (1957): River channel patterns: braided, meandering and straight. U.S. Geological Survey Prof. Paper, 282-B.

Lighthill, M. J. & Whitham, G. B. (1955): On kinematic waves, I: flood movement in long rivers.Proc. R. Soc. London A, vol. 229, no. 1178, 281-316.

Luk, S. H., Cai, Q. G. & Wang, G. P.(1993): Effects of surface crusting and slope gradient on soil and water losses in the hilly loess region, North China. Catena Suppl., 24, 29-45.

Mabbutt, J. A. (1977): Desert Landforms. Aust. Nat. Univ. Press. Canberra.

Mein, R. G. & Brown, B. M. (1978): Sensitivity of optimized parameters in watershed models. Water Resources Research, 14, 299-303.

Meirovich, L., Ben-Zvi, A., Shentsis, I. & Yanovich, E. (1998): Frequency and magnitude of runoff events in the arid Negev of Israel. Journal of Hydrology, 207, 204-219.

Melching, C. S. (1995): Reliability estimation. In: Computer models of watershed hydrology. Ed by V. P. Singh, 69-118. Water Resources Pub., Highlands Ranch, CO.

Michaud, J. & Sorooshian, S. (1994a): Comparison of simple versus complex distributed runoff models on a midsized semiarid watershed. Water Resources Research, 30, 593-605.

Michaud, J. & Sorooshian, S. (1994b): Effect of rainfall-sampling errors on simulations of desert flash floods. Water Resources Research, 30, 2765-2775.

Miller, R. M. & Ritter, J. B. (1996): An examination of the Rosgen classification of natural rivers. Catena, 27, 295-299.

Morin, J. & Benyamini, Y. (1977): Rainfall infiltration into bare soils. Water Resources Research, 13, 813-817.

Morin, J., Rosenfeld, D. & Amitai, E. (1995): Radar rain field evaluation and possible use of its high temporal and spatial resolution for hydrological purposes. Journal of Hydrology, 172, 275-292.

Mosley, M. P. & McKerchar, A. I. (1993): Streamflow. In: Handbook of Hydrology. Ed. by D. R. Maidment, 8.1-8.39, McGraw-Hill, New York.

Nash, J. E. (1958): The form of the instantaneous unit hydrograph. IAHS-Publ. no. 45, 114-121.

Natural Environment Research Council (NERC) (1975): Flood Studies Report, Vol. III, Flood Routing Studies. Institute of Hydrology. Wallingford. UK.

Nouh, M. (1990): Flood hydrograph estimation from arid catchment morphology. Hydrological Processes, 4, 103-120.

O'Connor, J. E. & Webb, R. H. (1988): Hydraulic modeling for paleoflood analysis. In: Flood Geomorphology. Ed. by V. R. Baker R. C. Kochel & P. C. Patton, 393-402. Wiley. New York.

Paul, A.H. (1973): The heavy hail of 23-24 July 1971 on the Western Prairies of Canada. Weather, 28, 463-471.

Perumal, M. (1992): Multilinear Muskingum flood routing method. Journal of Hydrology, 133, 259-272.

Picard, L. (1951): Geomorphogeny of Israel. The Hebrew University of Jerusalem. Jerusalem, Israel.

Pilgrim, D. H., Chapman, T.G. & Doran, D.G. (1988): Problems of rainfall-runoff modelling in arid and semiarid regions. Hydrological Science Journal, 33, 379-400.

Ponce, V. M. & Chaganti, P. V. (1994): Variable-parameter Muskingum-Cunge method revisited. Journal of Hydrology, 162, 433-439.

Refsgaard, J. C. (1996): Terminology, modelling protocol and classification of hydrological model codes, In: Distributed hydrological modelling. Ed. by M. B. Abbott & J. C. Refsgaard, 17-39. Kluwer Academic Publishers. Dordrecht. The Netherlands.

Refsgaard, J. C., Storm, B. & Abbott, M. B. (1996): Comment on 'A discussion on distributed hydrological modelling' by K. Beven. In Distributed hydrological modelling. Ed. by M. B. Abbott & J. C. Refsgaard, 279-288. Kluwer Academic Publishers. Dordrecht. The Netherlands.

Renard, K. G., Lane, L. J., Simanton, J. R., Emmerich, W. E., Stone, J. J., Weltz, M. A., Goodrich, D. C. & Yakowitz, D. S. (1993): Agricultural impacts in an arid environment: Walnut Gulch case study. Hydrological Science and Technology, 9, 145-190.

Renard K. G. & Keppel R. V. (1966): Hydrographs of ephemeral streams in the Southwest. Journal of the Hydraulics Division, 92, 33-52.

Riedl, J. (1995): Erforderliche Korrekturen und gebräuchliche Korrekturverfahren bei der Nutzung von Wetterradardaten. In: Herbstschule Radarmeteorologie. Ed. by DWD, Annalen der Meteorologie, 32, Offenbach.

Roded, R. (1983): The Geological Map of Israel, Sheet 19-III: Oron. Geological Survey of Israel. Jerusalem. Israel.

Rodriguez-Iturbe, I. & Valdes, J. B. (1979): The geomorphologic structure of hydrologic response. Water Resources Research, 15, 1409-1420.

Römkens, M. J. M., Prasad, S. N. & Whisler, F. D. (1990): Surface sealing and infiltration. In: Process Studies in Hillslope Hydrology. Ed. by M. G. Anderson & T. P. Burt, 127-172. Wiley. New York.

Rosenfeld, D., Wolff, D. B. & Amitai, E. (1994): The window probability matching method for rainfall measurements with radar. Journal of Applied Meteorology, 33, 682-693.

Rosenthal, E., Magaritz, M., Ronen, D. & Roded, R. (1987): Origin of nitrates in the Negev Desert, Israel. Applied Geochemistry, 2, 347-354.

Rosgen, D. L. (1994): A classification of natural rivers, Catena, 22, 169-199.

Salmon, O. & Schick, A. P. (1980): Infiltration tests. In: Arid Zone Geosystems. Ed. by. A. P. Schick, 55-115. Division of Physical Geography. The Hebrew University. Jerusalem.

Schick, A. P. (1968): The storm of March 11, 1966 in the southern Negev and its significance for flood control in deserts. Paper presented at the 21st international geographical congress. India. separatum. The Hebrew University of Jerusalem.

Schick, A. P. (1988): Hydrologic aspects of floods in extreme arid environments. In: Flood Geomorphology. Ed. by V. R. Baker R. C. Kochel & P. C. Patton, 189-203. Wiley. New York.

Schick, A. P. & Lekach, J. (1987): A high magnitude flood in the Sinai desert. In: Catastrophic flooding. Ed. by L. Mayer & D. Nash, 381-410. Allen and Unwin. Winchester.

Schick, A. P. & Lekach, J. (1993): An evaluation of two ten-year sediment budgets, Nahal Yael. Physical Geography, 14, 225-238.

Schick A.P., Lekach J., Grokek T., Lange J. & Leibundgut Ch. (1996): An artificial flash flood in a small arid stream channel, Eilat Mountains, Israel. EOS. AGU. F259.

Schick, A.P., Grodek, T & Lekach, J. (1997): Sediment management and flood protection of desert towns: effect of small catchments. IAHS-Publ. no. 245, 183-189.

Schroth, A. (1995): Theoretische Grundlagen der Radartechnik, in Herbstschule Radarmeteorologie. Ed. by DWD. Annalen der Meteorologie, 32. Offenbach.

Schumm, S. A. (1977): The Fluvial System. Wiley. New York.

Sehmi N. S. & Kundzewicz Z. W. (1997): Water, drought and desertification in Africa, IAHS-Publ. no 240, 57-65.

Shanan, L. A. (1975): Rainfall and runoff relationships in small watersheds in the Avdat region of the Negev Desert Highlands. PhD.-thesis. The Hebrew University of Jerusalem.

Shanan, L. A. & Tadmor, N. H. (1979): Micro-catchment systems for arid zone development, A Handbook for design and construction. Centre of International Agricultural Coorporation. Ministry of Agriculture. Rehovot. Israel.

Shanan, L. A. & Schick, A. P. (1980): A hydrological model for the Negev Desert Highlands: effects of infiltration, runoff and ancient agriculture. Hydrological Science Journal, 25, 269-282.

Sharma, K. D., Murthy, J. S. R. & Dhir, R. P. (1994): Streamflow routing in the Indian arid zone. Hydrological Processes, 8, 27-43.

Sharma, K. D., Menenti, M., Huygen, J. & Fernandez, P. C. (1996): Distributed numerical rainfall-runoff modelling in an arid region using Thematic Mapper data and a geographical information system. Hydrological Processes, 10, 1229-1242.

Sharma, K. D. & Murthy, J. S. R. (1998): A practical approach to rainfall-runoff modelling in arid zone drainage basins. Hydrological Science Journal, 43, 331-348.

Sharon, D. (1970): Areal pattern of rainfall in a small watershed a affected by wind and other climatic conditions, IAHS-Publ. no. 96, 3-11.

Sharon, D. (1972): The spottiness of rainfall in a desert area, Journal of Hydrology, 17, 161-175.

Sharon, D. & Kutiel, H. (1986): The distribution of rainfall intensity in Israel, its regional and seasonal variations and its climatological evaluation. Journal of Climatology, 6, 277-291.

Shentsis, I., Ben-Zvi, A. & Golts, S. (1997): A physically-related regional model for extreme discharges in Israel. Hydrological Science Journal, 42, 391-404.

Sherman, L. K. (1932): Streamflow from rainfall by the unit graph method. Eng. News Rec. 108, 501-505.

Singh, V. P. (1995): Watershed Modeling, in: Computer models of watershed hydrology. Ed. by V. P. Singh, 1-22. Water Resources Pub., Highlands Ranch, CO.

Smith, R. E., Goodrich, D. C., Woolhiser, D. A. & Unkrich, C. L. (1995): KINEROS - a kinematic runoff and erosion model. In: Computer models of watershed hydrology. Ed. by V. P. Singh, 697-732. Water Resources Pub. Highlands Ranch. CO.

Soil Conservation Service (SCS) (1985): National Engineering Handbook, Section 4 Hydrology. US Department of Agriculture. Washington D.C.

Storm, B. & Refsgaard, A. (1996): Distributed physically based modelling of the entire land phase of the hydrological cycle. In: Distributed hydrological modelling. Ed. by M. B. Abbott and J. C. Refsgaard, 55-69. Kluwer Academic Publishers. Dordrecht. The Netherlands.

Thomas, H. A.(1934): The hydraulics of flood movement in rivers. Eng. Bull., Carnegie Inst. of Technology. Pittburgh. PA.

Todini, E. (1988): Rainfall-runoff modelling - past, present and future. Journal of Hydrology, 100, 341-352.

Uhlenbrook, S., Holocher, J., Leibundgut, Ch. & Seibert, J. (1998): Using a conceptual rainfall-runoff model on different scales by comparing a headwater with larger basins. IAHS-Publ. no. 248, 297-305.

Uhlenbrook, S., Seibert, J., Leibundgut, Ch. & Rohde, A.: Prediction uncertainty of conceptual rainfall-runoff models caused by problems to identify model parameters and structure.Hydrological Science Journal. in press.

UNESCO (1979): Map of the world distribution of arid regions. MAB Tech. Notes, 7, UNESCO, Paris.

Van Zuidam, R. A. (1986): Aerial Photo-Interpretation in Terrain Analysis and Geomorphological Mapping. Smits Publishers. The Hague. The Netherlands.

Verhoog, F. H. (1987): Impact of climate change on the morphology of river basins. IAHS-Publ. no. 168, 315-326.

Walters, M. O. (1989): A unique flood event in an arid zone. Hydrological Processes, 3, 15-24.

Waymire, E., Gupta, V. K. & Rodriguez-Iturbe, I. (1984): A spectral theory of rainfall intensity at the meso-β scale. Water Resources Research, 20, 1453-1465.

Wheater, H. S., Woods Ballard, B. & Jolley, T. J. (1997): An integrated model of arid zone water resources: evaluation of rainfall-runoff simulation performance. IAHS-Publ. no. 240, 395-405.

Wheater, H. S. (1994): Modelling hydrological processes in arid and semi-arid regions. Proc. of the International Conference on the Efficient Utilization and Management of Water Resources in Africa. Khartoum. Sudan. 392-412.

Wood, E. F., Sivapalan, M., Beven, K. & Band, L. (1988): Effects of spatial variability and scale with implications to hydrological modelling. Journal of Hydrology, 102, 29-47.

Woods, R., Sivapalan, M. & Duncan, M.(1995): Investigating the representative elementary area concept: an approach based on field data. Hydrological Processes, 9, 291-312.

Yaalon, D. H. (1981): Environmental setting. In Aridic Soils of Israel, Properties, Genesis and Management. Ed. by J. Dan, R. Gerson, H. Koyumdjisky & D. H. Yaloon, 3-16. Division of Scientific Publications. Bet Dagan. Israel.

Yanovich, E., Ben-Zvi, A. & Shentsis, I. (1996): Enveloping curves for maximum discharges in the Negev wadis. Rep. HYD/6/96. Israel Hydrological Service. Jerusalem. Israel (in Hebrew).

Yair A. & Lavee, H. (1985): Runoff generation in the arid and semiarid zones. In: Hydrological forecasting. Ed. by M. G. Anderson & T. P. Burt, 183-221. Wiley. New York.

Yair, A. & Klein, M. (1973): The influence of surface properties on flow and erosion processes on debris covered slopes in an arid area. Catena, 1, 1-18.

Yair, A., Lavee, H., Bryan, R. B. & Adar, E. (1980a): Runoff and Erosion processes and rates in the Zin Valley badlands, Northern Negev, Israel. Earth Surface Processes and Landforms, 5, 205-225.

Yair, A., Sharon, D. & Lavee, H. (1980b): Trends in runoff and erosion processes over an arid limestone hillside, Northern Negev, Israel. Hydrological Science Bulletin, 25, 243-255.

Yair, A. (1987): Environmental effects of loess penetration into the Northern Negev. Journal of Arid Environments, 13, 9-24.

Yair, A. (1990): Runoff generation in a sandy area, the Nizzana sands Western Negev, Israel. Earth Surface Processes and Landforms, 15, 597-609.

Yair, A. (1992): The control of headwater area on channel runoff in a small arid watershed. In:Overland Flow. Ed. by T. Parsons & A. Abrahams, 53-68. University College Press.London.

Yechiely, Y., Elron, E. & Sneh, A. (1994): The Geological Map of Israel, Sheet 19-IV, 20-III: Neot Hakikar. Geological Survey of Israel. Jerusalem. Israel.

Ye, W., Bates, B. C., Viney, N. R., Sivapalan, M. & Jakeman, A. J. (1997): Performance of conceptual rainfall-runoff models in low yielding ephemeral catchments. Water Resources Research, 33, 153-166.

Zhang, X. C. & Miller, W. P. (1993): The effect of drying on runoff and interrill erosion of crusted soils. Catena Suppl., 24, 103-114.

Zilberman, E. (1989): The Development of the Landscape in the Central and Northwestern Negev in the Neogene and the Quarternary. PhD.-Thesis. Institute of Earth Science. The Hebrew University of Jerusalem (in Hebrew).

Zilberman, E. (1993): The Mahmal Graben and Nahal Hawwa, an introduction to paleogeography of the central Negev in the Miocene. Israel Journal of Earth Sciences, 42, 197-209.

Zilberman, E. & Eidelman, A. (1994): „Makhtesh“ - an erosion cirque at an anticlinal crest. unpublished manuscript. Jerusalem.

Acknowledgements

Only the support of my two supervisors enabled to perform the steps from a vague idea to a successful application of a newly developed rainfall-runoff model.

(a) In difficult times (after almost two years of waiting, a research proposal was rejected) Prof. Ch. Leibundgut provided financial backup from different sources. He provided finances for a portable computer and covered travelling expenses. By a temporary employment at the IHF he helped to bridge times of ‘no-money’.

(b) Prof. A. P. Schick was the ‘human and scientific backbone’ of the present study. He co-ordinated the access to different facilities (e.g. GIS) and data sources (rainfall- and runoff data, airphotos). Any time he was, and still is, open for thorough discussions and invested much time in valuable reviews of various papers.

Over the last four years the entire IHF-team provided a warm working atmosphere.

(a) Petra Schreiber gave initial aid in ‘Understanding GIS’.

(b) Any time, Franz-Josef Kern, Günter Gässler and Jürgen Strub were sympathetic listeners with all computer and printing problems.

(c) Paul Königer and Kerstin Stahl reviewed some chapters of the present volume.

(d) My bureau mate Stefan Uhlenbrook did not only invest much time in reviewing most of my abstracts and papers, he also provided many ideas in controversial discussions. This helped to stay on the right track in the delicate balance between virtual model simulations and the real world.

During my various stays in Israel I experienced help from many sides.

(a) Tamir Grodek offered his kind hospitality. Through him and his family I learned that Israel is a special place, not only in terms of arid zone hydrology.

(b) Dr. A. Ben-Zvi shared his experience on the accuracy of the hydrometric streamflow data and gave me free access to the hydrological data files of the Israel Hydrological Service.

(c) Adi Ben-Nun offered help in the local GIS-facilities at the Hebrew University of Jerusalem. Through him the borrowed airphotos could be scanned and sent electronically to Freiburg. Moreover, he put a DTM of the entire Nahal Zin at my disposal.

(d) Prof. A. Yair provided first hand information on infiltration properties of different lithologies and Prof. D. Sharon on arid rainfall.

(e) Without asking for any service in return, Efrat Morin sent the original radar data of the October 1991 event. Without this help there would have been no chance to perform a non-calibrated model run and to fully test this new approach. The radar data were collected by Mekorot, Electro-Mechanical Service Ltd.

(f) Noam Greenbaum played a decisive part in the various field trips that were necessary for the mapping. Starting in the middle of the night we spent many days inside Nahal Zin. There he shared his vast field experience with me, this also included a marvellous field-coffee.

The Förderverein Hydrologie at the University of Freiburg i. Br. provided a scholarship and financial support for several conference visits.

Dr. A. Schumann critically reviewed model structure and parametrization and gave useful ideas. Also the comments F. Watson, D. C. Goodrich and R. B. Grayson, in their function as the external reviewers of Water Resources Research, considerably improved parts of the present study.

Last but not least, the entire work would not have been possible without the kind private backup of Simone.

Jens Lange

Annex

Tab. A1 Rainfall simulator experiments conducted by GREENBAUM (1986)

Lithology	Granite	Schist	Amphibolite	Colluvium	Compressed Alluvium	Young Alluvium	Old Alluvium
Number of measurements (initial loss / final infiltration rate)	3/3	3/3	3/3	10/10	3/2	5/4	26/22
Initial loss (mean, mm)	0.6	1.7	0.8	3.4	6.7	6.2	4.2
Initial loss (RMSE, mm)	**0.8**	**1.2**	**0.4**	**0.8**	**2.7**	**1.2**	**0.8**
Final infiltration rate (mean, mm hr^{-1})	2.6	4.0	9.3	21.9	*	57.8	17.9
Final infiltration rate (RMSE, mm hr^{-1})	0.2	0.2	3.7	7.3	*	3.8	7.3
Final infiltration rate (RMSE. %)	**7.6**	**4.3**	**39.7**	**33.3**	*****	**6.5**	**41.2**

* only two independent measurements

Tab. A2 Field measurements of cross-sectional geometry

Channel Node	Channel Type	Width of inner channels [double steps]	Bankful width [double steps]	Width of inner channels [m]	Bankful width [m]	Percentage covered by inner channels
10	1	3	31	4.8	49.6	0.09677419
11	1	4	23	6.4	36.8	0.17391304
14	1	4	20	6.4	32	0.2
18	1	8	25	12.8	40	0.32
19	2	6	13	9.6	20.8	0.46153846
20	2	13.5	26	21.6	41.6	0.51923077
21	2	8	39	12.8	62.4	0.20512821
24	2	9	41	14.4	65.6	0.2195122
25	2	10	23	16	36.8	0.43478261
27	2	8	23	12.8	36.8	0.34782609
28	2	6	28	9.6	44.8	0.21428571
29	2	7	18	11.2	28.8	0.38888889
30	2	13	20	20.8	32	0.65
48	2	15	48	24	76.8	0.3125
51	2	18	39	28.8	62.4	0.46153846
52	2	26	35	41.6	56	0.74285714
54	2	9	30	14.4	48	0.3
55	2	19	36	30.4	57.6	0.52777778
60	2	11	42	17.6	67.2	0.26190476
61	2	15	50	24	80	0.3
78	2	7	52	11.2	83.2	0.13461538
79	2	10	46	16	73.6	0.2173913
80	2	15	28	24	44.8	0.53571429
84	2	12	33	19.2	52.8	0.36363636
85	2	12	18	19.2	28.8	0.66666667

86	2	8	17	12.8	27.2	0.47058824
87	2	13	17	20.8	27.2	0.76470588
89	2	4	16	6.4	25.6	0.25
90	2	8	48	12.8	76.8	0.16666667
91	2	13	44	20.8	70.4	0.29545455
100	2	30	55	48	88	0.54545455
101	2	19	26	30.4	41.6	0.73076923
105	2	31	75	49.6	120	0.41333333
113	2	35	60	56	96	0.58333333
114	2	20	42	32	67.2	0.47619048
115	2	28	55	44.8	88	0.50909091
139	1	3	14	4.8	22.4	0.21428571
141	2	15	22	24	35.2	0.68181818
158	2	40	67	64	107.2	0.59701493
159	2	17	73	27.2	116.8	0.23287671
160	3	36	173	57.6	276.8	0.20809249
161	3	44	209	70.4	334.4	0.21052632
162	3	59	270	94.4	432	0.21851852
171	3	58	496	92.8	793.6	0.11693548
174	3	91	403	145.6	644.8	0.22580645
178	3	34	472	54.4	755.2	0.0720339
180	3	50	273	80	436.8	0.18315018
183	3	49	108	78.4	172.8	0.4537037
187	3	34	104	54.4	166.4	0.32692308
189	2	10	16	16	25.6	0.625
202	2	6	25	9.6	40	0.24
209	2	5	12	8	19.2	0.41666667
220	2	8	11	12.8	17.6	0.72727273
223	2	5	13	8	20.8	0.38461538
227	2	15	41	24	65.6	0.36585366
251	2	9	31	14.4	49.6	0.29032258
262	3	29	134	46.4	214.4	0.21641791
266	3	14	188	22.4	300.8	0.07446809
268	3	28	125	44.8	200	0.224
269	3	10	180	16	288	0.05555556
279	2	11	19	17.6	30.4	0.57894737
280	2	10	19	16	30.4	0.52631579
281	2	15	32	24	51.2	0.46875
298	2	20	38	32	60.8	0.52631579
302	2	18	26	28.8	41.6	0.69230769
303	2	39	74	62.4	118.4	0.52702703
311	2	18	53	28.8	84.8	0.33962264
312	2	30	44	48	70.4	0.68181818
313	2	16	62	25.6	99.2	0.25806452
329	2	9	10	14.4	16	0.9
330	2	23	40	36.8	64	0.575
331	2	36	115	57.6	184	0.31304348
349	2	34	106	54.4	169.6	0.32075472
350	2	63	130	100.8	208	0.48461538
Mean	**1**					**0.20099459**
Mean	**2**					**0.45045367**
Mean	**3**					**0.19893321**

Fig. A1 **Typical Negev highlands: dissected limestone plateau (terrain type 2) with rocky upper slope areas (front) and colluvial mantles at the slope bottom**

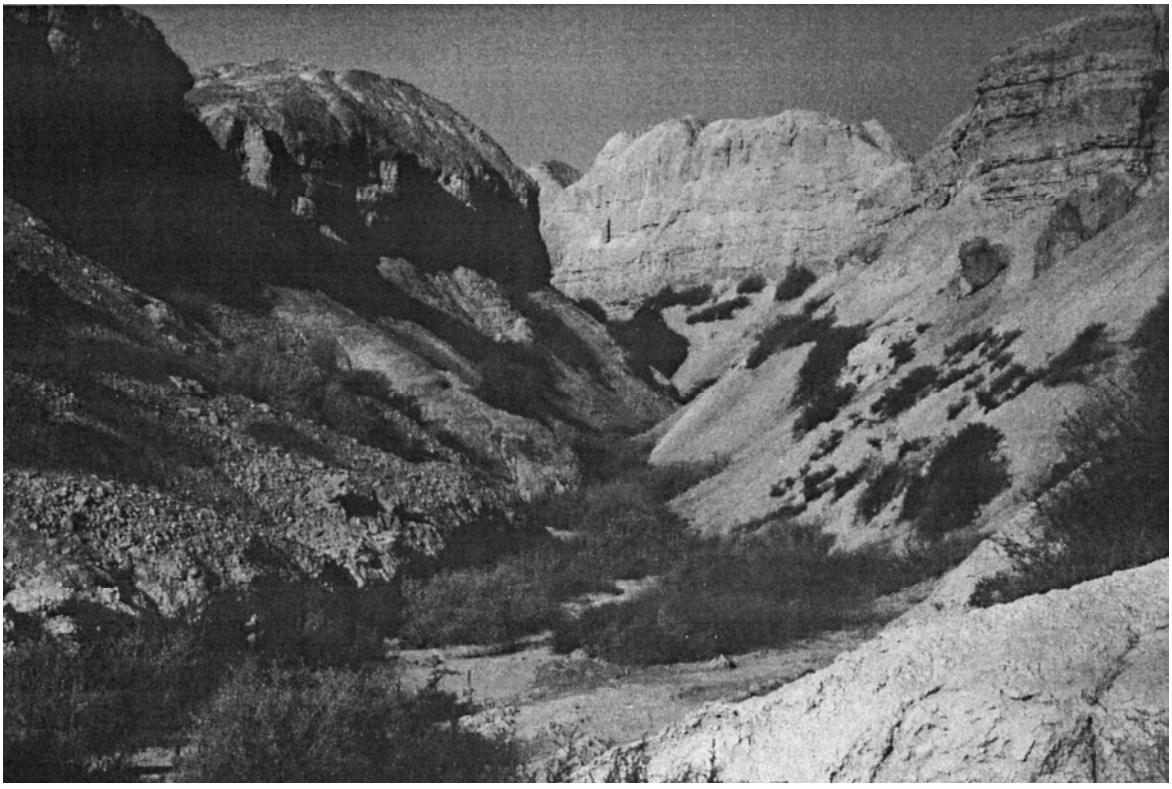

Fig. A2 **Steep slopes with still active erosion processes in the lower Zin catchment (terrain type 3)**

Fig. A3 **Left: Limestone slope (terrain type 2), right: dissected loessial colluvium representing a remnant of a Pleistocene valley fill (terrain type 4)**

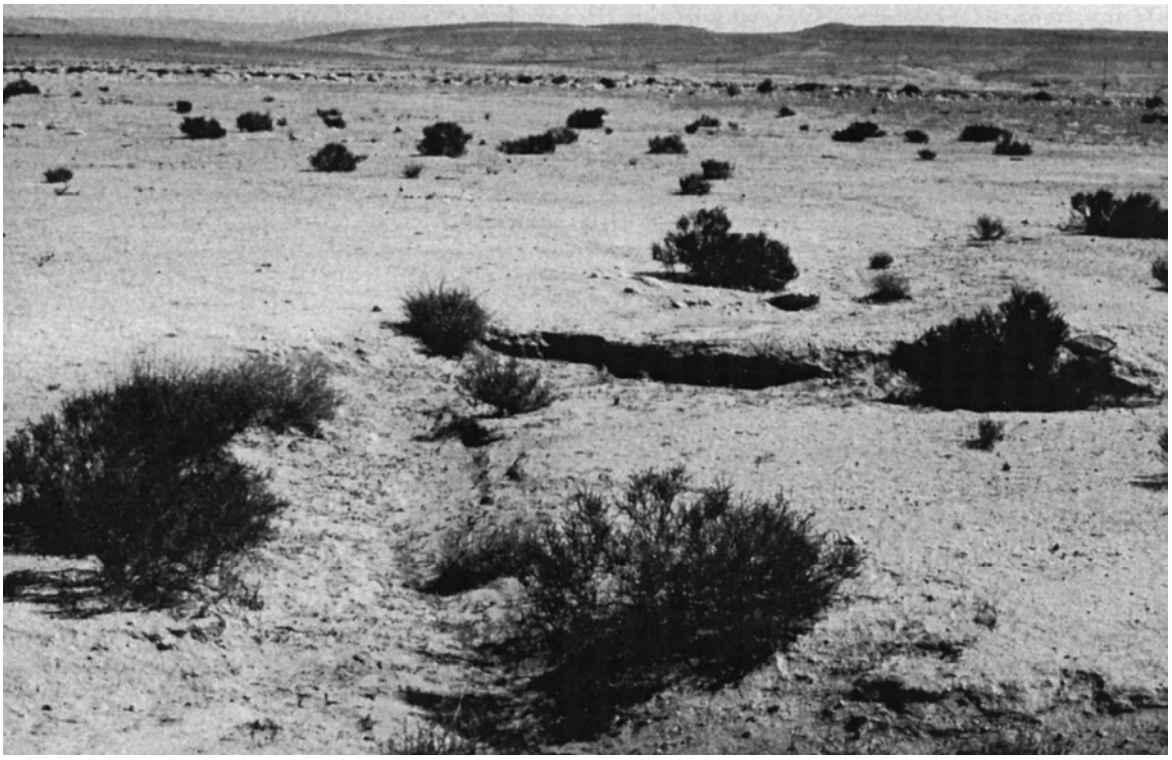

Fig. A4 **Plain loessial plateau (terrain type 5); accentuated runoff generation due to surface sealing by stable crusts**

Fig. A5 **The sandy Rotem Plain (terrain type 7); vegetation enhances infiltration; Hatira anticline with bare limestone (terrain type 1) in the background**

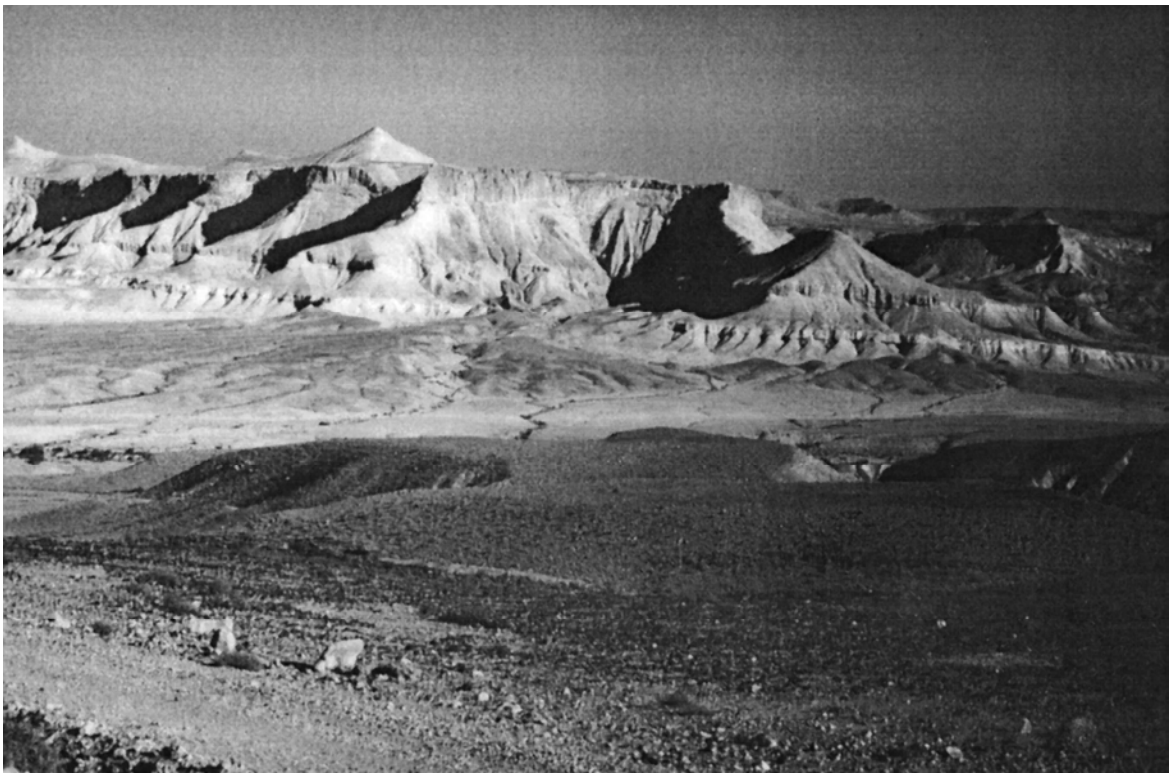

Fig. A6 **An old alluvial fan (terrain type 8) dissected by a recent channel in the Zin Valley; cliffs in the background rising up to the Avdat Plateau**

Fig. A7 Detail of an old, Pleistocene alluvial terrace (terrain type 8); well developed pavement and gravel-free horizon underneath; Zin Valley

Fig. A8 Detail of a young, Holocene alluvial terrace (terrain type 10); pavement unsorted and unstable; no gavel-free horizon developed; Zin Valley

Fig. A9 **Marly lithosol (terrain type 13); runnels indicate accentuated runoff generation; Zin Valley**

Fig. A10 **Disturbed area (terrain type 19); slag heap of the phosphate plant; Oron Syncline**

Fig. A11 Uppermost Nahal Zin flowing on a flat loessial valley fill; vegetation and loessial crust in channel (channel type 1)

Fig. A12 Straight, confined main channel (channel type 2); compacted channel alluvium with little roughness; lower Nahal Zin

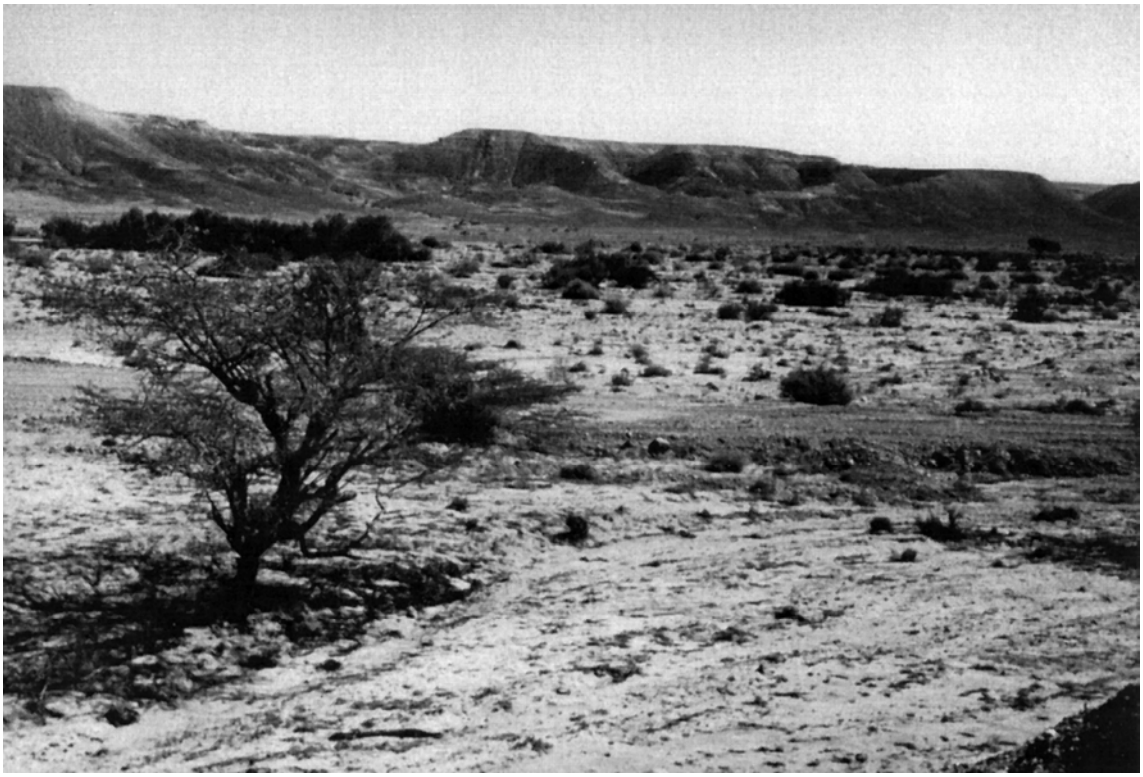

Fig. A13 Wide floodplain and system of braided sub-channels (channel type 3); accentuated transmission losses; Massos-Aqrabim reach

Fig. A14 Rocky waterfall with no channel alluvium (channel type 4); Zin Ein Avdat